Astrocyte calcium signaling under oxidative stress in acute and cultured brain tissue slices

Inaugural-Dissertation

zur Erlangung des Doktorgrades

der Mathematisch-Naturwissenschaftlichen Fakultät

der Heinrich-Heine-Universität Düsseldorf

vorgelegt von

Christian Kehl

aus Dormagen

Düsseldorf, Juli 2012

Aus dem Institut für Neurobiologie
der Heinrich-Heine Universität Düsseldorf

Gedruckt mit der Genehmigung der
Mathematisch-Naturwissenschaftlichen Fakultät der
Heinrich-Heine-Universität Düsseldorf

Referentin: Prof. Dr. C. R. Rose

Korreferent: Prof. Dr. D. Willbold

Tag der mündlichen Prüfung: 23.10.2012

Abstract

During evolution calcium (Ca^{2+}) has evolved into an essential signaling molecule, as it is involved in neurotransmission, muscle contraction and various metabolic processes of eukaryotic cells. Its function is highly dependant on preservation of cytosolic Ca^{2+} baseline levels in the nanomolar range. When oxidative stress arises after antioxidant mechanisms of the cell fail to fully reduce oxygen radicals, e.g. during aging, Ca^{2+} homeostasis becomes disturbed. To analyze in which way metabotropic Ca^{2+} signaling is affected by this, widefield Ca^{2+} imaging was performed in acute tissue slices of mouse hippocampus. Organotypic tissue cultures were used for analysis of medium-term effects. Analysis in both was focused on astrocytes because of their variety in function within the tissue of the central nervous system (CNS). For identification of astrocytes, two methods were compared, a pharmacological approach (Dallwig et al., 2000) and use of the fluorescent dye Sulforhodamine 101 (Kafitz et al., 2008). The latter one was found to be best for the performed experiments. Next, an appropriate H_2O_2 concentration for induction of oxidative stress was determined. Treatment with 200 µM H_2O_2 for 45 minutes caused a slight increase in intracellular Ca^{2+} and was subsequently used to analyze the effects of acute oxidative stress. Besides an increase in intracellular Ca^{2+} baseline levels, metabotropic Ca^{2+} response was found to be significantly reduced in these experiments. To narrow down the point of interference by oxidative stress in the metabotropic signaling cascade, filling level of internal Ca^{2+} stores was measured and testing for hints on adenosine triphosphate (ATP) shortage was performed. Neither a decrease of Ca^{2+} in internal stores was found after treatment, nor were hints on ATP shortage detected. Immunohistochemical analysis of tissue cultures provided evidence for reactive astrogliosis three days after treatment. In summary, these results show that acute oxidative stress disturbs Ca^{2+} homeostasis and drastically alters metabotropic Ca^{2+} signaling in astrocytes. Although it remains to be elucidated if alterations originated from receptor protein oxidation in the membrane or from impairment of the intracellular signaling cascade, it appears reasonable to assume that the precise spatially and temporal coding of Ca^{2+} signals necessary for the function of Ca^{2+} as second messenger is affected.

In addition to experiments that dealt with oxidative stress, unrestricted somatic stem cells (USSC) from human cord blood were analyzed on their functionality as a subproject of the FOR717. USSCs have been found before to support axonal regrowth and to increase locomotor recovery of rats after spinal cord injury (Schira et al., 2012). In widefield Ca^{2+} imaging experiments of our study, different neurotransmitters were applied on USSCs that have previously been treated to induce development into neurons. Except for ATP no substance was found to induce an intracellular Ca^{2+} response. To test the ability of untreated USSCs to integrate into the brain, cells were transplanted into hippocampal tissue cultures of mice directly after injury. Immunohistochemical staining detected USSCs to be still present in 6 out of 44 slices after seven days. Taken together, differentiated cells were able to show Ca^{2+} response which confirms their ability to respond to extracellular stimuli in principle. Yet, integration of USSCs into CNS tissue requires further analysis to make them usable for medical treatment of human beings.

Zusammenfassung

Im Laufe der Evolution hat sich Calcium (Ca^{2+}) zu einem essentiellen Signalmolekül entwickelt, das an der Signalübertragung von Nervenzellen, der Muskelkontraktion und vielen metabolischen Prozessen eukaryotischer Zellen beteiligt ist. Seine Funktion ist in hohem Maße abhängig von der Erhaltung der cytoplasmatischen Ca^{2+} Konzentration im nanomolaren Bereich. Wenn oxidativer Stress durch das Versagen antioxidativer Mechanismen der Zelle, Sauerstoffradikale vollständig zu reduzieren entsteht, z.B. im Laufe des Alterns, wird die Ca^{2+} Homöostase gestört. Um zu untersuchen inwieweit metabotrope Ca^{2+} Signale dadurch betroffen sind, wurden Ca^{2+} Fluoreszenzmessungen in Akutschnitten des Hippokampus von Mäusen durchgeführt. Organotypische Gewebekulturen wurden für die Untersuchung mittelfristiger Auswirkungen verwendet. In beiden Systemen standen Astrozyten aufgrund ihrer Vielzahl an Funktionen im zentralen Nervensystem (ZNS) im Vordergrund. Für die Identifikation von Astrozyten wurden hierzu zwei Methoden verglichen, eine pharmakologische (Dallwig et al., 2000) und eine unter Verwendung des Fluoreszenzfarbstoffes Sulforhodamine 101 (Kafitz et al., 2008). Die letztgenannte Methode wurde als am besten geeignet befunden. Als nächstes wurde eine für das Auslösen von oxidativem Stress geeignete H_2O_2 Konzentration bestimmt. Die Behandlung mit 200 µM H_2O_2 für 45 Minuten bewirkte einen geringen Anstieg des intrazellulären Ca^{2+} und wurde anschließend für die Untersuchung der Auswirkungen akuten oxidativen Stresses verwendet. Neben einem Anstieg der cytoplasmatischen Ca^{2+} Konzentration wurde eine signifikante Reduzierung der metabotropen Ca^{2+} Antwort festgestellt. Um die Stelle des Einwirkens von oxidativem Stress auf die metabotrope Signalkaskade einzugrenzen, wurde der Füllstand der internen Ca^{2+} Speicher ermittelt sowie Hinweise für einen Mangel an Adenosintriphosphat (ATP) gesucht. Weder eine verringerte Menge an Ca^{2+}, noch Hinweise auf einen ATP Mangel wurden gefunden. Die immunhistochemische Untersuchung der Gewebekulturen zeigte drei Tage nach Behandlung eine Astrogliose. Zusammengefasst zeigen diese Ergebnisse, dass akuter oxidativer Stress die Ca^{2+} Homöostase stört und die metabotrope Ca^{2+} Antwort von Astrozyten drastisch verändert. Obwohl noch zu klären ist, ob die Veränderungen auf eine Oxidation der Rezeptorproteine in der Membran oder auf eine Beeinträchtigung der intrazellulären Signalkaskade zurückzuführen sind, liegt es nahe anzunehmen, dass die präzise räumliche und zeitliche Verschlüsselung der Ca^{2+} Signale, die für die Funktion von Ca^{2+} als second messenger notwendig ist, beeinträchtigt wird.

Zusätzlich zu den Experimenten, in denen die Auswirkungen von oxidativem Stress behandelt wurden, wurden unrestringierte somatische Stammzellen (USSC) aus menschlichem Nabelschnurblut, im Rahmen des FOR717, auf ihre Funktionalität untersucht. Es wurde bereits herausgefunden, dass USSCs erneutes axonales Wachstum und die motorische Erholung von Ratten nach einer Rückenmarksverletzung unterstützen (Schira et al., 2012). In den Ca^{2+} Fluoreszenzmessungen der vorliegenden Arbeit wurden verschiedene Neurotransmitter auf USSCs appliziert, welche zuvor zur Entwicklung in Neuronen angeregt worden waren. Mit Ausnahme von ATP führte keine Substanz zu intrazellulären Ca^{2+} Antworten. Um die Fähigkeit unbehandelter Astrozyten zur Eingliederung in das Gehirn zu überprüfen, wurden die Zellen in hippokampale Gewebekulturen von Mäusen transplantiert, denen kurz zuvor eine Verletzung zugefügt worden war. Eine immunhistochemische Untersuchung zeigte, dass sich nach sieben Tagen in 6 von 44 Schnittkulturen noch USSCs befanden. Zusammengefasst zeigten differenzierte Zellen, dass sie zu einer Ca^{2+} Antwort imstande sind, was ihre Fähigkeit auf extrazelluläre Reize zu reagieren prinzipiell bestätigt. Dennoch erfordert die Integration der USSCs ins ZNS Gewebe weitere Untersuchungen um sie nutzbar für die medizinische Behandlung von Menschen zu machen.

Content

Abbreviations

ACSF	artifical cerebrospinal fluid
AD	Alzheimer's disease
AM	acetoxymethyl (-ester)
APP	amyloid precursor protein
ATP	adenosine triphosphate
Ba^{2+}	barium (ion)
BAPTA	1,2-bis(o –aminophenoxy)ethane-N,N,N',N'-tetraacetic acid
BBB	blood-brain barrier
BSO	buthionine sulfoximine
C	cytosine
CA1; CA3	cornu ammonis (area) 1; cornu ammonis (area) 3
Ca^{2+}	calcium (ion)
$[Ca^{2+}]_i$	intracellular calcium concentration
$CaCl_2$	calcium chloride
CaM	calmodulin
CNS	central nervous system
CO_2	carbon dioxide
CPA	cyclopiazonic acid
DAG	diacylglycerol
DAPI	4',6-Diamidino-2-phenylindol
DG	dentate gyrus (lat. *gyrus dentatus*)
DHPG	3,5-Dihydroxyphenylglycine
DIV	days *in vitro*
DMEM	Dulbecco's modified eagle medium
DNA	deoxyribonucleic acid
EGTA	ethylene glycol tetraacetic acid
E_m	membrane potential
ER	endoplasmic reticulum
F	fluorescence intensity (ratio value)
ΔF	alteration in fluorescence intensity (ratio value)

Fe^{2+}	iron (ion)
G	guanosine
GABA	γ-aminobutyric acid
GFAP	glial fibrillary acidic protein
GSH	glutathione
GSx	glutathione peroxidase
H_2O_2	hydrogen peroxide
HEPES	N-(2-hydroxyethyl)piperazine-N'-2-ethanesulfonic acid
hNuc	human nuclei (an epitope for immunohistochemical staining)
IP_3	inositol 1,4,5-triphosphate
$[K^+]_o$	extracellular potassium concentration
K^+	potassium (ion)
K^+_{high}	high potassium
K^+_{low}	low potassium
K-$MeSO_3$	potassium methansulfonate
KCl	potassium chloride
Kir	potassium inward rectifying (channels)
LTP	long-term potentiation (basis of memory consolidation)
MF	mossy fibres
Mg-ATP	magnesium adenosine triphosphate
$MgCl_2$	magnesium chloride
mGluR	metabotropic glutamate receptor
mtDNA	mitochondrial DNA
n	number of (experiments / analyzed cells)
n.s.	not significant
Na^+	sodium (ion)
Na^+/K^+-pump	sodium/potassium pump
NaH_2PO_4	sodium dihydrogen phosphate
Na_3-GTP	sodium guanosine triphosphate
NaCl	sodium chloride
$NaHCO_3$	sodium bicarbonate
NaOH	sodium hydroxide
NCX	sodium-calcium exchanger
NG2	a chondroitin sulfate proteoglycan

NGS	normal goat serum
NMDA	N-methyl-D-aspartate (specific agonist of a glutamate receptor family)
O_2^-•	superoxide anion
$^-$OH	hydroxyl
•OH	hxdroxyl radical
p-value	calculated probability in statistical analysis
P[x]	postnatal day [x]
PBS	phosphate-buffered saline
PIP_2	phosphatidylinositol 4,5-biphosphate
PLC	phospholipase C
PMCA	plasma membrane Ca^{2+}-ATPase
PP	perforant path
R	ratio value of fluorescence intensity
R_{max}	ratio value of maximum fluorescence intensity
R_{min}	ratio value of minimum fluorescence intensity
RoI	region of interest
ROS	reactive oxygen species
RT	room temperature (19-22°C)
S	Subiculum (hippocampal region)
S100β	a Ca^{2+} binding protein in astrocytes
SC	Schaffer collaterals
SERCA	sarco-endoplasmic reticulum Ca^{2+} ATPase
SLM	*stratum lacunosum moleculare* (hippocampal region)
SOD	superoxide dismutase
SP	*stratum pyramidale* (hippocampal region)
SR	stratum radiatum (hippocampal region)
SR101	Sulforhodamine 101
TTX	Tetrodotoxin
USSC	unrestricted somatic stem cells
VGCC	voltage-gated Ca^{2+} channel
Vitamin C	ascorbic acid
Vitamin E	α-tocopherol

1 Introduction

1.1 Astrocytes

1.1.1 Glial cells – more than glue

The central nervous system (CNS) consists mainly of the spinal chord and the brain, which itself is subdivided into several regions, e.g. cerebellum, cortex and hippocampus (for description of the hippocampal structure see chapter 1.2). Cells in the latter two regions are generally assigned to either neurons or glial cells, from which glial cells surpass neurons in number by up to 10-fold. Their name originates from the greek word for glue and was introduced by Rudolf Virchow in 1856. He described these cells as "neuroglia" to explain cohesion of the CNS tissue. Today, glial cells are subdivided further into macro- and microglia, from which macroglia are subdivided again into oligodendrocytes, astrocytes and NG2-cells (potential glial progenitor cells, see Kafitz et al., 2008), respective to their developmental origin, the neuroectoderm.

Astrocytes were the first subtype of "neuroglia" being found by staining experiments of Santiago Ramón y Cajal around 1913. Although he mainly used the term "neuroglia" for the protoplasmic and fibrous cells that he had found, it was him who introduced the name "astrocytes" (Kimelberg, 2004). Astrocytes have various functions that will be described further in chapter 1.1.3. Around 1920 one of Ramón y Cajal's pupils proved ectodermal origin for the protoplasmic and fibrous cells, and replaced the term "neuroglia" by dividing both cell types into astrocytes and oligodendrocytes (Somjen, 1988; Kimelberg, 2004). The latter are today known to be responsible for myelination of axons, allowing electrical signal conduction of neurons with higher velocity. In contrast to Schwann cells of the peripheral nervous system, oligodendrocytes in the CNS are capable of enveloping more than one axon. Ramón y Cajal's pupil also showed that some of the previously found "neuroglia" had mesodermal origin and were subsequently given their own group, the so-called microglia. These immunocompetent cells mainly function as defense against harmful substances by activation of other cells, e.g. astrocytes, and removal of cell debris (Liberto et al., 2004; Garden and Moller, 2006). Although the CNS is separated from

the immune system of the remaining body by the blood brain barrier, an influence of the immune system on microglia is still a topic of debate (Kim and Dustin, 2006; Lehnardt et al., 2007; Moser and Humpel, 2007).

1.1.2 Identification of astrocytes

The identification of astrocytes by Ramón y Cajal's staining procedure and subsequent exclusion of microglia and oligodendrocytes by their morphology was a valuable first step, but lacks reliability. Astrocytes in different brain regions show alterations in their morphology, which makes a distinct identification by this technique rather difficult (Kimelberg, 2004).

Over the years, use of specific biochemical markers has emerged as a widely accepted identification criterion. Especially positive staining against the glial fibrillary acidic protein (GFAP), an intermediate filament of astrocytes, has become a prominent marker for astrocytes (Bignami et al., 1972; Ridet et al., 1997; Eng et al., 2000; Nedergaard et al., 2003; Raponi et al., 2007; Verkhratsky et al., 2011) although its expression varies during development (Verkhratsky et al., 1998). GFAP is an intermediate filament and thought to be important in modulating astrocyte motility and shape by providing structural stability to astrocytic processes (Eng et al., 2000). Although it is an intermediate filament and can therefore be expressed everywhere in the cell's cytoplasm, staining against GFAP only reflects ~15 % of the total size of the astrocyte (Bushong et al., 2002). Mice with a disruption of the GFAP gene have been found to develop normally and show no obvious indication for anatomical abnormalities in the CNS (Gomi et al., 1995; Eng et al., 2000). Staining against GFAP, to verify astrocytes identity, holds basically two limitations. First, immunohistochemical staining against GFAP is time consuming and limited to fixed tissue. Consequently it is inappropriate for live cell imaging and all other live cell recordings. Second, not all astrocytes are positive for staining against GFAP. For example, Kafitz et al. confirmed in 2008 'that GFAP only labels a subset of astroglial cells' although electrophysiological properties indicated astrocyte identity. Utilization of other immunohistochemical markers is accompanied with additional difficulties. Expression of the calcium binding protein S100β, for example, is dependant on the developmental stage (Raponi et al., 2007) and consequently rather unreliable.

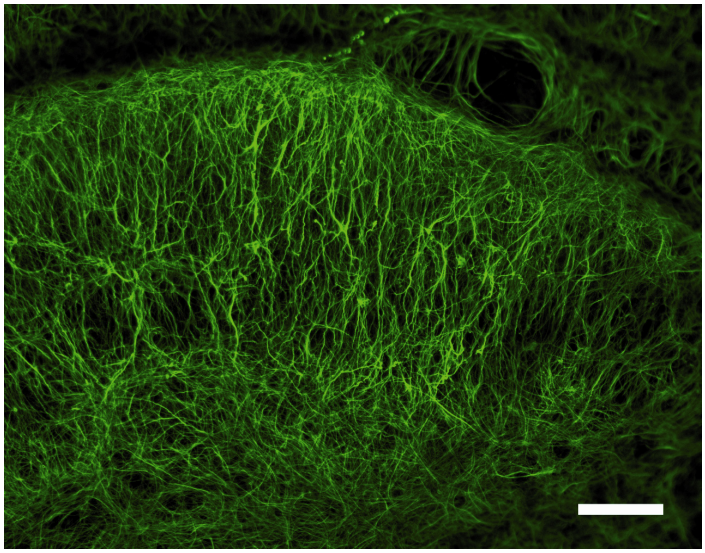

Figure 1: Immunohistochemical identification of astrocytes via staining against GFAP.

Organotypic tissue slice culture (preparation described in chapter 2.1.3; mouse, 17 DIV) stained against GFAP. Astrocytes of the shown hippocampal region (CA1; see chapter 1.2) are easily made visible by immunohistochemical labeling of the intermediate filament GFAP, which is predominantly expressed in astrocytes
Scalebar: 100 µm

Until Dallwig and Deitmer discovered an influx of calcium (Ca^{2+}) into astrocytes under certain circumstances, identification of astrocytes in live cell experiments was restricted to morphological and electrophysiological characterization or approaches with genetically modified animals, expressing a fluorescent protein under the control of the GFAP promoter (Zhuo et al., 1997; Nolte et al., 2001; Dallwig and Deitmer, 2002; Nimmerjahn et al., 2004). They found astrocytes, in contrast to neurons, to increase the intracellular calcium concentration ($[Ca^{2+}]_i$) when the potassium (K^+) concentration of the surrounding artificial cerebrospinal fluid (ACSF) was reduced from 5 to less than 1 mM (see also chapter 3.2.2). This effect was proposed to originate from Ca^{2+} influx through potassium inward rectifying (Kir) channels, because it could be blocked by the use of barium (Ba^{2+}) (Dallwig et al., 2000). Kir channels have gained more and more interest in the past two decades as they were found to be essential for maintenance of the membrane potential and uptake of K^+ in the CNS (Reimann and Ashcroft, 1999; Hartel et al., 2007; Hibino et al., 2010). One Kir channel subgroup, the Kir4.1 channel, is not expressed in neuronal cells but in glial cells and might therefore be responsible for the described influx. Although it is expressed in both, astrocytes and oligodendrocytes (Poopalasundaram et al., 2000; Hartel et al., 2007), it can be used as a first criteria to differ between neurons and glial cells in living tissue and suggest astrocyte identity for about 80 % of all astrocytes (Dallwig et al., 2000).

In 2004, Nimmerjahn et al. introduced Sulforhodamine 101 (SR101), a derivate of Texas Red, as a new dye that specifically and rapidly labels glial cells of the neocortex *in vivo*. This method was adapted and validated as a reliable technique to

identify astrocytes *in situ* by Kafitz et al. in 2008. Electrophysiological properties of labeled cells resembled those of classical astrocytes and immunohistochemical staining against GFAP was also positive in most cells. In fact, SR101 was found to label more astrocytes than immunohistochemical staining against GFAP. Besides the simple staining procedure, the major advantage of SR101 is that it possesses an excitation maximum at ~575 nm. Therefore, it allows a combination with ion indicator dyes of different excitation wavelengths, e.g. Fura-2 (see also chapter 3.2.1), which has to be excited with UV light.

1.1.3 Astrocytes – a cell type with multiple functions

More than 100 years were necessary to realize that glial cells are involved in much more than structural support for neurons, as Virchow proposed in the middle of the 19th century. The recognition of voltage-gated channels and neurotransmitter receptors in astrocytes in the late 1980s marks a moment in time, when these cells gained more attention and became considered active participants in neuronal communication (Volterra and Meldolesi, 2005). Today, the functional importance of astrocytes is established and various functions have been found, ranging from ion homeostasis, over modulation of synaptic transmission, to metabolic support and protective functions.

Astrocytes are involved in synaptogenesis (Nagler et al., 2001; Ullian et al., 2004) and because of their proximity to synapses, astrocytes are in the perfect place for taking up depleted neurotransmitters. By removing neurotransmitters from the synaptic cleft, they prevent neurotoxicity and maintain synaptic transmission while modulating synaptic activity by this in parallel (Araque et al., 1998; Nedergaard et al., 2003; Volterra and Steinhauser, 2004). Buffering of K^+ by uptake through Kir channels of astrocytes and distribution via gap junctions to other regions, additionally maintains synaptic transmission. This is important because variation in ion balance occurs during neuronal activity and its maintenance is a prerequisite for electrical signal conduction (Holthoff and Witte, 2000; Somjen, 2002; Kofuji and Newman, 2004). But Astrocytes are also responsible for pH homeostasis, regulation of blood vessel diameter (vasomodulation), and have been found to increase resistance of neural tissue against oxidative stress (Jendelova and Sykova, 1991; Desagher et al., 1996; Dringen, 2000; Takano et al., 2006; Obara et al., 2008; Liu et al., 2011).

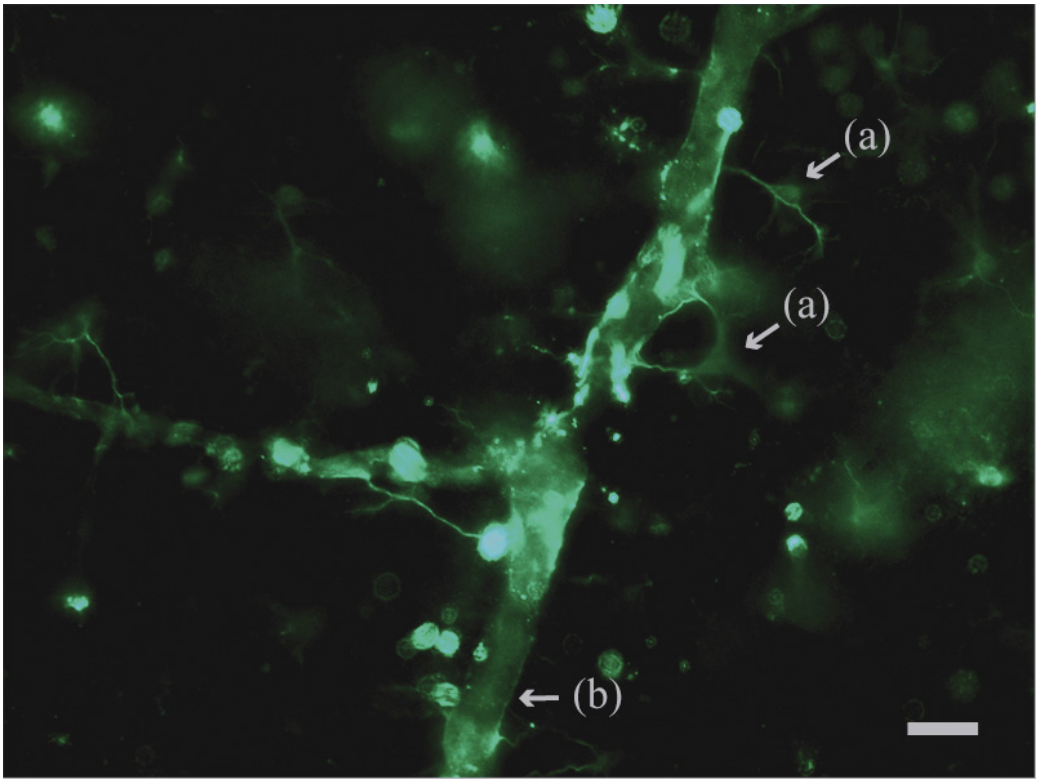

Figure 2: Astrocytes in proximity to a blood vessel.

Acute tissue slice (mouse, P14.) stained against GFAP to identify astrocytes (a). The image shows astrocytic processes contacting the blood vessel (b) for uptake of nutrients, which are subsequently transferred to neurons. Neurons are thereby isolated from the bloodstream to avoid infiltration by lymphocytes.
Scalebar: 20 µm

Another benefit for neurons is that astrocytes supply them with metabolites, e.g. glucose. This is necessary because neurons do not have direct contact to blood vessels and are consequently dependant on astrocytes, which contact blood vessels (see figure 2) with their endfeet, for transport of nutrients from the blood (Peters et al., 2004; Metea and Newman, 2006). While nutrients and energy metabolites are transported past the membranes that lie between the blood vessel endothelium and the neuronal plasma membrane, hydrophilic (immune) molecules are detained from entering the CNS. The blood-brain barrier (BBB), or the glia limitans to be more precise, gave the brain the status of being "immunprivileged" because it protects the CNS from intrusion of leucocytes (Becher et al., 2006; Bechmann et al., 2007). Invading leucocytes would induce inflammatory activity in the brain, as it can be found in multiple sclerosis, the most prominent disease implicated with failure of the BBB (Abbott et al., 2006; Becher et al., 2006). Protective functions of astrocytes also include the well-documented state of astrogliosis, in which astrocytes become "activated", e.g. by cytokines from

microglia, as a result of injury to the tissue (see figure 3; Ridet et al., 1997; Faulkner et al., 2004; Hauwel et al., 2005; Pekny and Nilsson, 2005; Buffo et al., 2010). Astrogliosis is hallmarked by hypertrophy, increased number of processes (Yong et al., 1991; Ridet et al., 1997; Tamagno and Schiffer, 2006; Wilhelmsson et al., 2006) and increased expression of the intermediate filament GFAP (Bignami et al., 1972; Ridet et al., 1997; Eng et al., 2000; Sofroniew, 2005). These "activated" astrocytes, also called "reactive astrocytes" (see figure 3 B), modulate inflammatory processes and repair-related functions that can, in case of severe damage to the tissue, lead to generation of a glial scar. This confines further damage to the nearby cells, but sets up a barrier of chondroitinsulphate proteoglycans that cannot be penetrated by neuronal growth (for review see Sofroniew, 2009; Buffo et al., 2010).

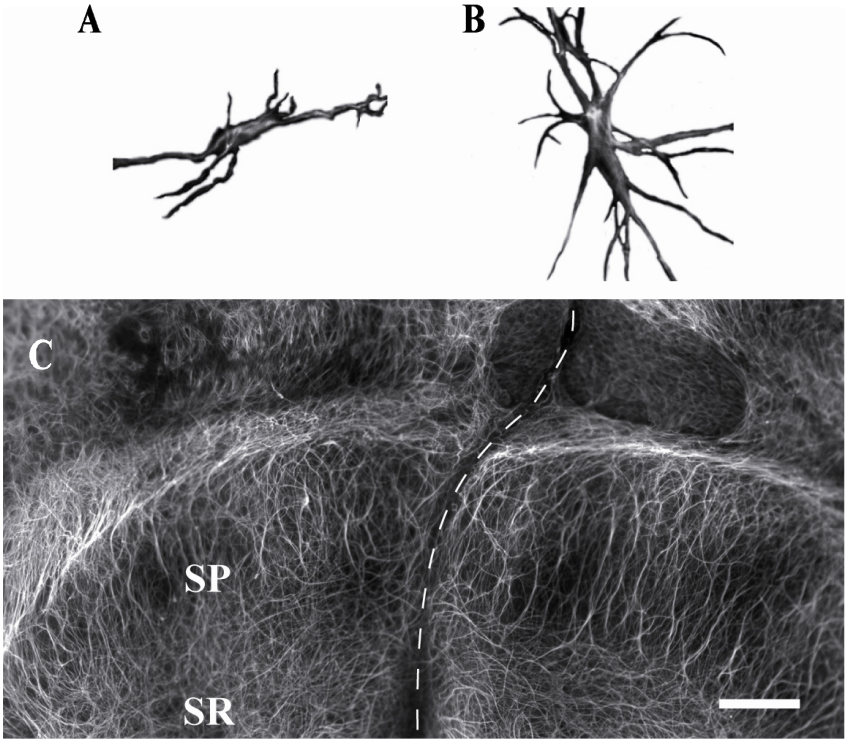

Figure 3: Astrogliosis in the CNS after an injury.

Injury to the CNS results in activation of astrocytes, which then modulate inflammatory processes and repair-related functions, the so-called astrogliosis. Those astrocytes are hallmarked by an increase in the number of processes and hypertrophy when they change from their classical (**A**) to their reactive (**B**) phenotype. Induction of astrogliosis in organotypic slice cultures can be performed by a mechanical injury to the tissue as shown in **C**. The hippocampal slice culture was injured by a cut through the CA1 region (dashed line), postincubated for 3 days and stained against GFAP afterwards.
SP: *stratum pyramidale*; **SR**: *stratum radiatum*; Scalebar: 100 µm

1.1.4 Ca^{2+} signaling in astrocytes

Ca^{2+} represents one of the most important intracellular messengers, for it can control numerous cellular functions, e.g. gene expression and release of neurotransmitters, by interacting with the corresponding biological molecules (for review see Johnson et al., 1997; Verkhratsky et al., 1998; Verkhratsky et al., 2011). As a prerequisite, Ca^{2+} concentrations are tightly controlled and held low within the cytosol of living cells. In this matter, the Ca^{2+} sensor Calmodulin (CaM) plays a central role. It coordinates about 30 different transporter proteins, enzymes, channels and receptors correlated with $[Ca^{2+}]_i$. These are, for example, the plasma membrane Ca^{2+}-ATPase (PMCA) that removes Ca^{2+} from the intracellular space and the IP_3-activated Ca^{2+} channels of the endoplasmic reticulum (ER), whose amounts of released Ca^{2+} are controlled by CaM via feeback inhibition (Squier and Bigelow, 2000). While extracellular concentrations of Ca^{2+} range from 1 to 2 mM, $[Ca^{2+}]_i$ of astrocytes is kept around 150 nM (Verkhratsky et al., 1998). For maintenance of this condition, elevated cytosolic Ca^{2+} is either taken up into intracellular stores or removed from the cell across the plasma membrane. Uptake into intracellular stores, such as the ER, is performed by ATP-driven pumps, the sarco-endoplasmic reticulum Ca^{2+} ATPases (SERCA). Ca^{2+} uptake by SERCAs leads to a concentration of up to 1 mM Ca^{2+} in the ER (Solovyova and Verkhratsky, 2002), which is comparable to the extracellular Ca^{2+} concentration. This is important for metabotropic Ca^{2+} responses because Ca^{2+} is released from the ER after activation of corresponding receptors (see below). For removal across the plasma membrane, Ca^{2+} is transported via the PMCAs. Additionally, the sodium-calcium exchanger (NCX) allows transport of Ca^{2+} in both directions across the membrane, depending on the sodium (Na^+) gradient (Verkhratsky et al., 2011).

Increase of $[Ca^{2+}]_i$ in astrocytes can be basically mediated by two pathways, influx from the extracellular space or intracellular depletion of the ER. Because of the lowered $[Ca^{2+}]_i$, a gradient is generated, which results in an influx of Ca^{2+} from the extracellular space into the cell when channels in the plasmamembrane are opened. Such channels can belong to the group of voltage-gated Ca^{2+} channels (VGCC), ligand-gated channels or nonspecific cation channels (Kimelberg et al., 1990; Puro, 1991; Steinhauser and Gallo, 1996; Verkhratsky et al., 1998). Analysis of astrocytes concerning the existence of VGCCs yielded controversy results *in situ* (Akopian et al., 1996; Carmignoto et al., 1998) although their presence was verified in cultured cells

(for review see Parpura et al., 2011; Verkhratsky et al., 2011). Ca^{2+} depletion of the ER is triggered by activation of inositol 1,4,5-triphosphate (IP_3) gated Ca^{2+} release channels of the ER (Verkhratsky et al., 1998). Initially, metabotropic neurotransmitter receptors in the cell membrane have to be activated. Subsequently phospholipase C (PLC) inside the cell is induced to cleave the membrane-bound phophatidylinositol 4,5-biphosphate (PIP_2) into diacylglycerol (DAG) and IP_3, which then diffuses to the intracellular receptors that lead to activation of Ca^{2+} release channels. Additionally, Ca^{2+}-induced Ca^{2+} release of the ER has been found in astrocytes after stimulation of ryanodine receptors (Berridge et al., 2000). Golovina and Blaustein proposed that different types of stores exist within the ER, one releasing Ca^{2+} after activation by IP_3 and one after activation by Ca^{2+} itself (Golovina and Blaustein, 2000). This form of Ca^{2+} release is involved in the propagation of Ca^{2+} waves by modulating the sensitivity of IP_3-triggered channels (Verkhratsky, 2006). Spreading of Ca^{2+} waves results from diffusion of IP_3 through gap junctions into neighboring astrocytes, followed by Ca^{2+} release from their ER, or by release of gliotransmitters, e.g. adenosine triphosphate (ATP). Released ATP can subsequently activate purinergic receptors of neighboring astrocytes, which again release Ca^{2+} from internal stores, i.e. the ER (Giaume and Venance, 1998; Arcuino et al., 2002; Perea and Araque, 2005; Nedergaard et al., 2010). This propagation of Ca^{2+} waves has been found to cross distances of several hundred micrometers and was proposed to form the basis for successful brain integration (Perea and Araque, 2005; Verkhratsky, 2006).

In addition to the distinct Ca^{2+} signals, which are partly the consequence of neuronal transmission and induce activation of specific cellular functions, astrocytes also show spontaneous Ca^{2+} signaling that appears independent from neuronal activity (Aguado et al., 2002). The function of these oscillations is still unknown, but a correlation with the modulation of neuronal excitability by mediating glutamate release from astrocytes, has been proposed (for review see Fellin, 2009). Abnormal and dysfunction of Ca^{2+} signaling, as well as failure of Ca^{2+} homeostasis in astrocytes has been associated with several neuropathologies, e.g. epilepsy, psychiatric disorders and Alzheimer's disease (AD), in whose late stages Ca^{2+} signaling is also affected. Alterations in Ca^{2+} homeostasis are followed by global elevation of resting Ca^{2+} levels and increased spontaneous oscillations, independent of neural activity (Kuchibhotla et al., 2009; Nedergaard et al., 2010).

1.2 The hippocampus

Key features of the CNS are information processing and memory formation. In the 1950s, a specific region was found to be correlated with learning, during treatment of a patient suffering from epileptic seizures (Scoville and Milner, 1957). The patient Henry M. showed a drastic reduction of seizures after partial removal of both medial temporal lobes. But in parallel, his ability to memorize new facts (episodic memory) was found to be impaired, he had developed an anterograde amnesia. The hippocampus, which lies in the medial lobe of each hemisphere, is a complex, yet clear arrangement of neurons and glial cells, today known to be responsible for consolidation of memories but not for the storage itself (Lavenex et al., 2007; Stella et al., 2011). If it would also be responsible for the storage, induced amnesia of patients like Henry M. would have also been retrograde (loss of memories made in the past).

Processing of neuronal signals in the hippocampus takes place in the "trisynaptic circuit" (Wojtowicz, 2012; see figure 4 C). It begins with the arrival of an excitatory neuronal signal in the enthorinal cortex. Via the perforant path, neurons project onto granule cells of the dentate gyrus. Subsequent signal conduction proceeds via axons of the granule cells, the so-called mossy fibers, to the pyramidal cells of the CA3 (*cornu ammonis*) region. Further projection via the Schaffer collaterals conducts the signals to the pyramidal cells of the CA1 region, whose axons enter the subiculum. Finally, signals are looped back into neurons of the enthorinal cortex. Neuronal cell bodies are arranged in an order, typical for the hippocampus, resulting in different layers (see figure 4 A+B). The *stratum pyramidale* contains the cell bodies of the CA1 and CA3 pyramidal neurons, and the *stratum granulosum* those of the dentate gyrus. Astrocytes can be found anywhere in between, e.g. the *stratum radiatum* or the *stratum lacunosum moleculare*.

The hippocampus has received great attention as a model system because of its high amount of interconnected neurons and the resulting function of memory consolidation. Although the hippocampus is not fully developed at birth, synaptic functionality is already given (Lavenex et al., 2007). Additionally, aside from the olfactory bulb, the hippocampus is the only region of the CNS in adult individuals, where the occurrences of neurogenesis is widely accepted. Neurogenesis in other regions of the CNS is still under debate (for review see Lledo et al., 2006; Bonfanti and

Peretto, 2011). This makes the hippocampus ideal for analysis of neuronal development and function under altered environmental conditions, e.g. oxidative stress.

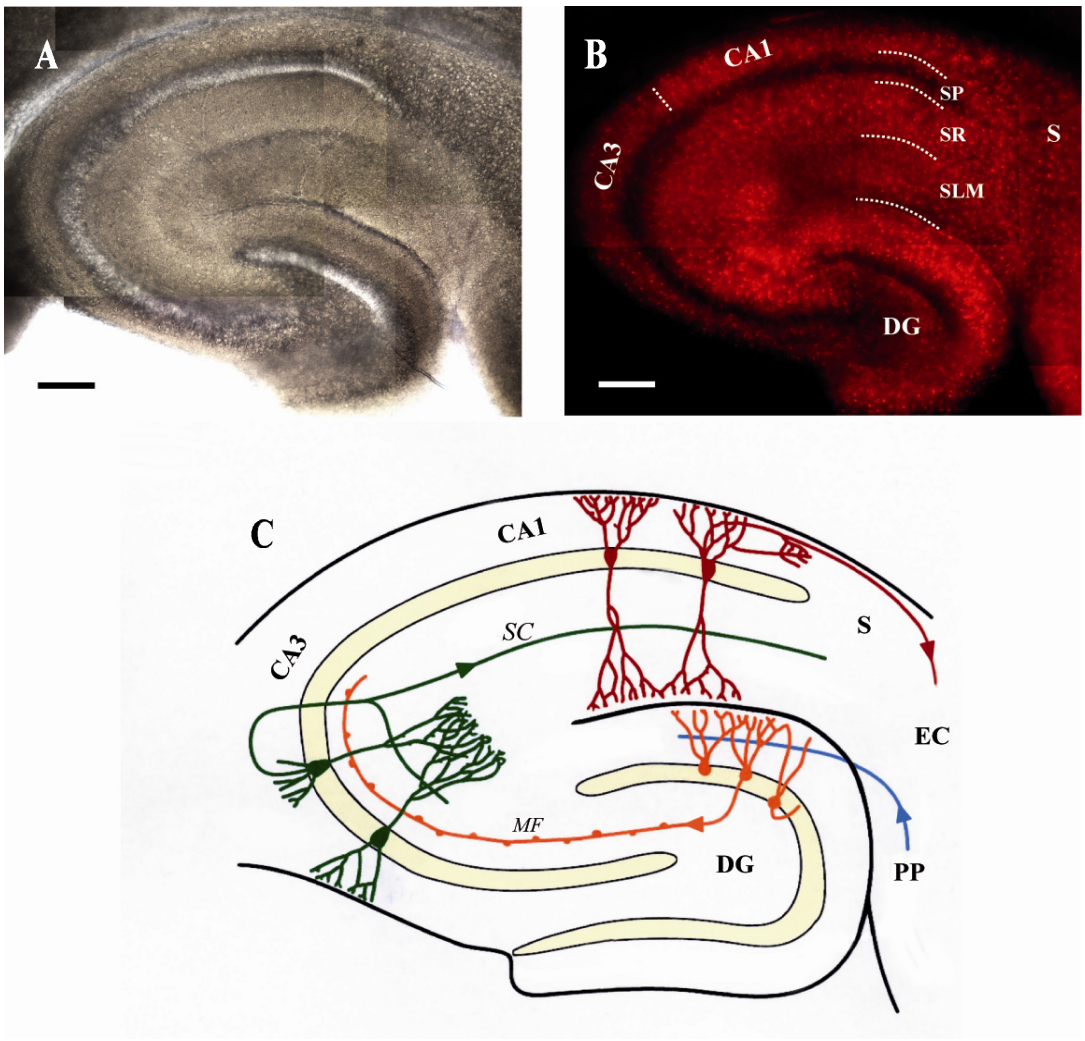

Figure 4: Hippocampal formation and signal processing.

Reconstruction of P14 mouse hippocampus from multiple Transmission images (**A**) and multiple fluorescence images (**B**), the latter showing SR101-labeled astrocytes. Differentiation of the different lamina (as indicated) can be made by observation of differences in structure and fluorescence intensity, respectively. The connectivity within the trisynaptic circuit of the hippocampus is illustrated below (**C**). Signals arriving via the perforant path are processed at different stations (for details see 1.2) and finally reach the enthorinal cortex via the Subiculum (direction of projections illustrated by arrowheads). Figure C taken from figure 2 in Meier, 2007 and modified afterwards.
CA1/CA3: different parts of the cornu ammonis; **DG**: dentate gyrus; **S**: Subiculum; **EC**: enthorinal cortex **SP**: *stratum pyramidale*; **SR**: *stratum radiatum*; **SLM**: *stratum lacunosum moleculare*; **PP**: perforant path; **MF**: mossy fibers; **SC**: Schaffer collaterals
Scalebar: 200 µm

1.3 Oxidative stress

1.3.1 Origins and defense mechanisms

Energy consumption in the brain is very high and requires therefore production of huge amounts of energy metabolites, e.g. ATP (Peters et al., 2004). This is always accompanied by the risk to generate radicals, which can induce disturbances of cellular functions or damage the surrounding tissue (for review see Valko et al., 2007). Especially oxygen radicals, i.e. superoxide anions (O_2^-•), emerge during ATP production in mitochondria. But also intermediate products of oxygen radical degradation, e.g. H_2O_2 are capable of interfering with cellular functions (see figure 6). All of these oxygen species are therefore classified as reactive oxygen species (ROS). In the presence of transition metals such as iron (Fe^{2+}), accumulation of ROS is increased even more as H_2O_2 is broken down into a hydroxyl ($^-$OH) and a hydroxyl radical (•OH). In the so-called Fenton reaction, Fe^{2+} is oxidized to Fe^{3+}, allowing breakdown of H_2O_2 ($Fe^{2+} + H_2O_2 \rightarrow Fe^{3+} + \bullet OH + {}^-OH$). As a result, lipid oxidation, protein dysfunction and failure of ion homeostasis occur, which can finally lead to cell death (for details see 1.3.2; for review see Valko et al., 2007; Facecchia et al., 2011).

To counteract an excess of ROS, several antioxidant mechanisms have developed that are basically divided into enzymatic and non-enzymatic processes (for review see Valko et al., 2007). The major enzymatic mechanisms are the conversion of O_2^-• to H_2O_2 by the superoxide dismutase (SOD), also described as the first line of defense (Olanow, 1993), and the subsequent detoxification of H_2O_2 by the catalase and the glutathione peroxidase (GPx). Whereas the GPx reduces H_2O_2 to water by oxidizing glutathione (GSH) in return, the catalase converts it into water and oxygen (see figure 6). In the brain, which is especially vulnerable to ROS (Pertusa et al., 2007), astrocytes have been found to remove H_2O_2 mainly by use of catalase activity that is strongly increased compared with that in neurons (Desagher et al., 1996). The non-enzymatic mechanisms contain antioxidants like GSH, ascorbic acid (Vitamin C), α-tocopherol (Vitamin E), carotenoids and flavonoids. GSH plays a multifunctional role as it functions as a cofactor of antioxidant enzymes, e.g. the glutathione peroxidase, and additionally scavenges free radicals, such as •OH. It also regenerates other antioxidants, e.g. Vitamin C and E back to their active form (Valko et al., 2007).

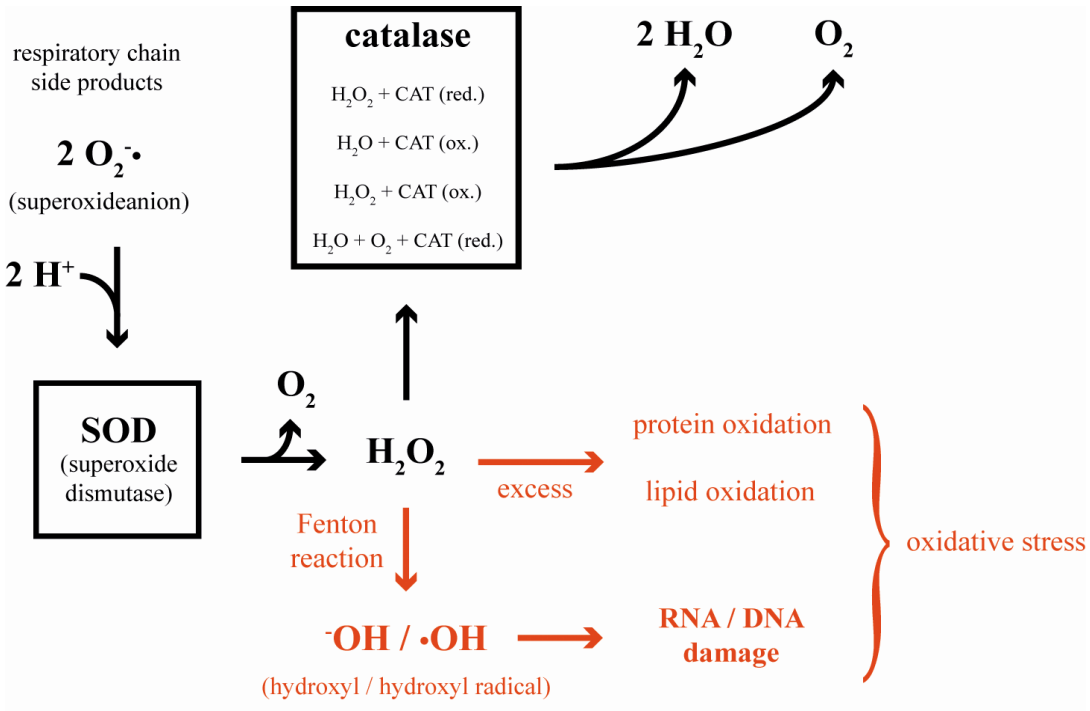

Figure 5: Simplified illustration of ROS emergence and reduction the cell.

ROS are constantly generated in the tissue. Superoxideanions are a side product of the energy production in mitochondria and reduced to H_2O_2 via the SOD. H_2O_2 is detoxified afterwards by reduction to water and oxygen via the catalase.
When H_2O_2 accumulates uncontrolled, for example because of redox mechanism failure, oxidative stress (red) arises with proteins and lipids becoming oxidized. Oxidative stress also arises when Fe^{2+} is present where H_2O_2 accumulates. Hydroxyls and hydroxyl radicals emerge from the Fenton reaction , leading to RNA and DNA damage. This can additionally increase the production of ROS and decrease the redox mechanisms' functionality, resulting in even more oxidative stress (not indicated).

However, antioxidant mechanisms are capable of decreasing the possibility that damage occurs by reducing the amount of ROS. But except for repair of DNA strands, in which GSH is also involved (Valko et al., 2007), they are unable to repair damage that has already occurred. Hence, reduction of ROS is essential for proper cell functions. Whenever emergence of ROS and compensation by antioxidant mechanisms become imbalanced, oxidative stress arises (Gille and Joenje, 1992).

1.3.2 Implications of oxidative stress on cellular functions

As long as ROS and antioxidant processes remain balanced, ROS can also perform physiological roles with beneficial effects. They can act as part of the immune system when pathogens are eliminated by oxidative bursts or function in various cellular

signaling pathways (Valko et al., 2007). But under conditions of increased oxidative stress, ROS induce rather malign effects. Oxidation of lipids and proteins leads to dysfunction of multiple proteins, e.g. pumps and enzymes (see also figure 6). One of the major disturbances is the impairment of ion homeostasis. Especially failure of Ca^{2+} homeostasis with subsequent global elevations of resting Ca^{2+} levels induces severe disturbances in cellular functions (for review see Squier and Bigelow, 2000; Nedergaard et al., 2010).

The regulation of $[Ca^{2+}]_i$ becomes affected when regulatory proteins, e.g. CaM, are oxidized. Under normal conditions, CaM functions as Ca^{2+} sensor and interacts with a huge number of proteins (see chapter 1.1.4) to keep $[Ca^{2+}]_i$ extremely low. An optimal spatial relationship of two globular domains of CaM was proposed to be critical for maintaining efficient activation of target proteins. But under conditions of oxidative stress, large changes in the spatial arrangementof these domains occur because of methionine oxidation, resulting in the nonproductive interaction of CaM with proteins, such as the plasma membrane Ca^{2+}-ATPases (Squier and Bigelow, 2000). Squier and Bigelow proposed alternatively that methionine oxidation causes a decreased binding energy which prohibits normal conformational changes in the target protein and consequently enzyme activation. When homeostatic processes are subsequently impaired, intracellular Ca^{2+} signals can hardly be coded in the correct manner. Signals, mediated by changes in $[Ca^{2+}]_i$, are spatially and temporally coded to induce specific functions, e.g. gene expression, release of neurotransmitters and K^+ buffering by astrocytes (Verkhratsky et al., 1998; Verkhratsky et al., 2011). As a consequence, these functions are also impaired during oxidative stress and have been partially associated with neural pathologies (see chapter 1.3.3). An additional failure of homeostasis arises from activation of ER Ca^{2+}-channels by H_2O_2. While H_2O_2 is generated during reduction of $O_2^{-}\bullet$, Ca^{2+} released by internal stores has been found to disturb Ca^{2+} homeostasis in mitochondria and enhance ROS production, leading to a vicious circle (van de Water et al., 1994; Bindokas et al., 1996; Jacobson and Duchen, 2002; Camello-Almaraz et al., 2006; Gonzalez et al., 2006; Droge and Schipper, 2007). Finally, if cellular functions are unable to restore Ca^{2+} homeostasis, apoptosis is induced by the high Ca^{2+} concentrations (Nicotera et al., 1992; Berliocchi et al., 2005; Nedergaard and Verkhratsky, 2010; Szydlowska and Tymianski, 2010). This applies to both, neurons and astrocytes, whereas neurons are more endangered as they are less efficient in removal of ROS. Therefore, neuronal survival is dependant on homeostasis support by

astrocytes, emphasizing the key role of astrocytes in proper function of the CNS (Desagher et al., 1996; Nedergaard et al., 2010).

Another severe effect of oxidative stress is the oxidation of DNA strands. Although cellular repair systems take care of damage that has been dealt to the DNA by ROS (Ghosh and Mitchell, 1999), depending on the conditions, repair mechanisms can become overstrained, resulting in an accumulation of damage. This is especially interesting in context with aging, because aging is often seen as being based on the accumulation of oxidative damage (see chapter 1.3.3; for review see Harman, 2003; Droge and Schipper, 2007). Damage that persists in the DNA has been found to result in transcriptional misfunction. Oxidation of guanosine (G) by •OH does not inhibit DNA replication, yet this oxidized base is read-through during replication and assists fixation of mutations by allowing increased mispairing with other bases than cytosine (C). When this occurs in the promoter region of genes, which are (G + C)-rich, initiation of the corresponding gene transcription is inhibited (Ghosh and Mitchell, 1999; Lu et al., 2004).

In mitochondria, DNA (mtDNA) is even more vulnerable to oxidative stress because the generation of ROS, as mentioned, takes place in the mitochondria. This exposes mtDNA to an about 10 times higher risk of damage than DNA in the nucleus. As a consequence, a vicious circle develops. ROS that arise during respiration, induce oxidative damage to mtDNA, which leads to an impaired transcription of proteins, e.g. ATP-synthetase, which is essential for the generation of the energy metabolite ATP. With shortage of ATP supply, ATP-dependant enzymes become unable to reduce the occurring ROS and cellular homeostasis fails (Richter et al., 1988; Finkel and Holbrook, 2000; Lu et al., 2004; Navarro and Boveris, 2004; Balaban et al., 2005; Droge and Schipper, 2007).

Oxidative stress was found further to induce an increase in GFAP expression. This is a hint on astrocyte activation (see also chapter 1.1.3), a process to keep the extent of damage to a minimum, after an insult to the brain has occurred (Rolls et al., 2009). Hence, overexpression of GFAP, probably resulting from lesions in the brain, was proposed to be useful as an indicator for oxidative stress (Morgan et al., 1997; Pertusa et al., 2007). Considering the “free radical theory of aging” (Harman, 1956), which describes the aging process as an accumulation of radical-based damage, it seems obvious that ‘an early stage of reactive gliosis is what characterizes the astrocytes of the aging brain’ (Cotrina and Nedergaard, 2002).

1.3.3 Oxidative stress and aging

A correlation of oxidative stress and aging was proposed first by Denham Harman. In his "free radical theory of aging", he theorized that aging and degenerative diseases are basically attributed to damage induced by free radicals (Harman, 1956). Over the years he expanded his theory with additional aspects such as mitochondrial aging and nutritional implications (for review see Harman, 2003). Today, there are numerous studies supporting Harman's theory (Toescu and Verkhratsky, 2003; Droge and Schipper, 2007; Lin et al., 2007; Pertusa et al., 2007; Zundorf and Reiser, 2011) but also publications that relate aging to a genetic program (for review see Glorioso and Sibille, 2010). However, undisputed are the consequences that emerge during aging, ranging from increased oxidant stress over damage to the DNA of cells and mitochondria, to increase of $[Ca^{2+}]_i$ baseline levels (for review see Squier and Bigelow, 2000; Droge and Schipper, 2007; Nedergaard et al., 2010).

Cells of aged individuals are less resistant to oxidative stress (Gottfried et al., 2002; Lin et al., 2007), although expression of SOD is upregulated and catalase activity increased. Upregulation of SOD is probably an attempt of the cells to compensate elevated ROS production, which cannot be controlled with the lower antioxidant activity of old individuals (Pertusa et al., 2007). The increased vulnerability to oxidative stress might result from the missing adaptation of the glutathione redox system to the altered conditions during aging, because its antioxidant efficiency remains unaltered (Pertusa et al., 2007). Consequently, the increasing amount of ROS aggravates the impairment of physiological functions, e.g. ion homeostasis and with it, the progress of several age-related diseases. Dysregulation of $[Ca^{2+}]_i$, as it can arise after oxidation of important proteins that maintain Ca^{2+} homeostasis, plays a decisive role in neuronal cell death, synaptic excitability and several neurodegenerative diseases (Kuchibhotla et al., 2008; Burke and Barnes, 2009; Zundorf and Reiser, 2011). In AD for example, β- and γ-secretases cleave the amyloid precursor protein (APP) in a way that the Aβ protein, whose increase has become a hallmark of AD, is generated. Subsequent oligomerization of elevated Aβ has been found to result in the generation of membrane pores, allowing uncontrolled entrance of Ca^{2+} (for review see Bezprozvanny and Mattson, 2008; Cai et al., 2011). Neurons experiencing this influx undergo apoptosis, leading to cognitive decline. Additionally, astrogliosis with all its hallmarks, e.g. upregulation of GFAP expression, arises because this apoptosis means an injury to the brain (Lin et al., 2007;

Sofroniew, 2009). But not only loss of neurons is responsible for impaired cognitive functions. A shift in the Ca^{2+} sources, responsible for $[Ca^{2+}]_i$ alterations, can already be sufficient. When, for example, involvement of N-methyl-D-aspartate (NMDA) receptors (glutamate activated receptors, which allow Ca^{2+} influx into the cell) in synaptic modifiability is decreased and replaced by increased participation of VGCCs and internal Ca^{2+} stores (as it is the case during aging of the hippocampus), cell excitability and synaptic plasticity might become altered (Foster, 2007). Long-term potentiation (LTP; the basis for memory consolidation) was also found to become impaired when the promoter region of genes, encoding for major signal transduction components, have been damaged by oxidative stress (Lu et al., 2004).

Taken together, oxidative stress and aging posses a lot of common implications, which makes it hardly plausible that radical formation is not, at least partially responsible for aging, but a genetic clock mechanism (Glorioso and Sibille, 2010). This is especially the case when increased vulnerability to oxidative stress in aged individuals is considered (Gottfried et al., 2002; Lin et al., 2007). It makes one remember the old question of what came first. The hen or the egg? Aging or oxidative stress? But no matter if accumulation of damage or a genetic program marks the beginning of aging, the end is formed by failure of Ca^{2+} homeostasis (Nedergaard and Verkhratsky, 2010). With cell death following an intracellular Ca^{2+} overload and failure of energy metabolism, oxidative stress and several age-related diseases are fatal.

Finally, it should be mentioned that increase in intracellular Ca^{2+} levels of aged individuals might also have compensatory effects. Propagation of intercellular Ca^{2+} waves, for example, is dependant on IP_3-mediated Ca^{2+}-release from the ER and ATP signaling (see chapter 1.1.4). Secretion of ATP as gliotransmitter activates purineric receptors, e.g. $P2X_7$, leading to influx of Ca^{2+} and consequently allows ATP depletion, which is Ca^{2+} triggered. With increased $[Ca^{2+}]_i$ even low amounts of ATP binding to the receptor are able to prolong the spreading of calcium waves. This is necessary because ATP metabolic activity is decreased with age due to the redox condition. In pathological conditions astrocytes can even upregulate expression of $P2X_7$ receptors inducing massive Ca^2 entry after activation by high levels of ATP (Joo et al., 1999; Arcuino et al., 2002; Nedergaard et al., 2002; Cotrina and Nedergaard, 2009; Verkhratsky et al., 2009).

1.3.4 Experimental induction of oxidative stress

Analysis of effects that result from oxidative stress requires an adequate way to induce oxidative stress. This can be archived by either addition of radicals or by decreasing the antioxidant defense mechanisms. Extracellular application of H_2O_2 is be an example for the first option. Because H_2O_2 is generated from O_2^-• by the SOD, this treatment imitates an imbalance between radicals and their removal by antioxidant mechanisms as it could develop in living cells for whatever reason. Use of H_2O_2, in a one-time, nonrecurring application, is limited to acute treatment though. Its concentration can diminish fast, depending on the amount of catalase in the concerning cell and the number of cells in the surrounding (Gille and Joenje, 1992; Pertusa et al., 2007). Use of buthionine sulfoximine (BSO) is be an example for the reduction of antioxidant mechanisms. BSO inhibits the gamma glutamyl cysteine synthetase, leading to a decline of GSH and consequently to an enhancement of oxidative stress (Griffith and Meister, 1979; Martensson et al., 1991). This reduction has been found usable in several organs and cell types (Andersen et al., 1996; Armstrong et al., 2002). Yet, although a longterm treatment (1-3 days) of tissue could be performed with BSO (Andersen et al., 1996; Hou et al., 1997; Armstrong et al., 2002) and oxidative stress increases with aging, a huge number of studies, analyzing changes in aged tissue, used old animals or *in vitro* aged tissue instead (Joo et al., 1999; Cotrina and Nedergaard, 2002; Lin et al., 2007; Pertusa et al., 2007). Aside from the experimental question, this is probably the case, because oxidative stress is just one feature of aging and it is still under debate, if it describes the main cause (Toescu and Verkhratsky, 2003; Droge and Schipper, 2007; Lin et al., 2007; Pertusa et al., 2007; Zundorf and Reiser, 2011; Glorioso and Sibille, 2010).

For experiments with induced oxidative stress, it is important to keep in mind, that indicators for alterations might be affected by the method used for stress induction. This is especially important when an excess of radicals is provoked. While an imbalance of the redox system can be detected by cell death or a decrease in GSH levels (Andersen et al., 1996; Armstrong et al., 2002), indicators for consequences of oxidative stress, e.g. fluorescent dyes for measuring increase in $[Ca^{2+}]_i$, might be oxidized. This has been found true for Fura-2 and Fura-3, when oxidative agents were applied together with enhancers, such as Fe^{2+}. In contrast to that, Fura-2 and Fura-3 are relatively resistant against oxidizing effects of H_2O_2 and O_2^-• alone (Sarvazyan et al., 1998), which suggests use of H_2O_2 without any enhancers when Ca^{2+} imaging wants to be performed.

1.4 Analysis of USSCs

Therapeutic use of stem cells is considered to be a promising strategy to compensate loss of cells, e.g. after an injury, and to allow recover from the functional impairments. To investigate the functional potential of unrestricted somatic stem cells (USSC) and to analyze the necessary regulatory mechanisms on the molecular level, the DFG founded the research group 717 (FOR717) "Unrestricted Somatic Stem Cells from Human Umbilical Cord Blood".

USSCs are non-hematopoietic, pluripotent stem cells which have been found in the umbilical cord blood and were described to be capable of developing into tissues of all three germ layers of the neural lineage (Greschat et al., 2008). In the subproject A2 of the FOR717, differentiation of USSCs into neuronal and glial cells was investigated. After establishment of a method for the cell-specific differentiation by Dr. Jessica Schira and co-workers in the department of neurology (head: Prof. Dr. H.W. Müller), a functional analysis of the differentiated USSCs was performed. USSCs were additionally transplanted into injured hippocampal tissue cultures of mice to test for successful integration of those cells (see chapter 3.1). Transplantation of USSCs was found to have beneficial results in the spinal chord of rats before, leading to an enhanced axonal regrowth and functional locomotor improvement after acute traumatic spinal cord injury (Schira et al., 2012).

Analysis of USSCs, which were differentiated to neurons, on their functionality, as well as preparation of hippocampal tissue cultures for testing on successful integration were performed by me in parallel to my work that dealt with oxidative stress. The results are therefore presented and discussed in separate chapters.

1.5 Aims of this study

With oxidative stress arising, after generation and reduction of ROS have become imbalanced, cells are affected by a variety of detrimental effects. Investigation of these effects in neurons and astrocytes of CNS tissue (for review see Squier and Bigelow, 2000; Valko et al., 2007; Facecchia et al., 2011) found DNA damage, lipid oxidation and oxidation of proteins to be the main consequences of oxidative stress. During aging,

these consequences have been described to arise as well. Especially failure of protein functions has gained great interest, because it is mainly responsible for failure of Ca^{2+} homeostasis and for subsequent increase in $[Ca^{2+}]_i$. This increase does not only impair important intracellular processes, e.g. mitochondrial electron transfer necessary for ATP synthesis, it can also cause cell death (Nicotera et al., 1992; Szydlowska and Tymianski, 2010). Astrocytes play a central role in this matter, as they are involved in several homeostatic processes of the tissue and also in protection of neurons by an improved ability to reduce ROS (Desagher et al., 1996; Nedergaard et al., 2010). Cell death of astrocytes is therefore in particular detrimental for CNS tissue, which is why neurological diseases that result from glial dysfunction have been suggested before to be considered as gliopathologies (Nedergaard et al., 2010; Zundorf and Reiser, 2011).

Until now, the effects of acute oxidative stress on metabotropic Ca^{2+} signaling of astrocytes have not been analyzed. It is consequently unknown, if oxidative stress impairs Ca^{2+} signals after metabotropic glutamate receptor (mGluR) activation in whichever way. Impairment of these signals, especially disturbance in spatial and temporal coding, might result in dysfunction of Ca^{2+} as second messenger and disturbance of astrocyte functions (see chapter 1.1.3 & 1.1.4). I therefore addressed the question, if oxidative stress and the resulting failure of Ca^{2+} homeostasis alter metabotropic Ca^{2+} signaling of astrocytes and if those alterations are similar for each signal when Ca^{2+} release is induced repeatedly with a short delay in between. My hypothesis was that Ca^{2+} response would show decreased amplitudes, which decrease even more with each mGluR activation. But as a prerequisite for this analysis, a reliable method for identification of astrocytes had to be determined first. For this identification method it was necessary that it would work in acute tissue slices and cultured slices because both model systems were compared to find the more adequate one for experiments dealing with oxidative stress. Use of acute tissue slices represents an approved model system, but use of a culture system would allow analysis of oxidative stress that can develop more slowly. This would make it more similar to oxidative stress as it accumulates during aging and might give insights into changes during aging. Another important experiments that had to be performed before analysis of metabotropic Ca^{2+} response, was the detection of an adequate H_2O_2 concentration for the induction of oxidative stress. A treatment had do be found that induces oxidative stress without overstressing the cells in both model systems. Analysis of intracellular Ca^{2+} store filling levels and search for hints on ATP shortage, subsequent to mGluR

activation experiments, were performed to test for underlying mechanisms of potential alteration in Ca^{2+} response.

For analysis of effects from oxidative stress on metabotropic Ca^{2+} signaling, including astrocyte identification experiments and dose-response experiments, I performed widefield Ca^{2+} imaging with the fluorescent, Ca^{2+}-sensitive dye Fura-2. My work concentrated on hippocampal astrocytes in the *stratum radiatum* of acute brain tissue slices as well as brain tissue cultures from Balb/c mice. For reliable identification of astrocytes, a pharmacological approach, which induces a specific Ca^{2+} influx in astrocytes (Dallwig and Deitmer, 2002), and use of the fluorescent dye SR101 (Nimmerjahn et al., 2004; Kafitz et al., 2008) were compared. Exposure of slices to different H_2O_2 concentrations for a short amount of time, followed by analysis of increase in $[Ca^{2+}]_i$ was performed in dose-response experiments. To additionally test if the chosen treatment results in mild oxidative stress, tissue cultures were treated and immunohistochemically analyzed for the occurrence of astrogliosis. By applying the mGluR agonist 3,5-Dihydroxyphenylglycine (DHPG) in Ca^{2+} imaging experiments, metabotropic Ca^{2+} response was triggered and signal amplitudes before and after treatment with H_2O_2 were subsequently compared. Application of DHPG was performed three times in each recording with a delay of one minute to analyze further if oxidative stress influences repeated release of Ca^{2+} from internal stores. Filling level of those stores was measured by depletion via cyclopiazonic acid (CPA) and detection of alteration in $[Ca^{2+}]_i$, whereas hints for energy shortage were tested for via electrophysiological recording of the membrane potential of astrocytes during exposure to H_2O_2.

In addition to analysis of the effects resulting from oxidative stress, unrestricted somatic stem cells (USSC) were tested on their functionality after differentiation and their ability to integrate into CNS tissue. These experiments were part of the FOR717 in collaboration with the department of neurology. Similar to other types of stem cells, USSCs are considered to be useful for treatment of injuries that come along with cellular loss. Earlier experiments already showed a beneficial effect on the recovery from spinal cord injury in rats. Implantation of USSCs into the site of injury led to axonal regrowth and improvement in locomotor recovery (Schira et al., 2012). For compensation of neuronal loss, USSCs have also been treated to differentiate into

neurons. These cells were found to develop into cells of the dopaminergic lineage and to express functional voltage-gated sodium channels (Greschat et al., 2008).

To further analyze the neuronal properties of those differentiated USSCs, cells were tested on their ability to respond to several neurotransmitters that are typically released during neurotransmission. The earlier described expression of functional voltage-gated sodium channels in differentiated USSCs was also checked. As described by Schira et al. (2012), USSCs are capable of supporting regeneration after spinal cord injury in rats and to persist in the lesion site. Yet, their ability to persist in other parts of the CNS as well as other model system had not been tested before and was therefore analyzed in my experiments.

Preparation of USSCs from human cord blood was performed by members of the department of neurology as well as the treatment for differentiation into neurons with the necessary medium. For analysis of cellular response to neurotransmitters, I performed widefield Ca^{2+} imaging experiments in which I applied several types of transmitters, i.e. glutamate, γ-aminobutyric acid (GABA) and ATP. Voltage-gated channels were stimulated by application of ACSF containing a high concentration of K^{+}. For analysis of USSC integration, I prepared hippocampal tissue cultures of Balb/c mice and made a cut shortly before transplantation of USSCs near the wound. Immunohistochemical analysis of cell survival was then done by members of the department for neurology.

2 Material & Methods

2.1 Model systems

2.1.1 Animals

Mice of the Balb/c strain were used for all experiments. For acute experiments animals of postnatal day (P) 18-20 were used, if nothing else is noted, as most basic developmental processes are completed at this time point. During comparison of methods for astrocyte identification, P5 animals were also used. Organotypic (tissue) slice cultures required younger animals to ensure structure preservation. Therefore, P7-8 mice were used.

USSCs were collected from human umbilical chord blood and cultured by Jessica Schira and co-workers in the institute of molecular neurobiology. After ~2.5 weeks, cells were used for experiments (see also chapter 2.3.5)

2.1.2 Slice preparation

All animal preparations were performed according to the animal protection laws. Mice being younger than P10, which had not opened their eyes yet, were decapitated without previous anesthesia. Animals of advanced age, in this case P18-20, were first anesthetized with CO_2 and decapitated afterwards.

Slice preparation for acute tissue experiments and organotypic slice culture was basically the same and performed as described earlier (Meier et al., 2006; Kafitz et al., 2008). In brief, brain tissue preparation was done in cold carbonate buffered ACSF. To maintain pH in the carbonate buffered ACSF, it was constantly gassed with carbogen (95 % O_2, 5 % CO_2). Hemispheres were separated, orientated and trimmed, to receive slices with a hippocampus as shown in figure 7. For acute tissue experiments slices were cut with a thickness of 250 µm (HM650V, Microm International GmbH, Walldorf, Germany). For preparation of organotypic slice cultures, slices were prepared with a thickness of 200 µm to decrease necessary time for tissue flattening. After slicing, tissue

sections were placed onto gauze in another, tempered glass (34°C) with ACSF. Depending on the type of following experiments, slices were either stained afterwards or immediately brought into cell culture. ACSF used during preparation differed between young (<P10) and older (>P10) animals. While "standard" ACSF (125 mM NaCl, 2,5 mM KCl, 1,25 mM NaH_2PO_4, 26 mM $NaHCO_3$, aqua dest., 2 mM $CaCl_2$, 1 mM $MgCl_2$, 20 mM glucose) was used throughout the complete preparation of young animals. Slicing of brains from older mice and subsequent SR101 labeling took place in ACSF with reduced $CaCl_2$ (0.5 mM) and increased $MgCl_2$ (6 mM). The aim was to minimize neuronal stress because of excessive receptor activation right after slicing. Lowered Ca^{2+} concentrations reduce the amount of Ca^{2+} influx into the cells by NMDA receptor activity. Additionally, elevated Mg^{2+} concentrations increase the availability of Mg^{2+} to block the NMDA receptors. Acute slices of older animals were put into "standard" ACSF after SR101 labeling. Chemicals for all experiments were, if nothing else is noted, purchased from Sigma-Aldrich (Taufkirchen, Germany).

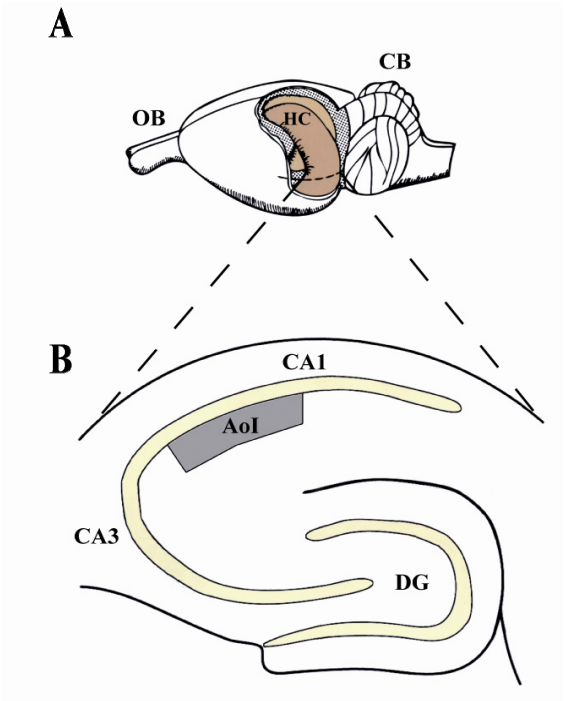

Figure 6: Mouse hippocampus.

(**A**) illustrates a schematic mouse brain after removal from the skull with opening, showing the hippocampus. **OB**: olfactory bulb; **HC**: hippocampus; **CB**: cerebellum. (**B**) shows the hippocampus after transversal cut as indicated in the upper image. The *Area of Interest* (**AoI**, grey) indicates where analysis during this work was performed. Figures were taken from figure 2 and figure 8 in Meier, 2007 and modified afterwards.
CA1/**CA3**: different parts of the *cornu ammonis*; **DG**: dentate gyrus

2.1.3 Organotypic slice cultures

Culture work with organotypic slice cultures was performed following the protocol of Stoppini et al. (Stoppini et al., 1991). For this, all work was done within a sterile workbench (Hera Safe KS12, Thermo, Langenselbold, Germany), except for the Ca^{2+} recordings. Media and solutions being used are listed in the appendix.

Before tissue preparation culture medium was prepared as listed in table 2+3, sterile filtrated afterwards and equilibrated in the incubator (Heraeus HERAcell 240 CO_2 incubator, Thermo, Osterode, Germany) at 37°C and 5% CO_2. After 24 hours pH was adjusted to 7.35 using NaOH. As another prerequisite for cell culture, 5 Petri dishes were filled with ~9 ml medium and for each brain one 6-well plate (Sarstedt AG & Co., Nürnbrecht, Germany) was equipped with culture membranes (Millicell-CM, Millipore corp., Ireland) and medium for every well. Petri dishes and 6-well plate were kept in the incubator until end of tissue preparation.

After preparation tissue slices were washed by transferring them sequentially through all 5 previously prepared Petri dishes, attempting to bring as little medium to the next Petri dish as possible. After that, slices were placed on the culture membranes in the 6-well plate. Medium on the top of the membrane was removed. Culture slices were kept in the incubator for at least 10 days to flatten down. With the cells having contact to air but no medium in the upper layers, cells underwent apoptosis, allowing the slices to reach a thickness of about 30-50 µm within less than 2 weeks. Medium was exchanged every 2-3 days and after the first 3 days, slices were washed with 1 ml medium to remove cell debris.

The advantage of this tissue culture is that the hippocampus and the surrounding tissue maintain their structure and interconnectivity, while allowing pharmacological treatment over a couple of days or weeks. Additionally, flattening of the tissue reduces the thickness of the slices to 2-3 cell layers, increasing its usability for immunohistochemical staining. But in contrast to acute tissue, one preceding procedure has to be performed. By slicing the tissue, the tissue is injured, leading to the generation of a so-called glial scar (see chapter 1.1.3). This thin, transparent barrier covers the slices and needs to be removed before staining and further experiments.

2.2 Principles of Ca^{2+}-imaging

Intracellular Ca^{2+} concentrations are kept extremely low in contrast to other ion concentrations. Na^+ for example, which is actively transported out of the cell via the sodium/potassium pump (Na^+/K^+-pump), is present in concentrations of about 10-20 mM in cultured astrocytes (Kelly et al., 2009). In contrast to that, Ca^{2+} is held at less than 200 nM (Verkhratsky et al., 1998). Therefore, measuring Ca^{2+} with a visual approach, e.g. epifluorescence widefield imaging, requires a molecule with a high binding affinity in the nanomolar range. Additionally, this molecule needs to change its extinction / emission characteristics when Ca^{2+} is bound, so that it can be differed between both forms and calculation of Ca^{2+} concentrations or at least detection of changes are possible. In Fura-2 (see below), for example, binding of free Ca^{2+} leads to a stabilization of the ground state, and therefore it also stabilizes the energy difference to the excited state (Deitmer and Schild, 2000). As a result, the absorption maximum of Fura-2 is shifted to light of a shorter wavelength.

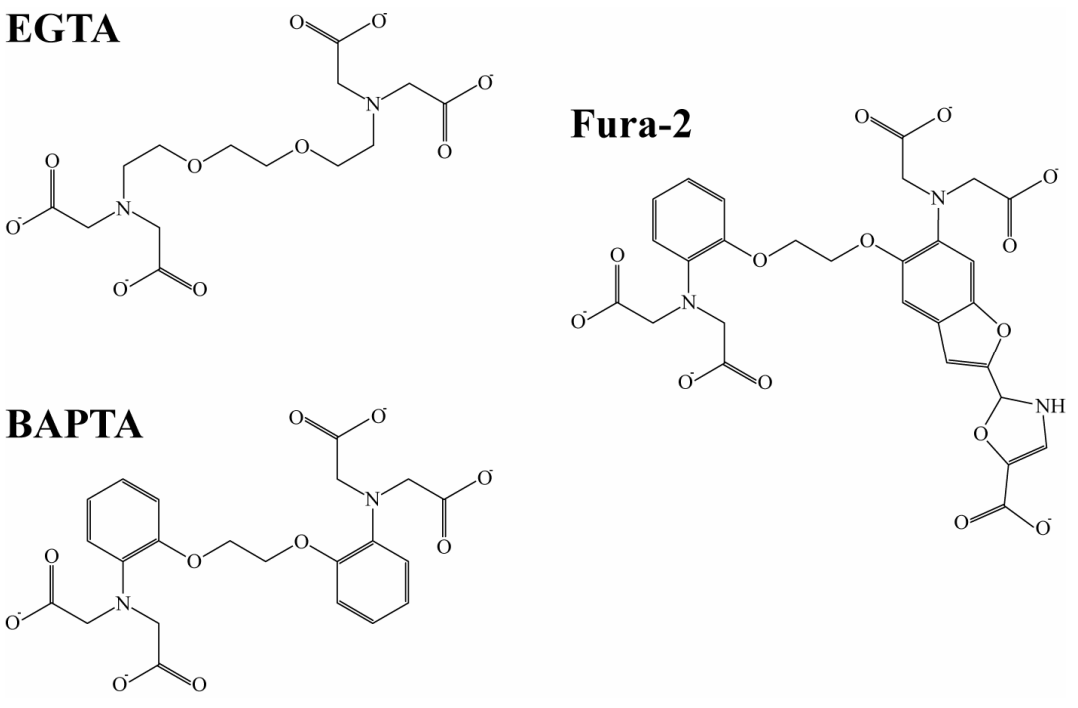

Figure 7: Ca^{2+} chelators and derivates.

The Ca^{2+}-sensitive dye BAPTA is a derivate of EGTA, modified with two aromatic ring systems for excitability, and an extinction maximum at ~250 nm (Deitmer and Schild, 2000). Fura-2 in its non-esterified form possesses even more aromatic ring systems, allowing this molecule to absorb light of the near UV spectrum which increases its usability. (molecule structures reproduced from figure 2.4 in Deitmer and Schild, 2000)

Today there are several calcium sensitive dyes available that capture Ca^{2+} with two carboxyl groups, similar to the chelating agent ethylene glycol tetraacetic acid (EGTA), which is used to eliminate free Ca^{2+} in solutions (Deitmer and Schild, 2000). The most similar one is 1,2-bis(o-aminophenoxy)ethane-N,N,N',N'-tetraacetic acid (BAPTA) that only differs in addition of two aromatic ring systems (see figure 8). Fura-2, the most commonly used dye for Ca^{2+} imaging, is synthesized from BAPTA and possesses a very high affinity for Ca^{2+} with a K_d of ~224 nM in presence of 1 mM magnesium (according to the manufacturer, Invitrogen). During this work a modified form of Fura-2, Fura-2 AM, was used especially for two reasons. First, Fura-2 AM is modified with an acetoxymethylester (AM) group which makes the polar Fura-2 molecule nonpolar and therefore membrane permeable (Deitmer and Schild, 2000). This simplifies cell loading for not each single cell needs to be loaded via patch pipette and the cell membranes are not disrupted while loading. Free esterases inside the cell cleave this ester binding, which restrains the dye from leaving the cell again (Deitmer and Schild, 2000). Second, Fura-2 shows different absorption maxima between its Ca^{2+}-bound and its Ca^{2+}-free form. This allows ratiometric measurements where changes in dye concentration become irrelevant.

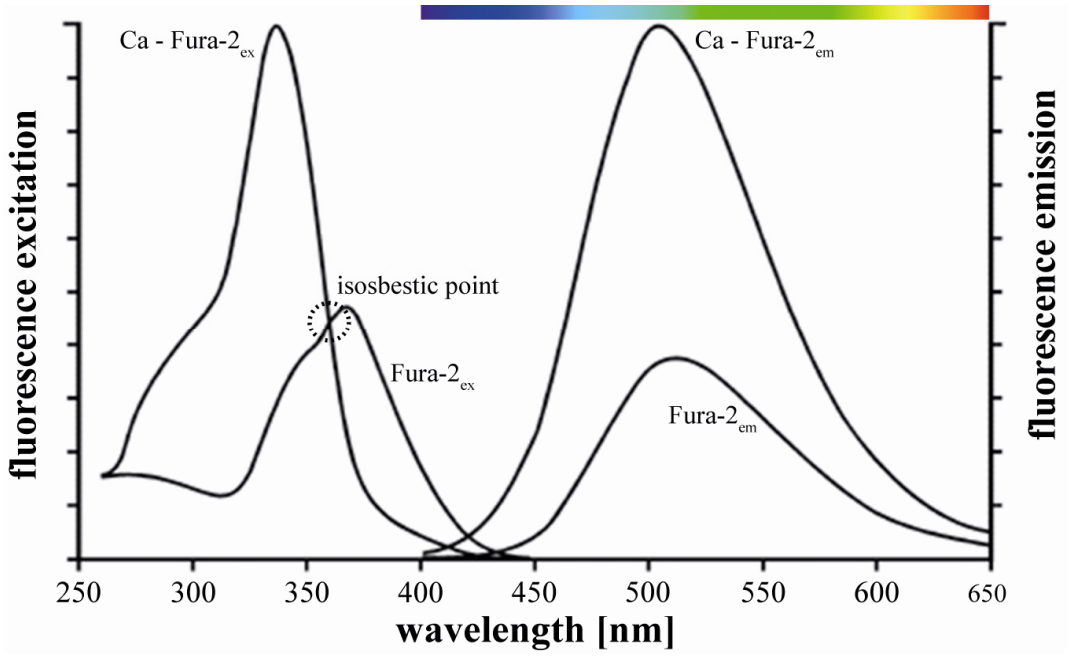

Figure 8: Excitation and emission spectra of Fura-2.

On the left side the excitation spectra of Ca^{2+}-bound Fura-2 (Ca-Fura-2_{ex}) and Ca^{2+}-free Fura-2 (Fura-2_{ex}) are shown, including the isosbestic point where Fura-2 absorbs equally. The corresponding emission spectra are shown on the right side. For better imagination the wavelengths from near UV to red are added above as color bar.
(image adapted from invitrogen.com and modified)

For recordings, alternating excitation with UV light of 340 nm and 380 nm is used to excite both forms of Fura-2 at their respective maximum (Yodozawa et al., 1991; Deitmer and Schild, 2000) and to compare the amounts of emitted light (F_{357}, F_{380}) afterwards by calculating the ratio value (F_{357} / F_{380}). Because in most cases optical devices, e.g. the microscope objective, have poor transmissibility for UV light excitation with 340 nm is replaced by excitation with ~357 nm. At this point both forms of Fura-2 absorb equally, the so called isosbestic point (see figure 9; Deitmer and Schild, 2000). By recording images during excitation with each wavelength via a CCD camera, regions of interest (RoI) can be selected in those images afterwards and mean intensities can be allocated. During this work RoIs were set on the soma of cells, because for its high signal intensity as intensity of Fura-2 in processes tends to fall below background threshold levels. This is important to note, because all measurements were made at a widefield imaging setup where imaging does not take place in a single focal plane of less than 1 µm in thickness. Labeled cells of lower and higher planes create a background signal intensity that needs to be corrected to receive reliable data. For this, a separate region was selected where neither astrocytes nor neurons were clearly visible. Fluorescence of this region after excitation with each wavelength was subtracted from all chosen RoIs to minimize signal intensity influence by other cells. Corrections were performed for each timepoint, i.e. each image taken.

Fura-2 can be excited in a confocal system via lasers as well, so that background correction would not be necessary. But in practice, ratiometric Ca^{2+} imaging with Fura-2 is mostly performed in widefield system, because of the high costs for UV lasers, from which two would be necessary. Moreover widefield imaging allows higher frequencies of capturing because the area of interest does not need to be scanned line by line, but is captured as one picture via a CCD camera. Therefore, and letting the costs aside, confocal imaging with Fura-2 would only make sense in small areas of interest when background correction shall be avoided. But in principle, use of a confocal system for Ca^{2+} imaging with Fura-2 is unnecessary.

2.3 Live cell imaging in cell cultures and organotypic slice cultures

Recording methods for widefield imaging experiments are described in 2.7.1 as well as methods and software used for the analysis of the recorded data.

2.3.1 SR101 and Fura-2 AM labeling

Staining of organotypic slice cultures was performed in two different ways, but before that, the glial scar was removed (see chapter 2.1.3) and slices were cut out. Slices for the H_2O_2 dose-response curve were basically labeled with SR101 via bathloading (see below) and labeled with Fura-2 AM as described in chapter 2.4.1 via bolus injection. Organotypic slice cultures of earlier H_2O_2 experiments, astrocyte identification experiments (see chapter 3.2.2) with $BaCl_2$ and experiments with unrestricted somatic stem cells (USSCs) were stained via bathloading. For this, SR101 labeling took place in a Petri dish with ACSF and ~500 nM SR101 in the incubator for 30 minutes at 36°C (not used for USSCs). After washing twice with preincubated ACSF, slices were put in ACSF with ~10 µM Fura-2 AM and for 45 minutes into the incubator again. Finally slices were washed with ACSF perfusion next to the imaging setup at room temperature (RT) for one hour. For cell culture experiments with organotypic slice cultures, slices of different postincubation age were used. The number of days *in vitro* (DIV) is noted at each experiment.

2.3.2 Detergents for supporting Fura-2 solubilization

Pluronic acid has been used to support solubilization of AM-dyes in water-based solutions for many decades now (Yodozawa et al., 1991; Rose and Ransom, 1997; Kafitz et al., 2008). As a nonionic detergent pluronic acid additionally facilitates diffusion of this dye over the membrane, which allows shorter incubation periods. For use in cell culture, Fura-2 AM was diluted in DMSO with 20 % pluronic acid (Invitrogen, Karlsruhe, Germany), similar to use in acute tissue slices. Due to staining quality and decreased cell viability (see chapter 3.3.1), pluronic acid was replaced by Brij-35. This substance is also a nonionic detergent and could therefore be used without

basic changes of the staining protocol. Brij-35 is, in contrast to pluronic acid, rarely used as detergent for staining with fluorescent dyes. Nonetheless it was found to improve transfection of cells with antisense oligonucleotides, coupled with fluorescent dyes. Increasing fluorescent intensity in these cells during the first 6 hours after transfection indicates no severe effects on cell viability (Zhang et al., 2007). For labeling cells in organotypic slice culture experiments of this work, Brij-35 was used in a concentration of 5 % in contrast to 20 % pluronic acid.

2.3.3 Experiments with alteration of $[K^+]_o$

K^+_{low} experiments in organotypic slice cultures were basically performed as they were in acute tissue slices (see chapter 2.4.2). Aside from changes in Fura-2 AM loading, which was done via bathloading, everything was kept the same, no changes in concentrations or perfusion times. Slices in experiments had an age of 11-27 DIV. Because experiments were only performed for proof of principle and were postponed after questionable results (see chapter 3.2.2), it was not determined which amount of days *in vitro* are comparable with P5 or P20 of acute slices.

2.3.4 Dose-response experiments with H_2O_2

H_2O_2 dose-response experiments were basically performed as described in chapter 2.4.3. In short, during 60 minute recordings, slices were perfused with different H_2O_2 concentrations for 10 minutes. Because organotypic slice cultures are thinner than acute tissue slices (see chapter 2.1.3) and posses therefore less cells for detoxification of H_2O_2, concentrations only ranged from 10 to 500 µM. For analysis, recorded fluorescence intensities were allocated as described in chapter 2.4.3. Staining methods were changed during experiments from bathloading to bolus injection as mentioned in chapter 2.4.1 because of unexpected side effects, as described in chapter 3.3.1.

2.3.5 Experiments with USSCs

For analysis of differentiated USSCs (see also chapter 1.4) on their neuronal function, USSCs were first of all collected from human cord blood (Schira et al., 2012). Afterwards, cells were plated on coverslips and preincubated for ~2.5 weeks. Treatment with differentiating medium (so-called XXL-medium) began 12 days before experiments to force neuronal development. All culture work to this point was performed by Dr. Jessica Schira and co-workers in the department of neurology (head: Prof. Dr. H.W. Müller).

After differentiation with the mentioned medium, cells were analyzed concerning their physiological properties i.e. receptor functionality by recording alterations in $[Ca^{2+}]_i$ (see chapter 3.1) to validate that USSCs had developed into functional neurons. Therefore, cells were labeled with Fura-2 AM via bathloading, similar to previously described procedures in organotypic slice cultures. Aberrant from this, labeling was performed in media instead of ACSF. USSCs from batch SA5/03 p11, SA5/03 p8 and SA8/25 were stimulated with 40-50 mM K^+, 10 mM glutamate, 1 mM ATP and 1-10 mM GABA to verify the presence of functional neuronal receptors and voltage-gated channels. For the first four days of experiments, carbonate buffered ACSF was used as bath solution. After that, experiments were performed in culture media (DMEM with amino acids) to reduce stress on the cells.

For testing on the ability of successful integration of USSCs in CNS tissue of mice, organotypic slice cultures of mice were prepared as described earlier (see chapter 2.1.2 & 2.1.3) and cultured for 10-13 days. Subsequent to this, a mechanical injury was set by making a vertical cut through the CA1 region, transecting the Schaffer collaterals. USSCs were immediately applied afterwards (~25000 cells) in proximity to the lesion by Dr. Jessica Schira. After 7 days of postincubtion cells in the tissue slices were immunohistochemically stained against human nuclei (hNuc) in the department of neurology to identify transferred USSCs and to determine the number of USSCs that were still present at this timepoint.

2.4 Live cell imaging in acute slices

Recording methods for widefield imaging experiments are described in 2.7.1 as well as methods and software used for the analysis of the recorded data.

2.4.1 SR101 and Fura-2 AM labeling

Slices for acute tissue experiments were stained with SR101 after preparation by adding this dye (end concentration ~500 nM) into the glass with temperated ACSF in which they were collected (see chapter 2.1.2), following incubation for 20 minutes at 34°C. After 10 additional minutes in a glass of SR101-free ACSF at 34°C, slices were used for experiments.

For measuring changes in intracellular Ca^{2+} Fura-2 AM was used. After placing a slice with 250 µm thickness in an experimental chamber and pinning it down with a grid, a glass pipette filled with 250 µM Fura-2 AM, diluted in Hepes-Ringer (125 mM NaCl, 3 mM KCl, 25 mM Hepes, Sigma-H_2O, 2 mM $MgSO_4$, 2 mM $CaCl_2$, 1.25 mM NaH_2PO_4, pH: 7.3), was used to load the area of interest via bolus injection. To clear the tissue from remains of the staining solution and to allow cellular esterases to cleave the dye from its acetoxymethyl group, the slice was washed for about 45 minutes with ACSF.

2.4.2 Experiments with alteration of $[K^+]_o$

For low potassium (K^+_{low}) experiments, acute slices were first perfused with ACSF containing 5 instead of 2.5 mM K^+ (for ACSF composition see chapter 2.1.2) to generate a more distinct difference towards ACSF with low K^+ concentration and to be consistent with experiments of Dallwig & Deitmer (Dallwig and Deitmer, 2002). Perfusion with 0.2 mM K^+ ACSF was then performed for 3-5 minutes followed again by 5 mM K^+ ACSF for about 10 minutes. A positive control was done by a 30 second perfusion with 50 mM K^+ ACSF to test for voltage-dependant response of neurons. To maintain osmolarity in all ACSF solutions with different K^+ concentration, increase in

K^+ was compensated with a decrease in Na^+ and vice versa. This perfusion series was performed four times with one slice and with different additional substances. The first series was recorded as control measurement without any other substances, so was the fourth recording to detect if $BaCl_2$ could be washed out. 500 nM Tetrodotoxin (TTX, Alomone Labs, Jerusalem, Israel), a blocker of voltage-activated Na^+ channels, was added to the 5 mM K^+ ACSF before the second series to reduce neuron-glia interaction, whereas K^+_{low} and K^+_{high} solutions were TTX-free, because TTX needs more than 5 minutes to become washed out (see also chapter 3.2.2). The third series contained 10 µM $BaCl_2$ in all solutions to block Kir channels as well as TTX. Aberrant to description in 2.1.1 animals of postnatal day 5 were used additionally during these experiments to verify developmental differences in astrocytes.

2.4.3 Dose-response experiments with H_2O_2

H_2O_2 dose-response experiments were performed by 60 minute recordings of Ca^{2+}-levels in astrocytes. The first 10 minutes were recorded under ACSF, followed by 10 minute perfusion with H_2O_2 in ACSF and 40 minutes under ACSF afterwards (see figure 10). Concentrations of H_2O_2 varied between 0.1-2 µM. For control measurements H_2O_2 was left out of the ACSF. Dose response experiments were done without use of TTX.

For analysis, ratio values (see chapter 2.2) were calculated from the fluorescence intensities of each time point. Subsequent, ratio values of the first 10 minutes were averaged to receive a baseline value (named 'F' in this work) for each cell. Alterations in $[Ca^{2+}]_i$ were obtained by averaging ratio values for each cell from the first minute after H_2O_2 perfusion (named 'ΔF' in this work) and setting it into relation with the baseline. ΔF/F was then calculated after baseline substraction, i.e. (ΔF-F)/F, to determine the increase in $[Ca^{2+}]_i$.

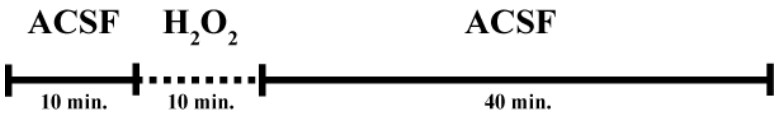

Figure 9: Schematic procedure for dose-response experiments.

To establish a dose-response curve of H_2O_2, slices were exposed to 0.1-2 µM H_2O_2 for 10 minutes. Before that, the slices were perfused with ACSF for 10 minutes to measure baseline Ca^{2+} levels. 40 minute perfusion with ACSF afterwards allowed observation if $[Ca^{2+}]_i$ recovers.

2.4.4 Metabotropic glutamate receptor activation

The mGluR agonist 3,5-Dihydroxyphenylglycine (DHPG; Schoepp et al., 1994) was used to study effects of 200 µM H_2O_2 on mGluR 1+5 function by observing Ca^{2+} signaling that results from the intracellular Ca^{2+} stores. Therefore 2 mM DHPG was applied via pipette for 200 ms three times in a five minute recording of Fura-2 (see figure 20). This recording was repeated with 500 nM TTX in the ACSF and after 45 min. of H_2O_2 perfusion again, including TTX and H_2O_2 as well. Exposure times were kept constant. Control experiments were performed with a 45 minute pause of imaging, but without ACSF containing H_2O_2.

2.4.5 Filling level of internal Ca^{2+} stores during oxidative stress

To measure filling levels of internal calcium stores and to analyze, if acute treatment with H_2O_2 induces changes, slices were treated with 30 µM cyclopiazonic acid (CPA) for 10 minutes in a 20 minute recording (see figure 22). CPA induces a total release of Ca^{2+} from the ER and inhibits further uptake (Plenge-Tellechea et al., 1997). Perfusion with CPA took at least 2 minutes to reach the experimental chamber; therefore the first 2 minutes of each recording were taken for baseline measurements. Before and after CPA perfusion, slices were perfused with ACSF. To minimize excitation-induced Ca^{2+} signaling of neurons, CPA perfusion contained 500 nM TTX. Amounts of depleted Ca^{2+} from the ER were analyzed as described in 2.4.3. Effects of H_2O_2 were studied in separate slices to exclude consequences of prior CPA usage. Therefore slices were pretreated for 45 minutes with 200 µM H_2O_2 before recording and perfusion with CPA. In this case, CPA solution contained H_2O_2 besides TTX as well.

2.4.6 Basic calibration of Fura-2 signals

In situ calibration of Fura-2 signals was performed as an approximation by recording maximum as well as minimum fluorescence intensities and calculating the corresponding ratio values (R_{min} and R_{max}). Because a linear dependency between $[Ca^{2+}]_i$ and fluorescence intensities was assumed for the intensities recorded in

experiments, use of a defined Ca^{2+} concentration for calibration, as performed by Deitmer and Schild (2000), was skipped. Before the first recording, cells of the acute tissue slice were perfused with ACSF containing no Ca^{2+}, 10 mM EDTA and 10 µM CPA for 10 minutes to remove Ca^{2+} from the internal stores. During the first recording, ACSF additionally contained 2 mM glutamate for 2 minutes, to ensure complete clearance of the Ca^{2+} stores by metabotropic receptor activation. Recordings were performed to observe decreasing metabotropic Ca^{2+} release. Subsequent, cell membranes were perforated for 30 minutes by perfusion with an ionophore, i.e. 5 mM ionomycine. 'Ionophores are hydrophobic molecules which form lipid soluble complexes with inorganic cations in membranes. They increase membrane permeability for specific inorganic cations by shielding their polar electrical charge from the apolar lipid bilayer' (Bolkent and Zierold, 2002). This allowed control of $[Ca^{2+}]_i$ in further recordings, simply by perfusion with ACSF containing a different Ca^{2+} concentration. The second recording was then performed to determine R_{min}. In this 10 minute recording, composition of the prior used 0 mM Ca^{2+} ACSF was kept. For determining R_{max}, cells were perfused with 10 mM Ca^{2+} ACSF for 30 minutes afterwards, followed by a 10 minute recording. In contrast to the ACSF used before, ACSF contained no CPA. After use of ionomycine all membranes were expected to be perforated, so that the Ca^{2+} gradient, which was originally directed into the cytosol, had to have collapsed during perfusion with 10 mM Ca^{2+}. Even if the internal stores would have been fully functional, opening of the store's Ca^{2+} channels wouldn't have induced a noticeable effect in the calculated ratio values.

Recordings were performed at a frequency of 0.1 Hz with constant exposure time. For calculation of $[Ca^{2+}]_i$, gathered data was background corrected and interpreted based on the standard calibrating equation by Grynkiewicz (Grynkiewicz et al., 1985):

$$\left[Ca^{2+}\right] = K_d \times \left(\frac{R - R_{\min}}{R_{\max} - R}\right) \times \left(\frac{F2_{low}}{F2_{high}}\right)$$

As mentioned before (see chapter 2.2), Fura-2 allows a ratiometric analysis of $[Ca^{2+}]_i$. Concentration of this dye inside the tissue was therefore irrelevant for determining the amount of intracellular Ca^{2+}. Basically, six values were necessary to determine $[Ca^{2+}]_i$:

- **R:** the calculated ratio (357 nm / 380 nm) for a chosen region (RoI)
- **R_{min}:** the calculated ratio minimum, based on recordings in 0 mM Ca^{2+} ACSF
- **R_{max}:** the calculated ration maximum, based on recordings in 10 mM Ca^{2+} ACSF
- **$F2_{low}$:** the recorded fluorescence intensity of Fura-2_{em} in 0 mM Ca^{2+} ACSF
- **$F2_{high}$:** the recorded fluorescence intensity of Fura-2_{em} in 10 mM Ca^{2+} ACSF
- **K_d:** the dissociation constant of Fura-2 (224 nM; according to the manufacturer, Invitrogen)

Those variables were determined in three cells of one slice and the respective values were averaged. After inserting the values into the equation, $[Ca^{2+}]_i$ in a chosen region could be calculated simply by using the recorded ratio value (R) of the RoI in the equation. However, calculated concentrations can only be seen as estimation, because no explicit concentration steps were performed for the calibration, and fluorescence illumination of the tissue was not uniform, resulting in different ratio values, depending on the cell's position. Additionally, the K_d was not explicitly determined, instead the K_d according to the manufacturer was used. As a consequence, alterations in $[Ca^{2+}]_i$ were described as $\Delta F/F$ or shown as ratio values in this work. Calculated concentrations are only named occasionally to give a rough idea of the changes in $[Ca^{2+}]_i$.

2.5 Patch clamp recordings

All electrophysiological recordings were done by Dr. Jonathan Stephan. In those recordings, the effects of H_2O_2 on the electrophysiological properties of astrocytes were investigated using the patch-clamp technique at a setup with an upright microscope (Nikon Eclips FN1, 60x water immersion objective, N.A. 1.00, Nikon Europe, Düsseldorf, Germany). Data were acquired with an EPC10 amplifier and "PatchMaster"-software (HEKA Elektronik, Lambrecht, Germany). Borosilicate patch-pipettes were pulled with a vertical puller (PP-830, Narishige, Japan) and filled with a

solution of 120 mM K-$MeSO_3$, 24 mM KCl, 10 mM N-(2-hydroxyethyl)piperazine-N'-2-ethanesulfonic acid (HEPES), 12 mM NaCl, 4 mM Mg-ATP and 0.4 mM Na_3-GTP, adjusted to pH 7.3. For measurements, astrocytes in a depth of approximately 20 µm were brought into whole-cell configuration and clamped to a potential of -85 mV, which is near the presumed membrane potential. Subsequent current-clamp recordings were performed at a frequency of 50 Hz and processed with "IGOR Pro"-software (WaveMetrics Inc., Lake Oswego, OR).

2.6 Medium-term effects of oxidative stress in organotypic slice cultures

Documentation of immunohistochemically stained tissue is described in chapter 2.7.2 as well as methods and software used for the analysis of the documented cells.

2.6.1 H_2O_2 treatment

After 10 days in culture, organotypic slice cultures were treated with different concentrations of H_2O_2 or ACSF as control. H_2O_2 was diluted with sterile filtered ACSF to concentrations of 10, 100 and 200 µM. Slices in each well were then provided with 1 ml of one concentration or ACSF and kept in the incubator for 45 minutes. Afterwards slices were washed three times with ACSF to remove H_2O_2 and provided with fresh medium below the membrane. Organotypic slice cultures were kept in the incubator for three more days and removed then for fixation and immunohistochemical staining.

2.6.2 Fixation and immunohistochemical staining

Fixation and immunohistochemical staining was performed based on the procedure of Kelly et al. (2009) and modifications of Kehl (2007) and Lepka (2010). After glial scar removal and excision, slices were put into a 24-well plate with 4 % PFA over night at 4°C. Interim halts in ice-cold phosphate-buffered saline (PBS) were kept as short as

possible. Afterwards, slices were washed two times with PBS before blocking with 2 % normal goat serum (NGS) and permeabilization with 0.25 % Triton-X for 1.5 hours at 4°C. Subsequent, staining against GFAP (dilution 1:1000) and S100β (dilution 1:200) was performed overnight at 4°C. On the next day, slices were washed with PBS containing 0.25 % Triton-X and 2 % NGS several times to remove unbound antibodies. Incubation with adequate secondary antibodies (see table 5) was performed afterwards for two hours at RT, as well as subsequent repeatedly washing with PBS. A short treatment with DAPI followed to stain nuclei and after washing again, slices were put onto glass slides and sealed with a drop of Mowiol (see table 4) and a coverslip. All steps after incubation with the first antibodies were performed in the dark to avoid early bleaching. Staining procedure is also listed in table 6.

2.7 Methods for image capturing and analysis

2.7.1 Widefield imaging

Widefield imaging was performed using a TILL (TILL Photonics GmbH, Munich, Germany) imaging system on a Zeiss Axioscope 2 FS microscope with a 40x Olympus objective (LUMPlanFI, N.A. 0.80). Selected areas of interest (see figure 7) contained an elevated number of distinct visible astrocytes under excitation of SR101. To ensure imaging in the upper focal layers of the tissue, z-axis was adjusted to include neurons in the *stratum pyramidale* as well. Only those neurons at the top can be focused, therefore astrocytes being imaged are presumably near the tissue surface. Imaging of Fura-2 was performed for different periods of time with exposure times between 15-60 ms. Exposure times differed slightly between slices, depending on the effectiveness of the dye loading. In the majority of recordings, such as those of the H_2O_2 experiments, no additional grey filter was inserted into the beam.

Averaged RoI intensity was background corrected after recording, using Microsoft Excel (Redmond, Washington, USA) and then documented in Origin 8 (OriginLab Corporation, Northampton, MA 01060 USA). Fitting curves were also made using Origin while evaluation of changes in Ca^{2+} levels and statistical validation was performed in Excel.

2.7.2 Documentation of immunohistochemically stained culture slices

Slices that were immunohistochemically stained against GFAP, S100β and additionally labeled with DAPI, were documented on a confocal laser scanning microscope (Nikon C1), based on a Nikon Eclipse E600FN with a 60x oil-immersion objective (Nikon, Plan Apo VC, N.A. 1.40). For excitation of DAPI, an argon laser (405 nm) was used, whereas excitation of the secondary antibodies, by which antibodies against GFAP and S100β were labeled, was performed via two helium-neon lasers (488 nm / 590 nm). Z-stacks consisted of 7-8 focal planes with a thickness of 0.5 µm each. The documented areas of interest were the same as in widefield imaging experiments, i.e. the *stratum radiatum*.

For analysis, stacks were exported using NIS Elements Viewer (Nikon) and turned into a maximum projection using NIH ImageJ (National Institute of Health, USA). ImageJ was also used to create merged image files and to analyze diameter of processes.

All illustrations were made with Adobe Illustrator CS2 (Adobe Systems GmbH, Munich, Germany), partly after exporting from Excel and Origin. For images, Adobe Photoshop CS2 (Adobe Systems GmbH, Munich, Germany) and ImageJ were additionally used.

3 Results

3.1 Analysis of USSCs

3.1.1 Ca^{2+} signaling in differentiated USSCs

Work with USSCs was performed to investigate the developmental potential of these stem cells and to analyze the underlying molecular processes. In the subproject A2 (see also chapter 1.5) USSCs were tested on their developmental potential in the neurological field and the functionality of cells that were differentiated into possible neurons. The question was if USSCs, which were treated with differentiating medium, had really differentiated into fully functional neurons. For this purpose, several substances, mainly neurotransmitters, were applied via pressure application. Ca^{2+} response was detected via Fura-2 AM, using widefield fluorescence imaging. Labeling with Fura-2 AM was performed in the incubator using bathloading techniques in ACSF (see chapter 2.3.1).

During the first four experimental days with USSCs a total number of 78 cells were analyzed. Control recordings were performed with each of those 78 cells, but not all substances were tested on each cell. 60 cells were treated with 50 mM K^+ ACSF, 56 with 10 mM glutamate, 47 with 1 mM ATP and 42 with 10 mM GABA. Response was found after application of 50 mM K^+. All applied neurotransmitters failed to induce alterations in $[Ca^{2+}]_i$. However, detection of response on 50 mM K^+ application was only the case in 1 out of all 60 cells and could not be repeated within the same cell. Independent of these results, about 44 % of analyzed cells (34 of 78) showed spontaneous Ca^{2+} oscillations. For stress reduction, cells were measured in culture medium (DMEM with amino acids) instead of ACSF afterwards.

After changing experimental procedures from ACSF as bath solution to culture medium, cells were divided into four groups respective of their morphology (see figure 11). Bipolar or bipolar-like cells (n = 4) were assigned to group “T1” (type 1). Cells with short or no processes at all (n = 4) were assigned to group “T2” (type 2). “T3” (type 3) consisted of cells with a flat morphology which possessed either many processes showing minor branching or few processes showing major branching

(n = 10). Cells of the "T4" (type 4) group showed 3-4 processes with minor branching. From these four groups (21 cells) only one contained cells that could be stimulated repeatedly with 1 mM ATP. All other applied substancess (40 mM K^+, 1 mM glutamate and 1 mM GABA) showed no effect (data not shown). Within group "T4" all tested cells (n = 3) exhibited at least partial rise in $[Ca^{2+}]_i$ (see figure 12). Repeated application resulted in similar Ca^{2+} responses, representing a reliable response to the given stimulus.

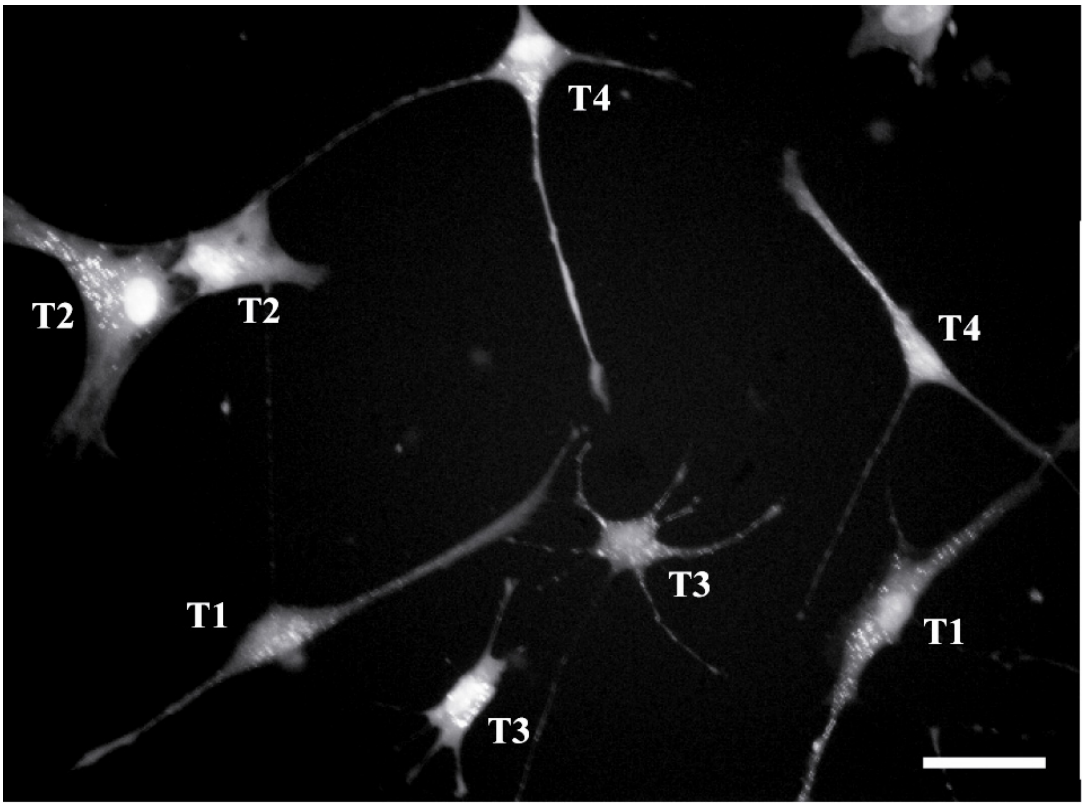

Figure 10: Morphology of USSCs.

Differentiated USSCs were stained with Fura-2 AM and measured at a widefield imaging setup. For analysis, cells were divided into four groups based on their morphology: type-1 cells with bipolar or bipolar-like morphology (**T1**), type-2 cells with short or no processes at all (**T2**), type-3 cells with flat morphology which posses either many processes that show minor branching or that posses few processes that show major branching (**T3**), and type-4 cells with 3-4 processes which show minor branching (**T4**). Scalebar: 50 µm

In summary, verification of neuronal properties of differentiated USSCs yielded a variety of different cell morphologies. Most of these cells did not respond to stimulation with substances that are supposed to induce $[Ca^{2+}]_i$ response, such as K^+_{high} ACSF, glutamate, ATP or GABA, except for a small group of cells. These 3 cells out of 21 exhibited a response to ATP which was repeatable. However, the observed response behavior cannot only be found in neurons, but in other cell types of the CNS as well,

e.g. astrocytes and microglia (Verderio and Matteoli, 2001; Wang et al., 2005; Light et al., 2006; North and Verkhratsky, 2006).

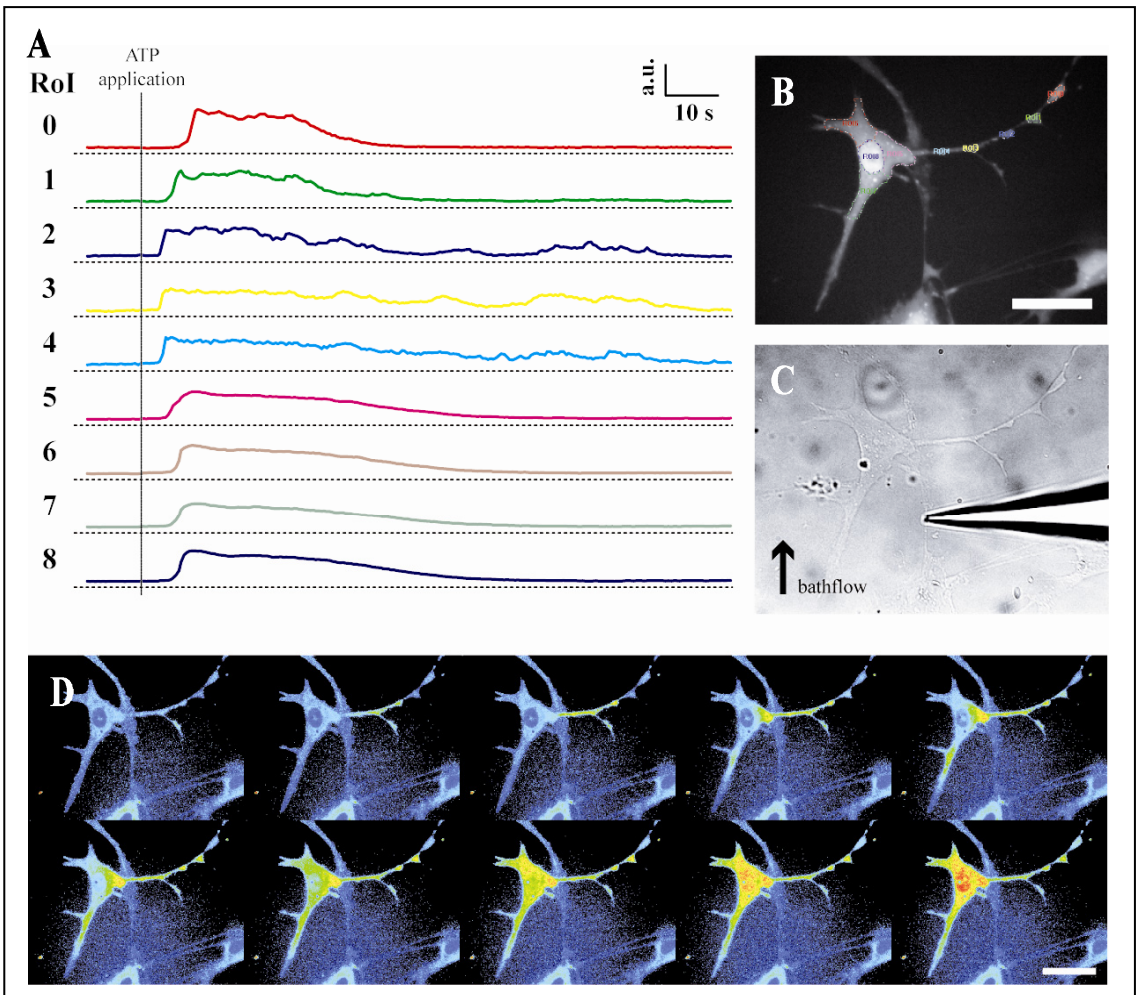

Figure 11: Ca^{2+} response after ATP stimulation.

Analysis of one exemplary USSC (T4) that responded to ATP stimulation with alteration of $[Ca^{2+}]_i$. The traces (**A**) show the occurrence of Ca^{2+} signals in different regions (**B**) of the cell. Signals are spreading from RoI2 in the right process towards the soma after application of 1 mM ATP for 2 s. (B) shows the localization of RoIs for analysis (cells are stained with Fura-2) and (**C**) a transmission image of the stimulated cell. The course of occurring alterations in $[Ca^{2+}]_i$ indicated by the colored image series (**D**; blue = low concentration; red = high concentration). Images were recorded in 0.5 sec. intervals. Bath flow was from the bottom to the top (as indicated).
P: pipette; a.u.: arbitrary units (ratio); Scalebar: 50 µm

3.1.2 Transplantation of USSCs into injured tissue culture slices

Successful integration of USSCs into the tissue is a basic prerequisite before considering treatment of injuries with these stem cells. We therefore tested if USSCs can integrate themselves into the tissue of a rodent model system and survive for 7-14 days. For simulating the injured tissue, organotypic (tissue) slice cultures were prepared

with an incubation time of 10-13 days. After making a cut with a sterile steel blade, USSCs were applied into the lesion and the tissue was postincubated for the intended amount of days. Slices were fixed and cells immunohistochemically stained against human nuclei on day 7, 10 and 14 after application. To make all cells visible, staining with DAPI was also performed (see figure 12).

Cells of human origin were only found in 6 out of 44 tissue slices with a lesion after 7 days of incubation (see figure 12). In slices without an injury USSCs were not detected on any timepoint. Finally, these results allowed no conclusion if USSCs had successfully integrated into the tissue or simply survived 7 DIV.

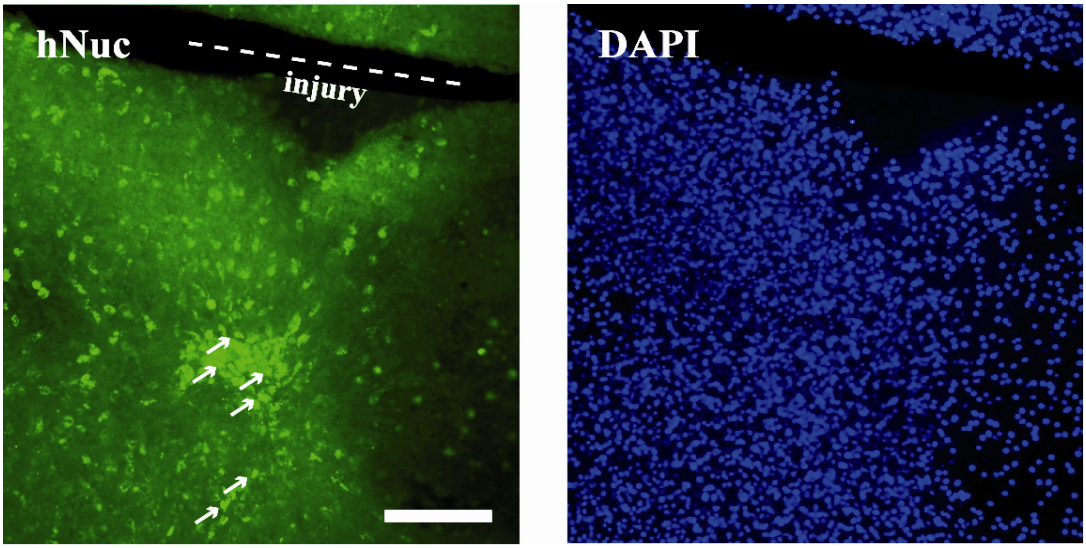

Figure 12: Transplanted USSCs in an organotypic culture slice.

An organotypic slice of mouse was cultured for 13 days before setting a lesion and injecting USSCs near the injury. After 7 more days, USSCs (exemplarily indicated by arrows) were partially detected by staining against human nuclei (hNuc). All cells were additionally stained with 4',6-Diamidino-2-phenylindol (DAPI) to detect all nuclei. (images received from Dr. Jessica Schira)
Scalebar: 100 µm

Taken together, differentiated USSCs showed a variety of morphologies and did not react with an increase in $[Ca^{2+}]_i$ on the application of most of the common substances used for stimulation of neurons. Nonetheless 3 out of 21 cells reacted repeatedly on ATP, showing that these cells are in principle capable of listening to extracellular transmitters. Transplantation experiments exhibited survival of USSCs only in the minority of slices. Yet, the organotypic slice culture is a model system in which such experiments have not been performed before. Experiments have already yielded different results in the CNS of living animals (Schira et al., 2012).

3.2 Identification of astrocytes

3.2.1 Identification of astrocytes via SR101 labeling

Besides mechanical injury, there are several neural pathologies which also result in apoptosis of neurons and might be counteracted by developing replacement strategies for dead neurons. However, analysis of cellular process impairments that arise before apoptosis is important to gain an improved understanding of those pathologies and to find potential points of intervention to avoid neuronal death. Pathologies in the CNS have already been described as gliopathologies before (Nedergaard et al., 2010) because neurons are highly dependant on homeostatic functions of astrocytes. Analysis of astrocytes is therefore obvious, especially in slowly developing pathologies which show hints on homeostasis failure. But for this, the reliable identification of astrocytes is a crucial prerequisite.

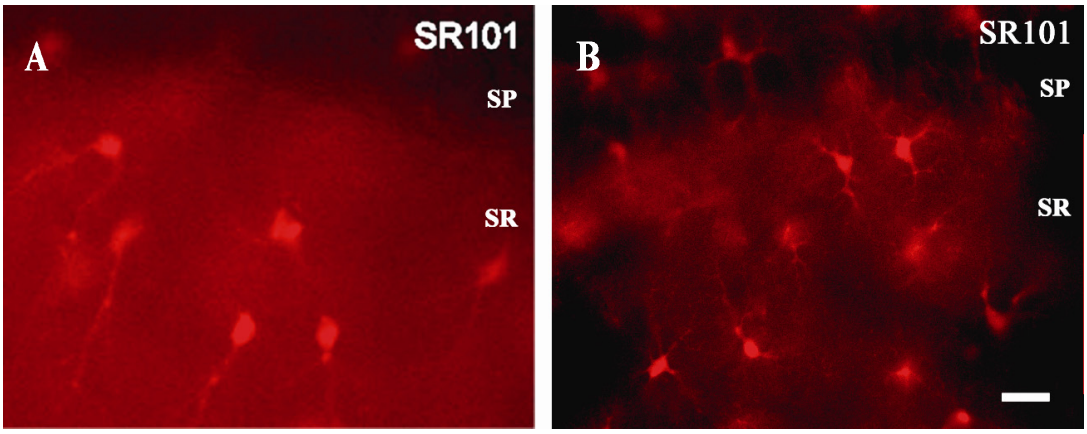

Figure 13: SR101 staining in acute tissue slices.

Comparison of SR101 staining in acute tissue slices of earlier work and staining of acute tissue slices
***A**:* Acute tissue slice stained with SR101 in earlier work (image taken from figure 6 in Kafitz et al., 2008
***B**:* Acute tissue slice stained with SR101 during experiments of this study (Scalebar: 20 µm).

Both images were recorded with a 40x objective on a widefield imaging setup. Staining procedures were identical. (**SP**: *stratum pyramidale*; **SR**: *stratum radiatum*)

Two methods for identification of astrocytes were compared in this work; use of Sulforhodamine 101 (SR101), a red fluorescent dye for staining of living cells, and a pharmacological approach (see chapter 3.2.2). SR101 has been previously described and

validated in detail as a method for specific labeling of astrocytes in living tissue (Nimmerjahn et al., 2004; Kafitz et al., 2008).

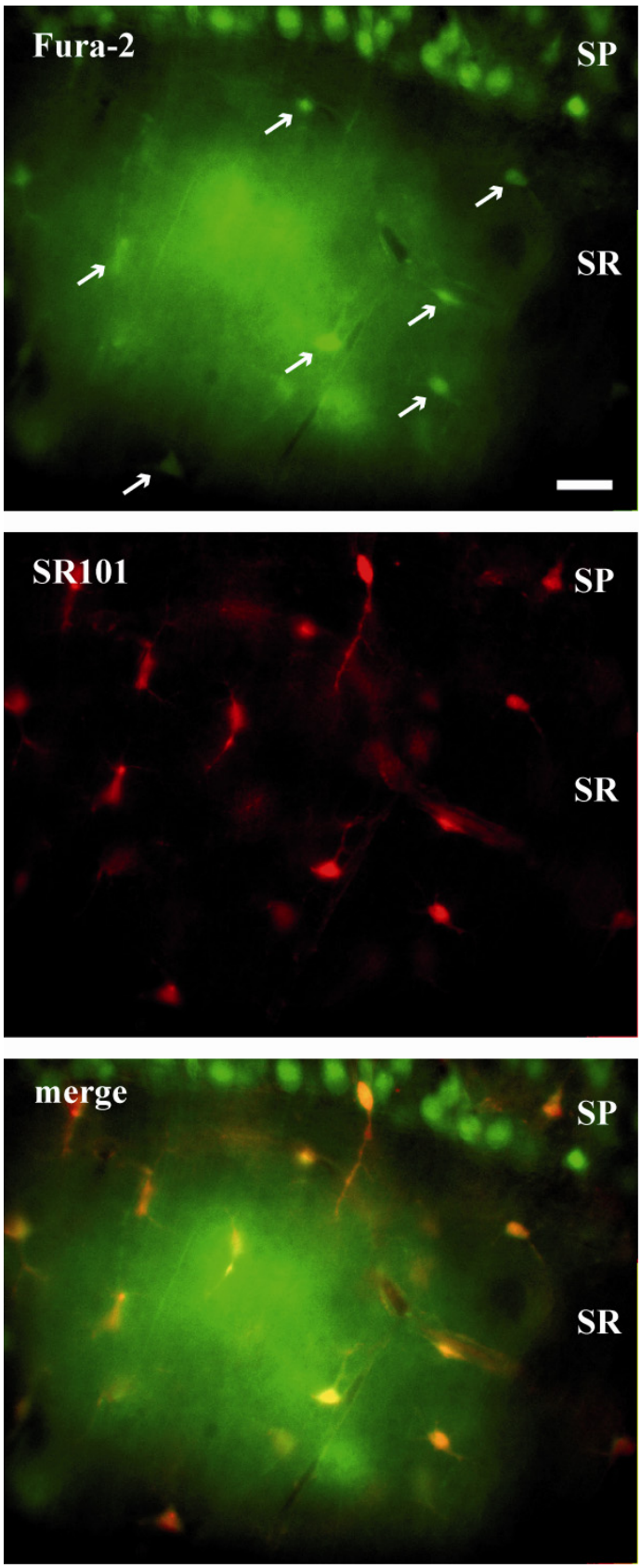

Figure 14: Astrocyte identification via SR101.

Acute tissue slice from a Balb/c mouse, that was stained with SR101 and Fura-2 AM.
Fura-2: Tissue staining with Fura-2 AM under excitation of UV light (380 nm wavelength). Neuronal cell bodies are good visible in the *stratum pyramidale* (**SP**) and scattered in the *stratum radiatum* (**SR**). Fine structures such as processes are hardly distinguishable.
SR101: Tissue staining with SR101 under excitation with light of 575 nm wavelength. Cell bodies are distributed through the tissue but reduced in the *stratum pyramidale*. Finer structures are visible but the apparent amount of processes is far from the actual number.
Merge: Merged image of Fura-2 and SR101 staining showing co-localization of both dyes, identifying astrocytes that can be used for Ca^{2+} imaging (exemplary cells indicated by arrows).
Scalebar: 20 µm

During this work, SR101 showed reliable labeling results, which are in consistence with earlier work mentioned above (see figure 13). Cells that were labeled by SR101 were found throughout the entire slices, but reduced in regions with an increased number of neuronal cell bodies, e.g. *stratum pyramidale*. Morphological appearance was also comparable with former results, as SR101-labeled cells exhibited a small soma and several fine processes. Hence, correlation of SR101 and Fura-2 labeling in regions with presumed presence of astrocytes was taken as an indicator for astrocytes, usable for Ca^{2+} imaging experiments (see figure 14).

3.2.2 Identification of astrocytes by specific Ca^{2+} influx

In 2000, Dallwig et al. discovered that one cell type in CNS tissue showed increase in $[Ca^{2+}]_i$ during perfusion with K^+_{low} ACSF (Dallwig et al., 2000). Analysis identified them as astrocytes and revealed a Ca^{2+} permeability of Kir channels in those cells under these conditions. In order to take advantage of this identification method for astrocytes, acute tissue and cultured tissue slices were exposed to K^+_{low} (0.2 mM K^+) ACSF and blocking experiments were performed as described earlier (Dallwig and Deitmer, 2002). Short perfusion with K^+_{high} (50 mM K^+) ACSF was used for positive controls, because the membrane potential of cells is depolarized for about 60 mV by changing $[K^+]_o$ from 5 to 50 mM, which then activates VGCCs. For better differentiation, experiments were split into 4 recordings. The first and the last recording were controls without any blocking substances. TTX was used in the second recording to block signal conduction via sodium channels of neurons and to ensure that recorded Ca^{2+} signals in astrocytes were not altered by neuronal interference. In the third recording Ba^{2+} was used to additionally block Kir channels as described earlier (Dallwig and Deitmer, 2002). Changes in $[Ca^{2+}]_i$ were measured by recording fluorescence intensities of cells after labeling with Fura-2. Astrocytes were pre-identified by SR101 labeling (Kafitz et al., 2008).

In slices of mice of early postnatal age, namely postnatal day 5, which were expected to express only minor amounts of functional Kir channels (Seifert et al., 2009), perfusion with K^+_{low} ACSF induced a drastic increase in $[Ca^{2+}]_i$ of astrocytes (see figure 15). Signal kinetics and amplitudes of recorded transients were rather variable. Some cells exhibited fast Ca^{2+} spikes whereas others increased and decreased $[Ca^{2+}]_i$

more slowly. Although TTX reduced some Ca^{2+} spikes, only Ba^{2+} was able to suppress nearly all Ca^{2+} signals evoked by K^{+}_{low} ACSF. Washing for 20 minutes proved sufficient for removal of Ba^{2+} from most of the Kir channels and partially restored Ca^{2+} signals during K^{+}_{low} ACSF perfusion. However, heterogeneity of Ca^{2+} signals' kinetics and amplitudes remained. In most cases, recorded signals were different compared with those of the first recording (see figure 15).

Compared to astrocytes, neurons were not found to show similar effects in earlier studies (Dallwig and Deitmer, 2002). In accordance with that, K^{+}_{low} ACSF did not induce Ca^{2+} transients in cells that were not labeled by SR101, i.e. neurons (see figure 16). Perfusion with K^{+}_{high} ACSF as positive control provoked Ca^{2+} responses in both, astrocytes and neurons. Astrocytes exhibited Ca^{2+} transients with a single peak, which was diminished but not vanished by TTX. After 20 minutes of washing, signal amplitude was restored. Neurons in contrast showed two peaks. They were reduced to one by TTX, but the amplitude was not altered. As in astrocytes, this effect was reversible by 20 minutes of washing. Ba^{2+} had no influence on any Ca^{2+} signal induced by K^{+}_{high} ACSF.

In astrocytes of P20 mice, which were expected to possess fully functional Kir channels (Seifert et al., 2009), perfusion with K^{+}_{low} ACSF also induced an increase of $[Ca^{2+}]_i$. Ca^{2+} signals were rather variable in amplitude as well, but Ca^{2+} spikes, as seen in P5 astrocytes, were not observed. Amplitudes were smaller in average though and in some recordings, $[Ca^{2+}]_i$ of astrocytes was not altered. Blocking of Kir channels by use of Ba^{2+} was rather variable as well. In some slices $[Ca^{2+}]_i$ increase in astrocytes was fully blocked during K^{+}_{low} perfusion whereas in others a partial block was observed. However, blocking effects of Ba^{2+} were removable in astrocytes that had shown a partial block. In cells which exhibited a full block of Kir channels, Ca^{2+} signaling was not restored within 20 minutes of washing (see figure 17).

Neurons were not affected by perfusion with K^{+}_{low} ACSF, similar to findings in P5 mice (see figure 18). Perfusion with K^{+}_{high} ACSF also provoked Ca^{2+} response in astrocytes and neurons of P20 animals. In both cell types Ca^{2+} signals showed one peak and were reduced during blocking with TTX. This is different to results of P5 neurons, where TTX did not alter neuronal response. In addition, 20 minutes of washing was insufficient for both cell types to return to signaling kinetics from the first recording. Again, Ba^{2+} had no influence on any Ca^{2+} signal induced by K^{+}_{high} ACSF.

In organotypic culture slices (11-20 DIV) astrocytes showed Ca^{2+} signaling similar to those of astrocytes in P5 acute tissue slices during K^{+}_{low} ACSF perfusion. But response to K^{+}_{high} ACSF perfusion was missing (data not shown) and neurons were hardly detectable because of difficulties with the Fura-2 loading (see also chapter 3.3.1). Therefore blocking attempts were not performed and identification of astrocytes via Ca^{2+} response to K^{+}_{low} ACSF was postponed.

Taken together, identification of astrocytes by detection of Ca^{2+} influx through Kir channels was found to be useful for acute tissue slices in this study. Astrocytes showed rather variable signaling but neurons lacked a response, allowing a clear distinction. Signaling of astrocytes which should not have expressed functional Kir channels yet and missing restorability of signals after use of blockers in slices of older animals, lowered usability of this method though. Additionally, use of ACSF with varying K^{+} concentration for identification might have induced unnecessary stress to cells in later experiments dealing with oxidative stress. For this, labeling with SR101 has proven well. SR101 showed a reliable labeling quality in consistence with earlier findings, where it labeled probably all astrocytes in the slice (Kafitz et al., 2008). In combination with Fura-2 specific selection of astrocytes or neurons was possible in Ca^{2+} imaging experiments without the risk of side effects.

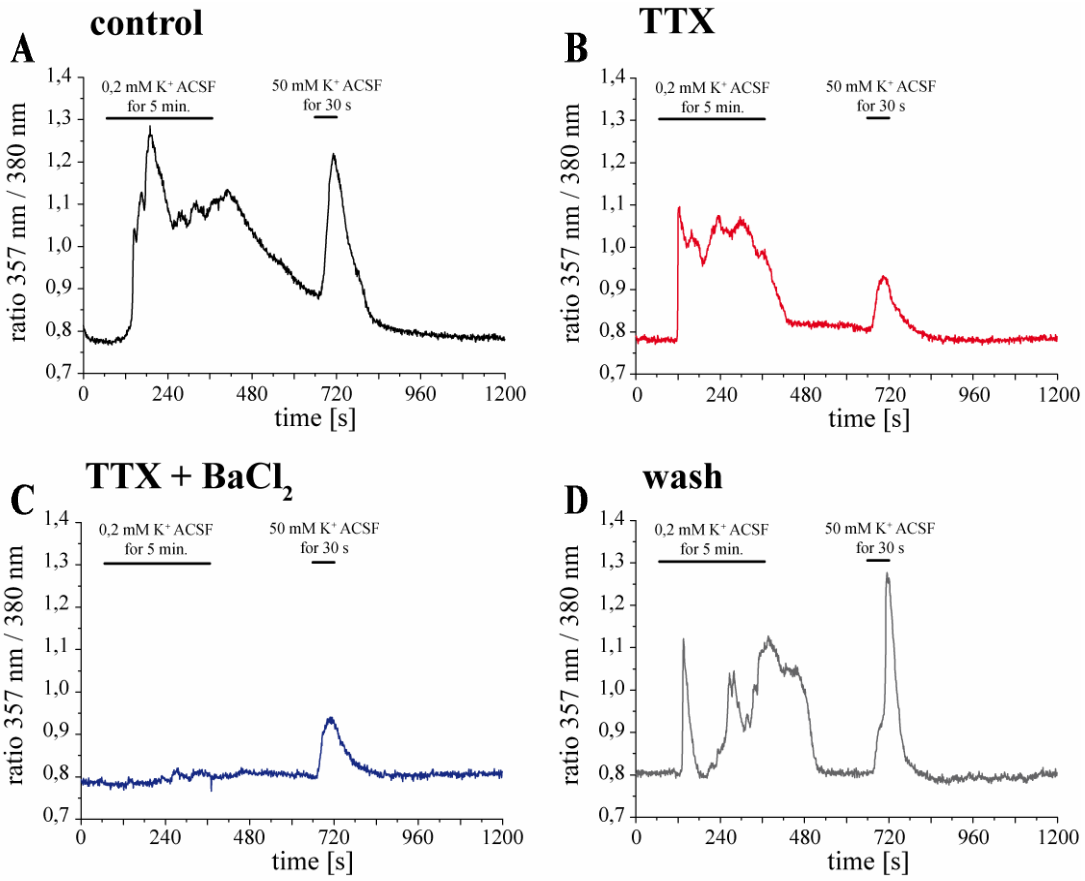

Figure 15: Ca^{2+} signals in astrocytes of a P5 acute tissue slice.

Ca^{2+} signals of all measured astrocytes from one slice were averaged and plotted exemplarily. In A-D the same cells were analyzed. Analysis showed the occurrence of Ca^{2+} signals during perfusion with K_{low} ACSF, which could be blocked with $BaCl_2$. Washing for 20 minutes was sufficient to remove the block.

***A**:* Control measurement with 0.2 mM and 50 mM K^+ ACSF without blockers.
***B**:* Measurement with 0.2 mM and 50 mM K^+ ACSF under the influences of 500 nM TTX.
***C**:* Measurement with 0.2 mM and 50 mM K^+ ACSF under the influence of 500 nM TTX and 100 µM $BaCl_2$.
***D**:* Control measurement with 0.2 mM and 50 mM K^+ ACSF without blockers after 20 minutes of washing.

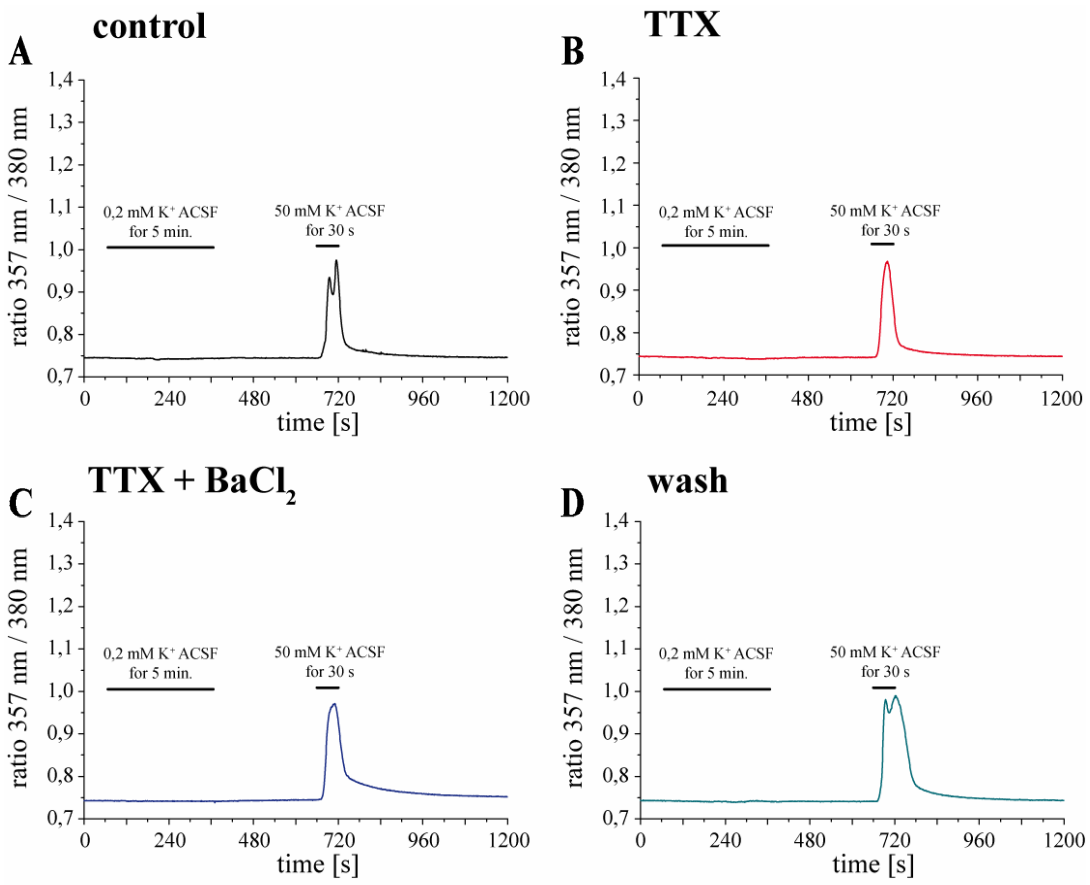

Figure 16: Ca^{2+} signal in neurons of a P5 acute tissue slice.

Ca^{2+} signals of all measured neurons from one slice were averaged and plotted exemplarily. In A-D the same cells were analyzed. Analysis did not show the occurrence of Ca^{2+} signals during perfusion with K_{low} ACSF.

***A**:* Control measurement with 0.2 mM and 50 mM K^+ ACSF without blockers.
***B**:* Measurement with 0.2 mM and 50 mM K^+ ACSF under the influences of 500 nM TTX.
***C**:* Measurement with 0.2 mM and 50 mM K^+ ACSF under the influence of 500 nM TTX and 100 µM $BaCl_2$.
***D**:* Control measurement with 0.2 mM and 50 mM K^+ ACSF without blockers after 20 minutes of washing.

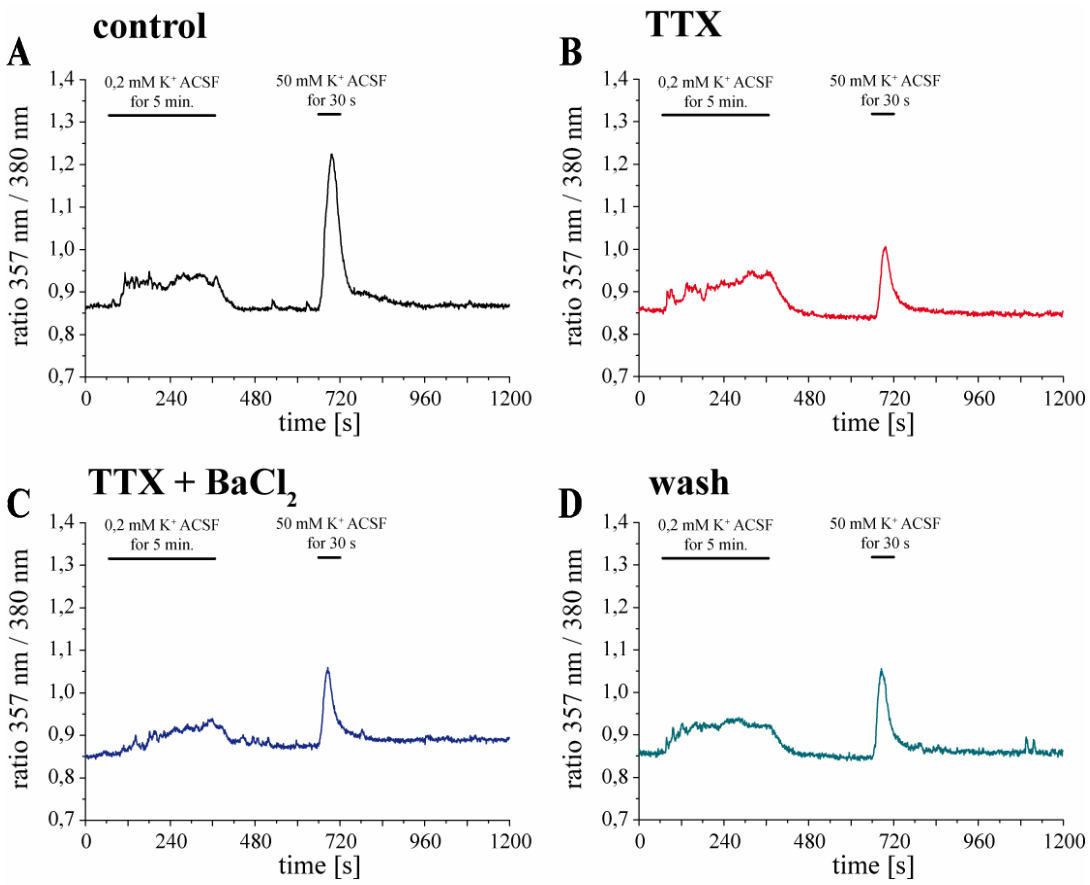

Figure 17: Ca^{2+} signal in astrocytes of a P20 acute tissue slice.

Ca^{2+} signals of all measured astrocytes from one slice were averaged and plotted exemplarily. In A-D the same cells were analyzed. Analysis showed the occurrence of small Ca^{2+} signals during perfusion with K_{low} ACSF, which could partially be blocked with $BaCl_2$. Washing for 20 minutes was only sufficient to remove the block in cells, which showed a partial block.

***A**:* Control measurement with 0.2 mM and 50 mM K^+ ACSF without blockers.
***B**:* Measurement with 0.2 mM and 50 mM K^+ ACSF under the influences of 500 nM TTX.
***C**:* Measurement with 0.2 mM and 50 mM K^+ ACSF under the influence of 500 nM TTX and 100 µM $BaCl_2$.
***D**:* Control measurement with 0.2 mM and 50 mM K^+ ACSF without blockers after 20 minutes of washing.

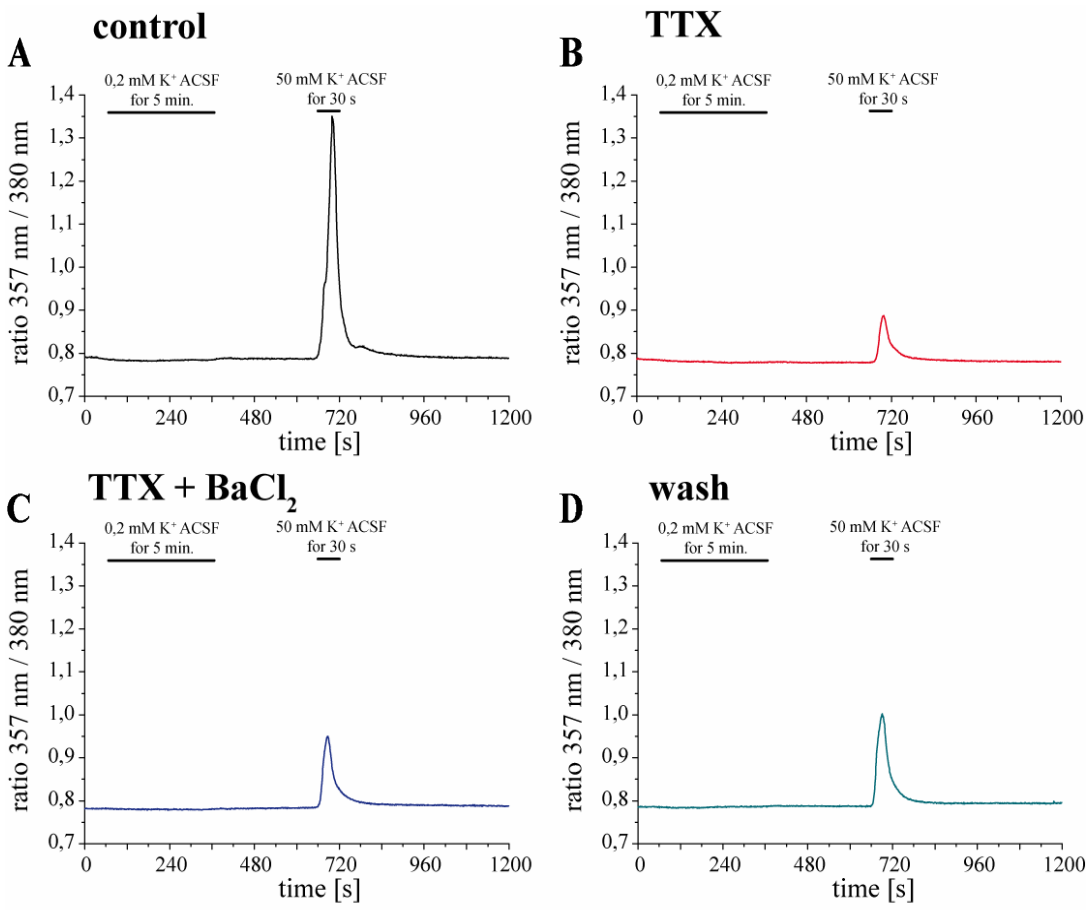

Figure 18: Ca^{2+} signal in neurons of a P20 acute tissue slice.

Ca^{2+} signals of all measured neurons from one slice were averaged and plotted exemplarily. In A-D the same cells were analyzed. Analysis did not show the occurrence of Ca^{2+} signals during perfusion with K_{low} ACSF. Ca^{2+} signaling during K_{high} perfusion was drastically decreased during use of TTX. Blocking effects were not fully removed after 20 minutes of washing.

***A**:* Control measurement with 0.2 mM and 50 mM K^+ ACSF without blockers.
***B**:* Measurement with 0.2 mM and 50 mM K^+ ACSF under the influences of 500 nM TTX.
***C**:* Measurement with 0.2 mM and 50 mM K^+ ACSF under the influence of 500 nM TTX and 100 µM $BaCl_2$.
***D**:* Control measurement with 0.2 mM and 50 mM K^+ ACSF without blockers after 20 minutes of washing.

3.3 Acute oxidative stress in organotypic slice culture

In earlier work, organotypic (tissue) slice cultures have been found to represent a useful model system for observation of injury in the CNS over several days (Kehl, 2007). Therefore it was considered to be used to analyze the effects of long-term oxidative stress in this study, which requires interference with the redox system for several days, as well. Organotypic slice cultures flatten down to a thickness of 30-50 µm within 10 days which makes them ideal for experiments in which the thickness of acute slices might cause difficulties, e.g. immunohistochemical staining. And additionally, the tissue's structure is preserved during the process of flattening (see figure 24).

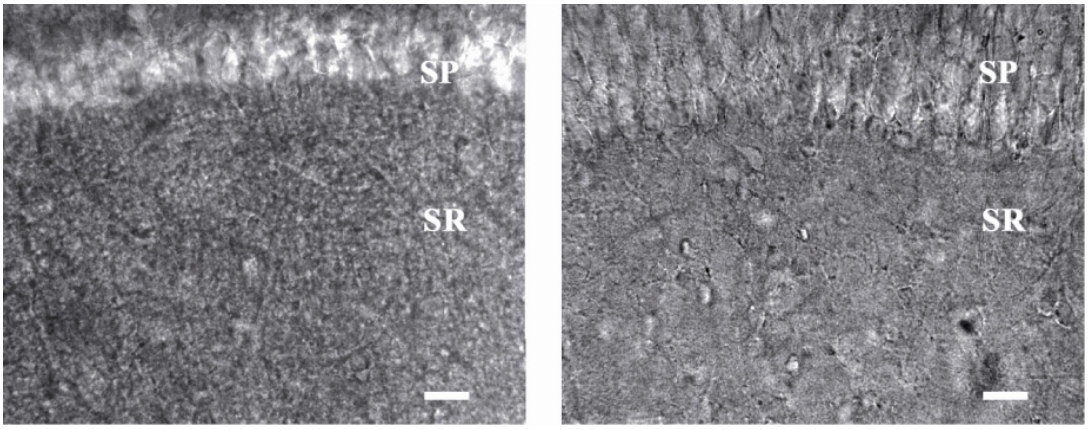

Figure 19: Transmission image of an organotypic culture slice.

Tissue structure of the hippocampus is preserved in organotypic culture slices, even after several weeks in culture. This makes the model system ideal for pharmacological interference over several days and allows experiments where tissue thickness might cause difficulties, e.g. immunohisto-chemical staining.
The image shows a part of the CA1 region in culture slices 17 DIV.
SP: *stratum pyramidale;* ***SR:*** *stratum radiatum;* scalebar: 20 µm

For labeling with Fura-2, different procedures were tested in culture to establish a culture pendant to labeling of acute slices, which was a prerequisite for analysis of long-term treatment effects of H_2O_2. Staining of organotypic slice cultures via bathloading allowed distinct differentiation between astrocytes and neurons (see figure 25 and figure 26). Processes of astrocytes were even better visible than in acute tissue slices after replacing the detergent pluronic acid with Brij-35. Additionally, the tissue was equally stained. Bolus injection, which was finally used to analyze dose-response behavior, allowed differentiation as well but with decreased image quality (see figure 27).

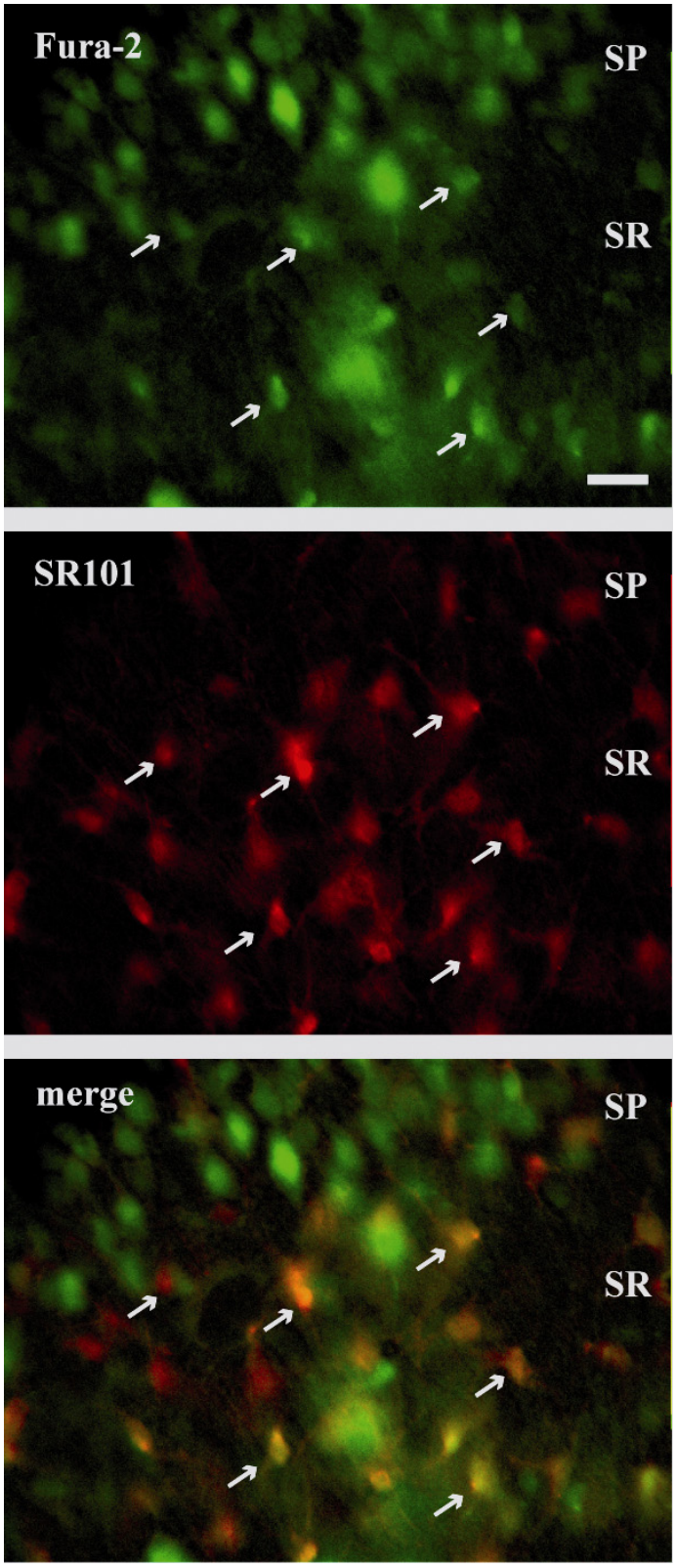

Figure 20: Fura-2 staining in organotypic slice cultures via bathloading (pluronic).

Images are showing the working area within the CA1 region of hippocampus. *Stratum pyramidale* (SP) and *stratum radiatum* (SR) can be distinguished by their staining with Fura-2 AM and SR101. Fura-2 binds calcium and allows detection of living cells whereas SR101 specifically labels astrocytes. Cells that were positive for both signals (merge) were used for measurements (indicated by arrows).
For staining of cells in this slice with Fura-2, bathloading technique was used with pluronic acid as detergent. SR101 staining was performed via bathloading as well.
(organotypic slice culture from a Balb/c mouse, 19 DIV; scalebar: 20 µm)

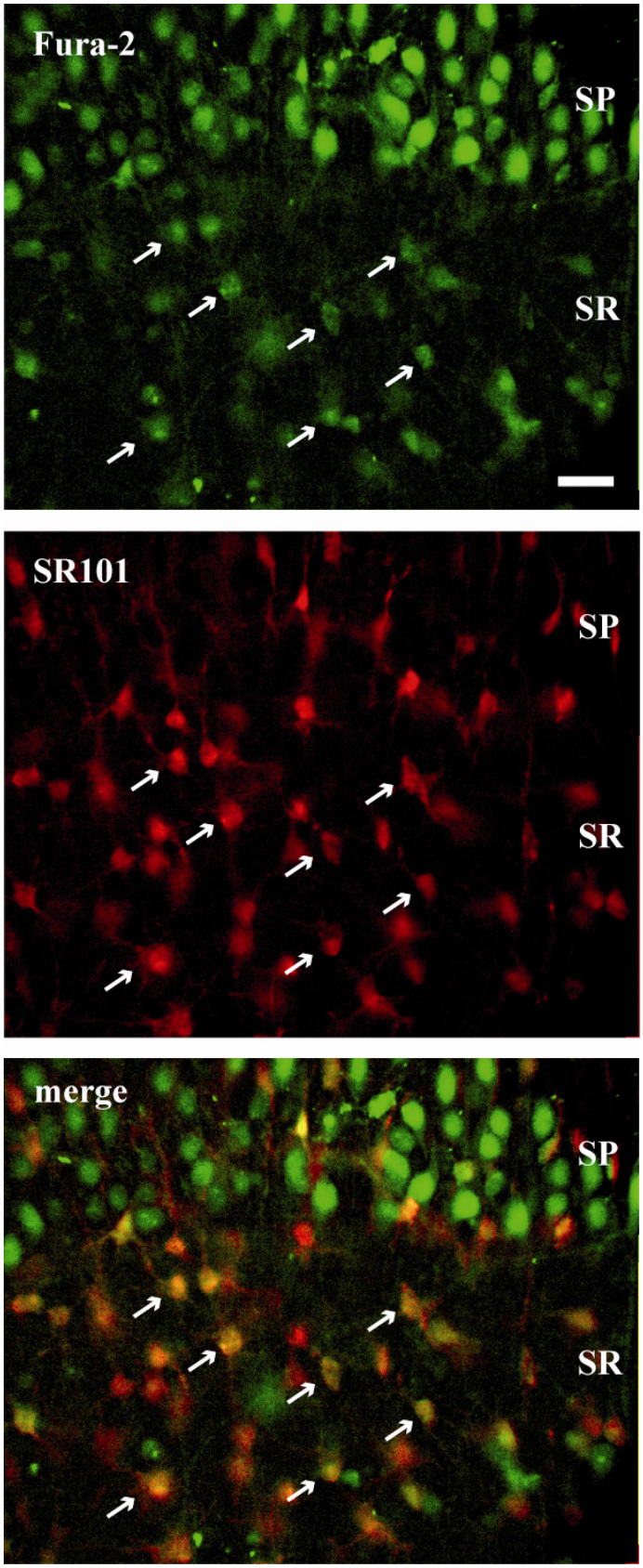

Figure 21: Fura-2 staining in organotypic slice cultures via bathloading (Brij-35).

Images are showing the working area within the CA1 region of hippocampus. *Stratum pyramidale* (SP) and *stratum radiatum* (SR) can be distinguished by their staining with Fura-2 AM and SR101. Fura-2 binds calcium and allows detection of living cells whereas SR101 specifically labels astrocytes. Cells that were positive for both signals (merge) were used for measurements (indicated by arrows).
For staining of cells in this slice with Fura-2, bathloading technique was used with Brij-35 as detergent. SR101 staining was performed via bathloading as well.
(organotypic slice culture from a Balb/c mouse, 17 DIV; scalebar: 20 µm)

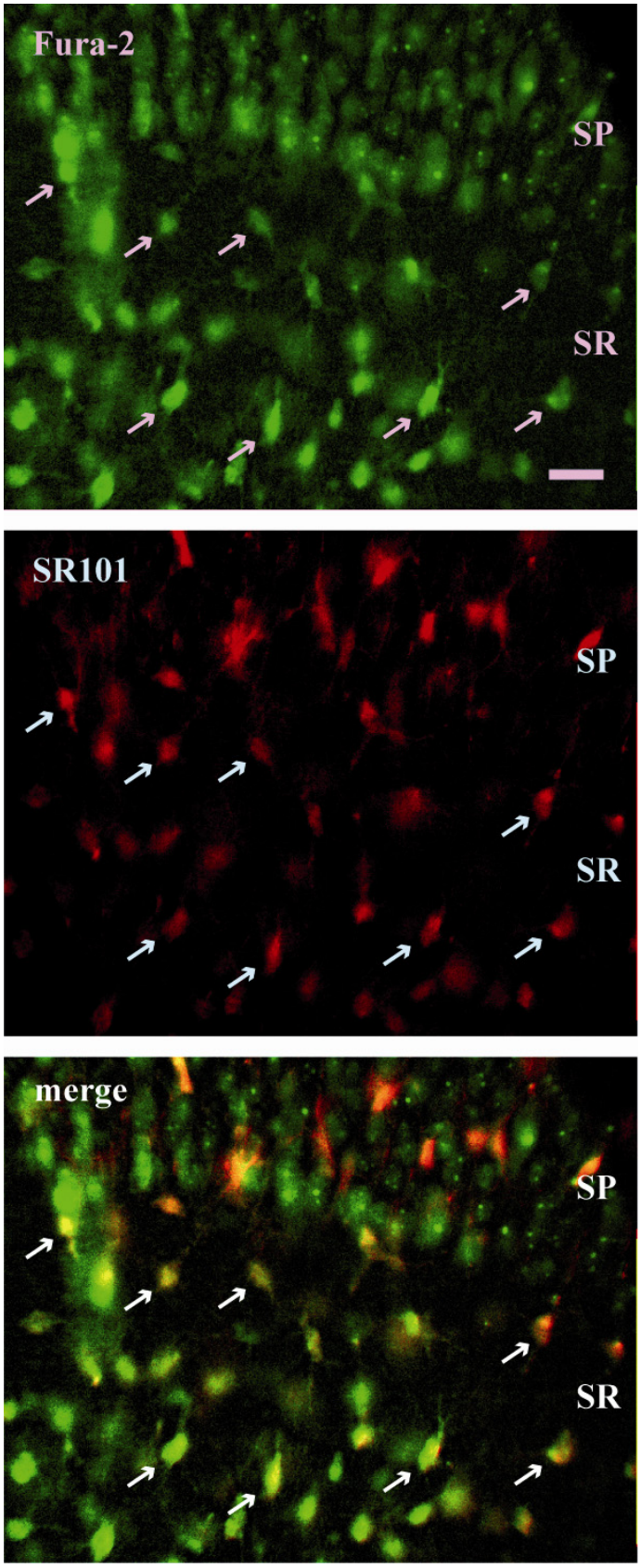

Figure 22: Fura-2 staining in organotypic slice cultures via bolus injection.

Images are showing the working area within the CA1 region of hippocampus. *Stratum pyramidale* (SP) and *stratum radiatum* (SR) can be distinguished by their staining with Fura-2 AM and SR101. Fura-2 binds calcium and allows detection of living cells whereas SR101 specifically labels astrocytes. Cells that were positive for both signals (merge) were used for measurements (indicated by arrows).
For staining of this slice with Fura-2, bolus injection was used. In contrast to bathloading, neurons showed an inferior staining quality and partly exhibited dye uptake in vesicles (see bright spots of Fura-2 in cells of the *stratum pyramidale*. SR101 staining was performed via bathloading. (organotypic slice culture from a Balb/c mouse, 11 DIV; scalebar: 20 µm)

3.3.1 Switch from bathloading to Bolus staining

At the beginning of dose-response experiments in organotypic cultures, slices were stained with Fura-2 AM via bathloading in the incubator. As a derivation from staining solutions used for Bolus staining, Fura-2 AM was also dissolved in DMSO and 20 % of pluronic acid, which is a common technique to facilitate the staining process. Organotypic cultures stained this way showed cellular degradation in the *stratum pyramidale*, in most cases. In slices, in which neuronal loss did not occur, staining results were comparable with those of acute tissue after Bolus staining (see figure 25). Neurons and astrocytes were discriminable in combination with SR101 labeling. In an attempt to prevent cellular degradation and side-effects originating from this damage, pluronic acid was replaced with another non-ionic detergent. The detergent Brij-35 was found to be usable in lower concentrations (10 %) and resulted in improved staining quality (see figure 26) without cellular degradation in even one slice. Co-labeling with SR101 was comparable with earlier staining procedures.

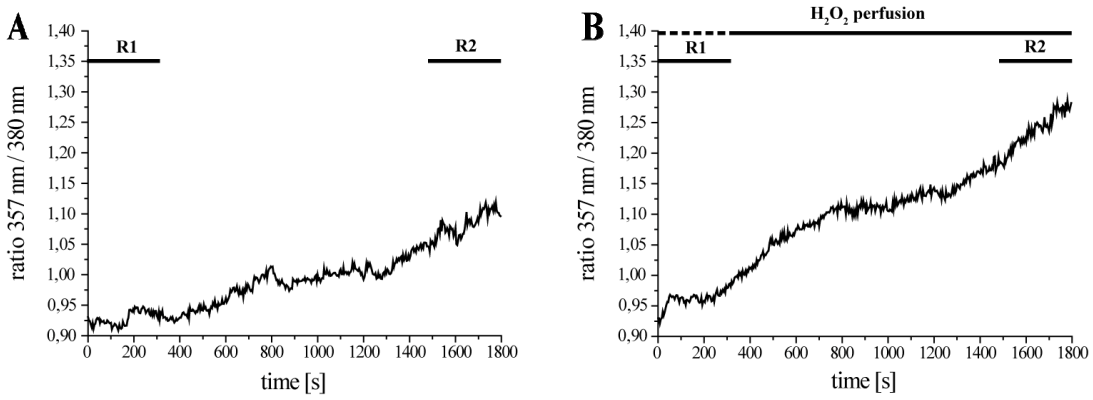

Figure 23: Ca^{2+} baseline increase after Fura-2 bathloading.

Recording of one astrocyte in organotypic slice culture for 30 minutes during control (**A**) and subsequent 100 µM H_2O_2 treatment (**B**). For analysis, mean baseline ratio values (R1) were compared with mean ratio values of the last five minutes (R2) to assess increase in Ca^{2+}. Perfusion of H_2O_2 took five minutes to reach the bath (dashed line), therefore the first five minutes were used to determine the baseline level.

During Ca^{2+} recordings, occurrence of an increase in $[Ca^{2+}]_i$ was found, even when the slices were not treated with H_2O_2, indicating difficulties with the use of Brij-35 under these conditions as well. Explicit analysis of this issue was performed by a 30 minute recording without exchange of the perfusion solution and another recording with H_2O_2 perfusion, beginning 5 minutes after start of the recording. Again, an “increase” of

$[Ca^{2+}]_i$ was detected in the control measurement, which was much smaller as in the recording with H_2O_2, but yet present (see figure 28).

In the end, attempts to preserve bathloading by reduction of Brij-35 and pluronic acid concentrations, or varying incubation intervals were not successful. Fura-2 bathloading without any detergents was tested as well with staining results similar to those shown in figure 26. However, neurons lacked necessary uptake of Fura-2. Therefore dose-response experiments were performed after Fura-2 was applied into the tissue via pressure injection (Bolus staining), as it was performed in acute tissue experiments.

3.3.2 Dose-response experiments with H_2O_2

Dose-response measurements in organotypic slice cultures were performed identically to those of acute tissue slices, but H_2O_2 concentrations were different (see also chapter 3.4.2). In astrocytes, a concentration of 0.1 mM H_2O_2 in the ACSF used for perfusion was already sufficient to reach $\Delta F/F$ values of $[Ca^{2+}]_i$ that were comparable with about 1.3 mM in acute slices. Consequently, the H_2O_2 concentration necessary for maximum peak amplitude of $[Ca^{2+}]_i$ in astrocytes was also much lower in organotypic slice cultures (see figure 29). Additionally, increase in $[Ca^{2+}]_i$ turned into a significant decrease (statistics not shown) when slices were treated with 75 µM H_2O_2, compared to treatment with 50 µM. To ensure that measurements were not based on an occasional incident, the number of analyzed astrocytes was increased from 66 to 118, but that did not yield any other results (see figure 29). For fitting, neither linear nor sigmoid fitting was found to be usable for dose-response curves of organotypic slice cultures. Analysis of neurons could not be performed, because staining was too weak in the majority of cells in the *stratum pyramidale*. In those neurons, which were stained, Fura-2 was also taken up in vesicles (see figure 27). As a consequence of both, live cell experiments with H_2O_2 were stopped in organotypic slice cultures (see also chapter 4.3.2).

In summary, bathloading techniques were able to stain the tissue, allowing differentiation between astrocytes and neurons, but held difficulties for proper analysis of received data from Ca^{2+} imaging experiments. Use of Bolus staining, as in acute tissue slices, showed also challenges that have to be resolved first. An H_2O_2

concentration and treatment time for induction of oxidative stress in organotypic slice culture was not derived from theses dose-response experiments. Therefore Ca^{2+} imaging experiments in organotypic slice cultures were stopped and revisited in acute tissue slices.

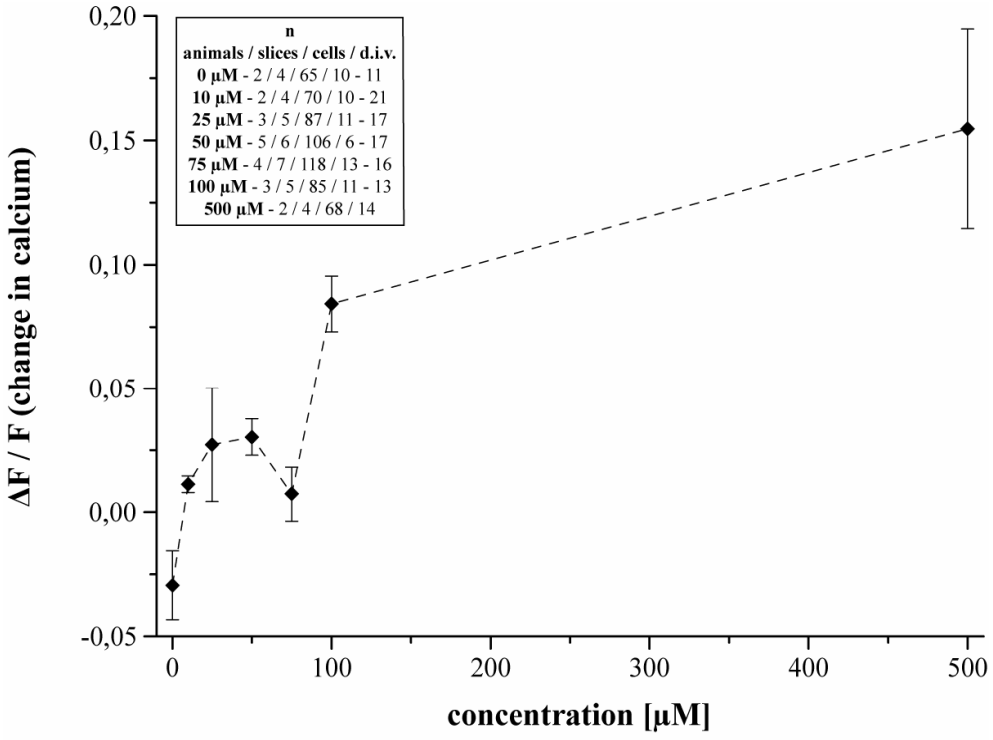

Figure 24: Dose-Response curve of H_2O_2 treatment in organotypic slices.

Astrocytes of organotypic slice cultures showed beginning of maximum peak amplitude of intracellular Ca^{2+} increase after treatment with 100 µM H_2O_2 for 10 minutes. In contrast to dose-response curves of acute tissue slices, control recordings showed negative ΔF/F calculations and treatment with 75 µM resulted in calculations that were significantly lower than those of 50 µM treatment. No fitting with an adequate R^2 was found. All values are given as means ± S.E.M.

3.4 Acute oxidative stress in acute tissue slices

This work primarily dealt with effects of oxidative stress on CNS tissue. Therefore, H_2O_2 exposure was used and effects on intracellular Ca^{2+} and metabotropic glutamate receptor activation were analyzed via fluorescence imaging. Before acute treatment experiments were started, proper H_2O_2 concentrations had to be determined first that would induce oxidative stress but not cell death.

3.4.1 Basic calibration of Fura-2 signals

For estimating the changes in $[Ca^{2+}]_i$ of cells in experiments, which dealt with H_2O_2 as well as metabotropic receptor activation, a basic calibration of Fura-2 signals was performed. This calibration was based on determining the minimum and maximum ratio values for recordings with Fura-2 in the employed imaging setup. First, intracellular Ca^{2+} stores of cells in the slice were cleared by CPA and membranes were perforated by use of the ionophore ionomycine. Afterwards, slices were perfused with ACSF containing 0 mM Ca^{2+} to receive the R_{min} value. R_{max} was then determined by perfusion with 10 mM Ca^{2+} ACSF.

Because similar results were found in parallel work of the institute, only recordings from one tissue slice were used for the calculation. Three astrocytes were analyzed and results averaged because of the nonuniform illumination. The results are listed in table 1. After inserting the received values into the standard calibrating equation (see chapter 2.4.6), the following equation was used for calculating the amount of alteration in $[Ca^{2+}]_i$ during experiments:

$$\left[Ca^{2+}\right] = 224\,nM \times \left(\frac{R - 0{,}81}{2{,}95 - R}\right) \times \left(\frac{568{,}45}{38{,}49}\right)$$

Or in a reduced form:

$$\left[Ca^{2+}\right] = 3307{,}92 \times \left(\frac{R - 0{,}81}{2{,}95 - R}\right) nM$$

	cell 1	cell 2	cell 3	mean
R_{min}	0,825	0,795	0,794	0,805
R_{max}	2,664	3,011	3,163	2,946
$F2_{low}$	681,807	325,549	698,002	568,453
$F2_{high}$	69,136	11,031	35,314	38,493

Table 1: Data for the Ca^{2+} calibration equation.

Recorded and calculated ratio values from calibration experiments are listed, as well as the averaged values that were inserted into the standard calibration equation. All values are backgroundcorrected and were determined in the same slice. Variations between the cells might originate from effective differences in $[Ca^{2+}]_i$, but reflect also the nonuniform illumination of the slice.

As already mentioned in the material & methods section, such a calibration can only give a rough estimation of the effective $[Ca^{2+}]_i$. Nonetheless, a basic calibration with the corresponding calculation was performed to gain an idea of the alterations in $[Ca^{2+}]_i$ concentrations and to see if concentrations do not drop out of the physiological range. Baseline levels of $[Ca^{2+}]_i$ were found to be below than 200 nM in controls (~100 nM in mGluR activation experiments), which is in accordance with Verkhratsky et al. (1998). But because this calibration only gives an estimation on the $[Ca^{2+}]_i$, concentrations in this work are noted exemplarily and graphs displaying alterations in $[Ca^{2+}]_i$ are shown as background corrected ratio values or amplitudes in relation to a baseline ($\Delta F/F$).

3.4.2 Dose-response experiments with H_2O_2

Dose-response experiments in acute tissue slices were performed as 60 minute recordings with 10 minute perfusion of ACSF containing defined H_2O_2 concentrations. In these measurements astrocytes showed an almost linear relation between H_2O_2 concentration in ACSF perfusion and increase in $[Ca^{2+}]_i$, calculated as $\Delta F/F$. Calculations resulted in $\Delta F/F$ values of 0.012 ± 0.015 for controls ($n = 40$), 0.023 ± 0.016 for 0.1 mM ($n = 32$), 0.038 ± 0.029 for 0.5 mM ($n = 36$), 0.069 ± 0.03 for 1 mM ($n = 33$) and 0.055 ± 0.018 for 2 mM H_2O_2 ($n = 28$). A maximum peak amplitude of $[Ca^{2+}]_i$ in astrocytes was not detected within the analyzed range of H_2O_2 concentrations. Calculations based on the basic calibration of Fura-2 (see chapter 3.4.1) resulted in approximately $[Ca^{2+}]_i$ alterarions of ~15 nM for controls, ~30 nM for

0.1 mM, ~50 nM for 0.5 mM, ~ 85 nM for 1 mM and ~175 nM for 2 mM H_2O_2 in astrocytes. Neurons in contrast showed an earlier rise in ΔF/F values with 0.013 ± 0.024 for controls (n = 34), 0.042 ± 0.021 for 0.1 mM (n = 23), 0.165 ± 0.068 for 0.5 mM (n = 28), 0.343 ± 0.117 for 1 mM (n = 25) and 0.427 ± 0.075 for 2 mM H_2O_2 (n = 22). $[Ca^{2+}]_i$ alterations showed an almost linear relation to H_2O_2 concentrations up to 1 mM which had a higher slope than that of astrocytes. After this concentration slope was reduced and $[Ca^{2+}]_i$ approached maximum peak amplitude. Hence, fitting curves were different (see figure 19). Calculations based on the basic calibration of Fura-2 (see chapter 3.4.1) resulted in approximately $[Ca^{2+}]_i$ alterarions of ~20 nM for controls, ~65 nM for 0.1 mM, ~355 nM for 0.5 mM, ~ 550 nM for 1 mM and ~795 nM for 2 mM H_2O_2 in neurons. For the concentrations used, astrocytes were fitted best with a linear model (a = 0.01288; b = 5.69365*10^{-5}):

$$y = a + b \times x$$

Neurons could be fitted with either an exponential or a sigmoid model. Because the dose-response curve did not show linearity when x-axis was scaled logarithmically (not shown) and presence of antioxidants in neurons was taken into consideration (details see chapter 4.3.1), a sigmoid type was chosen (A1 = -0.04395; A2 = 0.43075; $LOGx_0$ = 566.4945; p = 0.00147):

$$y = \left(\frac{A2 - A1}{1 + 10^{(\log x0 - x) \times p}} \right)$$

An R^2 value of 0.999 additionally supported this fitting. Furthermore, in astrocytes as well as in neurons ΔF/F calculations indicated a slight increase in $[Ca^{2+}]_i$ even in the controls. Because similar changes were detected in both cell types and changes were minimal, this findings were not taken into account further (see also chapter 4.3.2).

Recover of $[Ca^{2+}]_i$ levels during dose-response experiments was not analyzed in detail. Yet, observation of recorded traces showed full recovery to baseline levels in almost all cells (astrocytes: ~90 %; neurons: ~85 %) after 10 minute treatment with 0.1 mM and most astrocytes (75 %) after 0.5 mM. Neurons instead showed decrease in $[Ca^{2+}]_i$, but most cells did not completely recover to baseline levels (~65 %). This was also the case after perfusion with 1 mM (~70 %) but astrocytes exhibited incomplete

recovery as well (~80 %). After perfusion with 2 mM H_2O_2 at least half of all cells did not even show a decrease of $[Ca^{2+}]_i$ (astrocytes: 50 %; neurons: ~60 %).

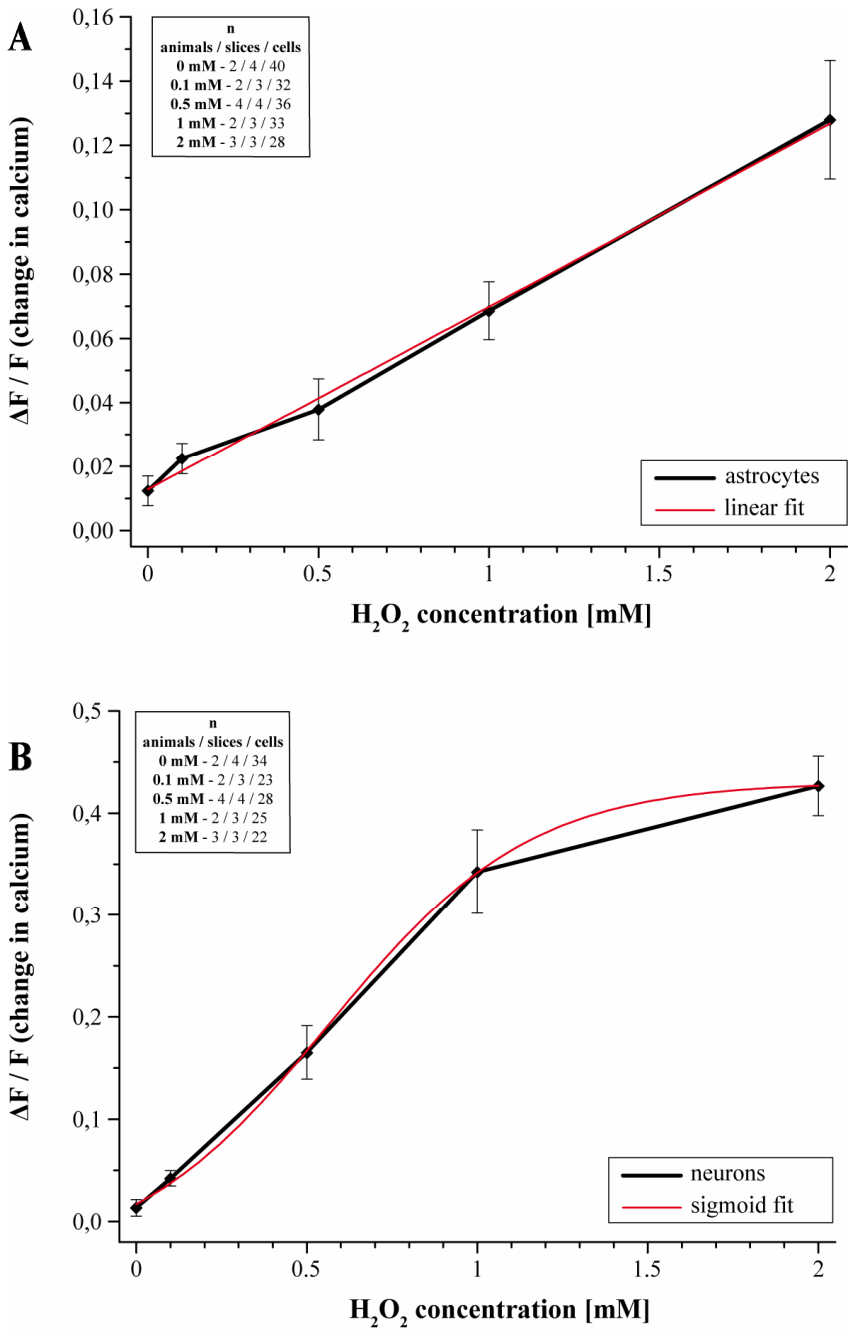

Figure 25: Dose-Response curves of H_2O_2 treatment in acute tissue slices.

Increase of $[Ca^{2+}]_i$ after 10 minutes of H_2O_2 treatment differs between astrocytes and neurons. In astrocytes $[Ca^{2+}]_i$ rises with a linear slope (R^2=0.99) in dependence of the concentrations used (**A**). Maximum peak amplitude was not reached within 2 mM. In contrast, neurons showed approach to maximum peak amplitude at concentrations of 1 mM H_2O_2 already (**B**). A sigmoid trace, having a R^2 of more than 0.99, gives an adequate fit. All values are given as means ± S.E.M.

In these dose-response experiments neurons were shown to be less tolerant to oxidative stress than astrocytes. In contrast to neurons, increase of $[Ca^{2+}]_i$ in astrocytes was much smaller and maintained a linear slope up to the highest H_2O_2 concentration used for dose-response experiments. Neurons showed a nearly linear increase up to a concentration of 1 mM H_2O_2 for 10 minutes, followed by a reduction of increase in $[Ca^{2+}]_i$ instead. As a consequence for further experiments, induction of oxidative stress had to result in less increase in intracellular Ca^{2+} of neurons than 1 mM H_2O_2 did in 10 minutes (~550 nM). This was because the reduced increase in $[Ca^{2+}]_i$ from this point on indicated that cellular mechanisms for compensation had reached their limit and neurons might experience detrimental effects, e.g. induction of apoptosis. Assuming a linear dependancy between alteration in $[Ca^{2+}]_i$ and treatment time (see also chapter 4.3.1), a treatment with 200 µM H_2O_2 for 45 minutes before the experiments was derived from dose-response experiments. Experiments with mGluR activation confirmed this treatment to be sufficient for the induction of oxidative stress (see chapter 3.4.3).

3.4.3 Metabotropic glutamate receptor activation

For analysis of effects on metabotropic signaling during acute oxidative stress, the mGluR agonist DHPG was applied three times in a 5 minute recording. Each application lasted 200 ms, with a one minute interval between each application. Recordings on acute tissue slices were performed under three different conditions. The first recording was a control without any pretreatment or perfusion with other substances. The second recording was performed with ACSF containing 500 nM TTX to ensure that blocking of potential Ca^{2+} signals, following neuronal activity, did not alter measured Ca^{2+} responses. The third recording followed after 45 minutes of pretreatment with 200 µM H_2O_2 and was used for calculations of $[Ca^{2+}]_i$ changes (see figure 20). 93 of 118 analyzed cells were still responding to DHPG after perfusion with H_2O_2. Prior experiments with 60 minute treatment were stopped after 2/3 of the slices' astrocytes showed no more responses. Amplitudes were calculated based on the peak value that corresponds to each application time point and on baseline levels immediately before this application. That means, for the first application the previous

60 seconds were averaged and taken as baseline while for the second and third application only the 10 seconds before the application were used.

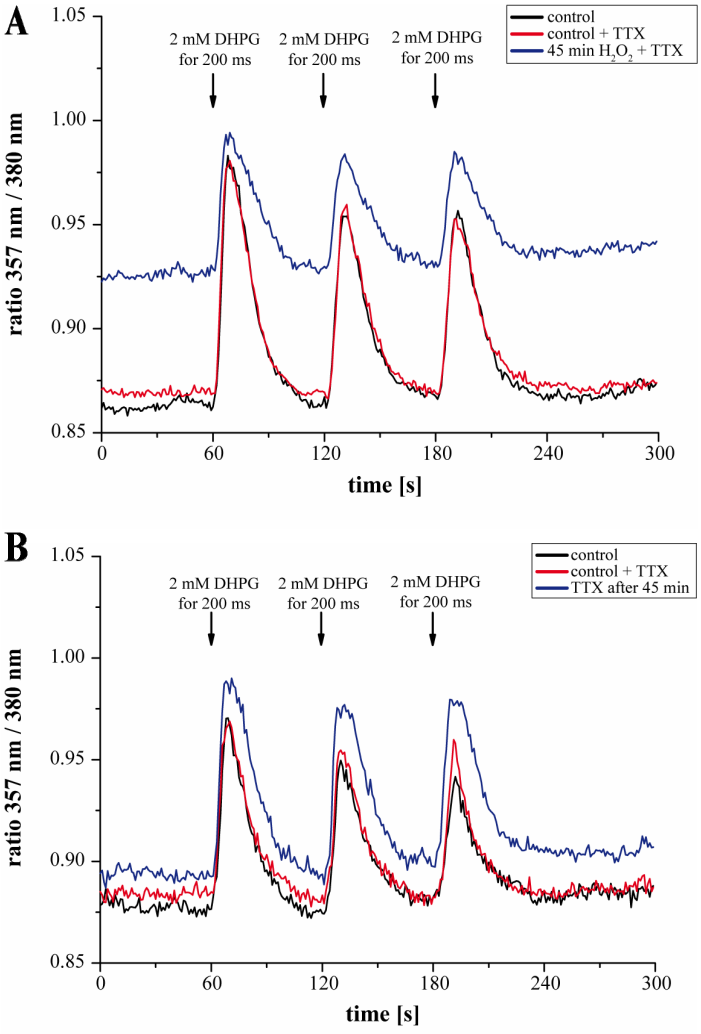

Figure 26: mGluR mediated Ca^{2+} responses in acute tissue slices.

Recorded ratio values of all DHPG application experiments were averaged and plotted. Application of 2 mM DHPG for 200 ms each and with a delay of 1 minute showed a slight decrease in signal amplitude in which the second and third Ca^{2+} rise had basically the same amplitude (black line; $[Ca^{2+}]_i$ baseline: ~90 nM; $[Ca^{2+}]_i$ 1st application: ~340 nM; $[Ca^{2+}]_i$ 2nd & 3rd application: ~300 nM). After 45 minute treatment with 200 µM H_2O_2 amplitudes were significantly decreased (**A**, blue line; $[Ca^{2+}]_i$ baseline: ~200 nM; $[Ca^{2+}]_i$ 1st application: ~360 nM; $[Ca^{2+}]_i$ 2nd & 3rd application: ~340 nM), which is independent of TTX (red line). Control experiments (**B**) to verify that detected effects result from oxidative stress and not from 45 minutes pause, showed no significant differences before and after pause (see figure 21).

Averaged metabotropic Ca^{2+} responses of astrocytes showed a slight decrease in amplitude between the first and the second application of DHPG, whereas the second and third were nearly identical. $[Ca^{2+}]_i$ changed from ~90 nM (baseline) to ~340 nM during the first application, but the second and third application induced a ~40 nM lower increase in $[Ca^{2+}]_i$. TTX, which was used to eliminate signaling between neurons, had no influence on neither the amplitudes nor the signal kinetics of astrocytes (see figure 20 A). Pre-treatment with 200 µM H_2O_2 did not only lead to a drastic increase in the intracellular Ca^{2+} baseline level of about 6,4 % (increase in calculated ratio) and from ~90 nM to ~200 nM in $[Ca^{2+}]_i$, but also to significant effects on metabotropic signaling (see figure 20 and figure 21). After H_2O_2 treatment, astrocytes showed an average decrease in amplitude of Ca^{2+} signal response of about 36,5 % as to their ΔF/F

values. This applied to each of the three responses following DHPG application during one recording. Increase in $[Ca^{2+}]_i$ during DHPG applications showed a Ca^{2+} concentration maximum of ~360 nM for the first and ~340 nM for the second and third application.

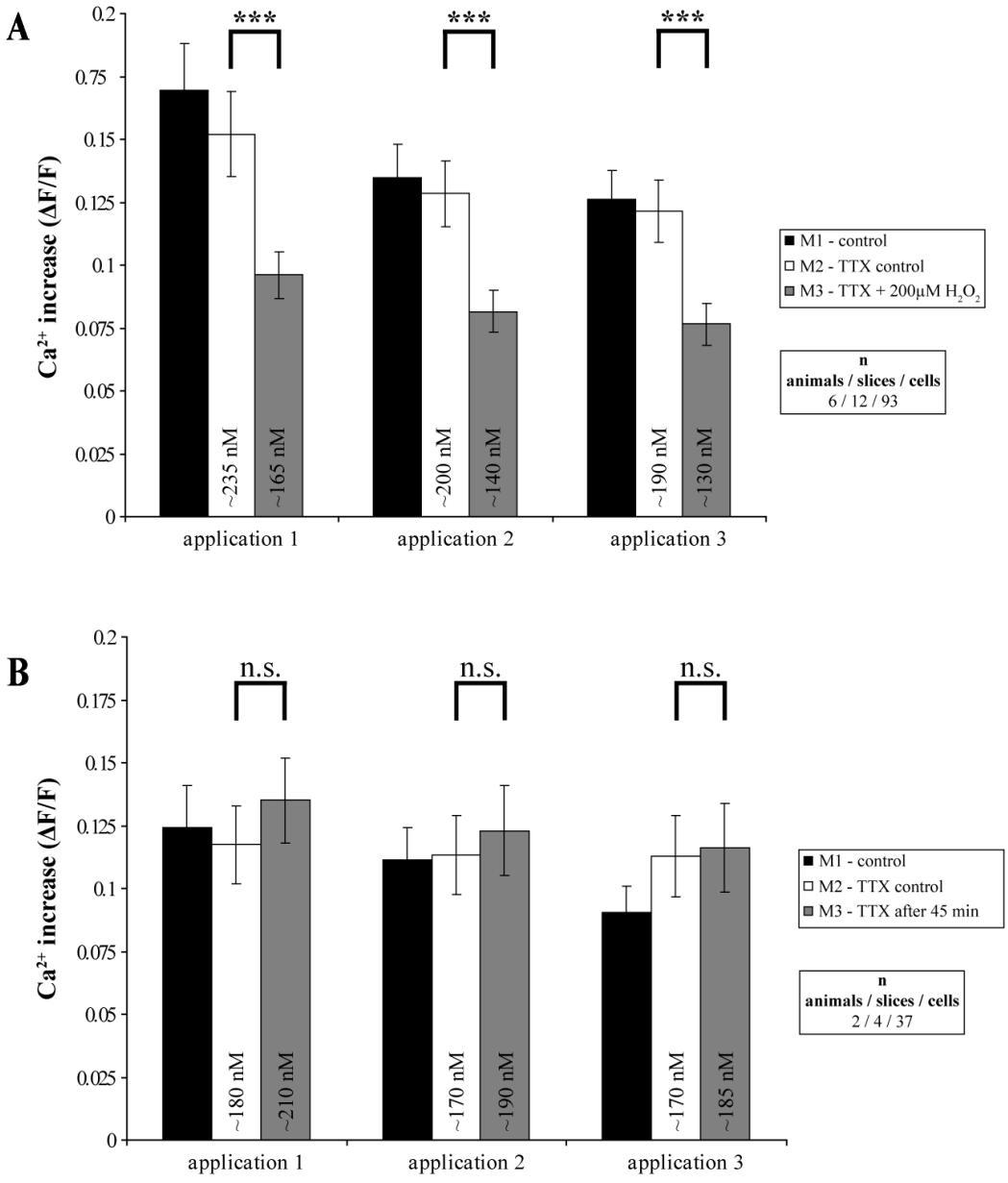

Figure 27: Amplitudes of mGluR mediated Ca^{2+} responses in acute tissue slices.

Calculated Ca^{2+} signal amplitudes after mGluR stimulation were averaged for each type of experiment (control, TTX control and after H_2O_2 treatment). In all three types of experiments, the second and third response showed slightly decreased amplitude in comparison with the first. While control and TTX control measurements exhibited nearly no difference, after 45 minutes of 200 µM H_2O_2 treatment amplitudes were significantly decreased (**A**).
Control experiments with a pause of 45 minutes instead of H_2O_2 treatment showed no significant changes in amplitude (**B**). All values are given as means ± S.E.M..
(significance: n.s. = not significant ($p > 0.01$); * = $p < 0.01$; ** = $p < 0.001$; *** = $p < 0.0001$)

Control measurements to check if these effects were a simple consequence of a 45 minute pause, exhibited a minor increase in $[Ca^{2+}]_i$. However, metabotropic Ca^{2+} responses were not significantly altered in control experiments (see figure 20 B and figure 21 B).

3.4.4 Effect of oxidative stress on internal Ca^{2+} stores

With decrease of Ca^{2+} response amplitudes after DHPG application, the question arose whether this reduction was based on lowered filling levels of internal stores, caused by oxidative stress. To analyze this, ER depletion experiments with CPA were performed. Use of Ca^{2+}-free ACSF, to prevent refill of stores with extracellular Ca^{2+}, was resigned to avoid further stress on the cells. For analysis the amplitude of the first increase in $[Ca^{2+}]_i$ after begin of CPA perfusion was measured and compared with that of slices which were pretreated with 200 µM H_2O_2 for 45 minutes.

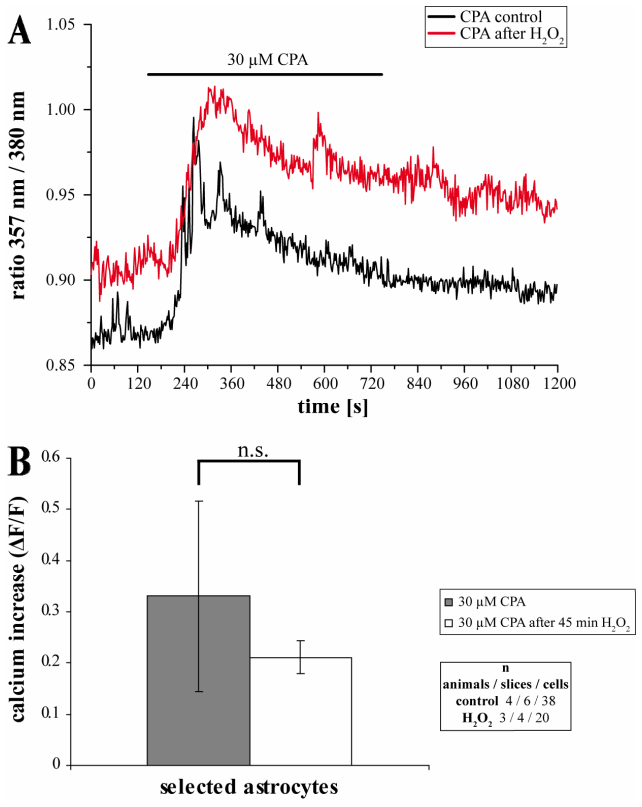

Figure 28: Depletion of internal Ca^{2+} stores.

A: Averaged Ca^{2+} signals during 10 minutes of 30 µM CPA perfusion (background corrected). Colors indicate recording with prior H_2O_2 perfusion (red) and control (black).
B: Statistical analysis of Ca^{2+} signal amplitudes showing no significant difference (unpaired t-test, because experiments had to be performed in separate slices). All values are given as means ± S.E.M.
(n.s. = not significant ($p > 0.05$)

The averaged $[Ca^{2+}]_i$ baseline level was increased after H_2O_2 treatment, similar to earlier findings (see chapter 3.4.3). But although depletion of intracellular Ca^{2+} stores via CPA showed a ~50 nM lower increase in $[Ca^{2+}]_i$ after 45 minutes of H_2O_2 treatment, calculation of $\Delta F/F$ values between baseline and maximum peak did not result in a significant difference. This indicates no significant alteration in Ca^{2+} filling levels of the ER by H_2O_2 treatment. It is therefore implausible that the reduced metabotropic Ca^{2+} response after mGluR activation (see chapter 3.4.3) resulted from decreased filling levels of the intracellular Ca^{2+} stores. Additionally, signaling kinetics had not been altered noteworthy.

3.4.5 Effect of H_2O_2 on astroglia membrane potential

Patch-clamp experiments were performed to test for hints on reduced ATP availability during H_2O_2 treatment, because reduction of ATP and consequently functionality of ATP-dependant Ca^{2+} uptake into the ER, may be involved in the increased $[Ca^{2+}]_i$ and the reduced Ca^{2+} signal amplitude after perfusion with H_2O_2 (see chapter 3.4.3). For this, membrane potential (E_m) of astrocytes was analyzed by using current-clamp recordings. Perfusion with 250 µM H_2O_2 was started right after stable membrane potential was verified and continued for 20 minutes. Afterwards, perfusion was changed to H_2O_2-free ACSF. The hypothesis was that when ATP availability was decreased, ATP-dependant pumps, e.g. the Na^+/K^+-pumps, were affected as well. The consequence would have been a depolarization of the cell membrane.

While 2 of 5 astrocytes did not exhibit an alteration of E_m upon treatment with H_2O_2, 3 cells did. Recordings of those astrocytes showed an instant hyperpolarization directly after begin of H_2O_2 perfusion (see figure 23 A). E_m became hyperpolarized by about 2 mV and repolarized incompletely within the following 30 minutes after wash-out of H_2O_2. Resulting from these recordings, no indication of decreased Na^+/K^+-pump activity was found, which might give a hint on ATP shortage.

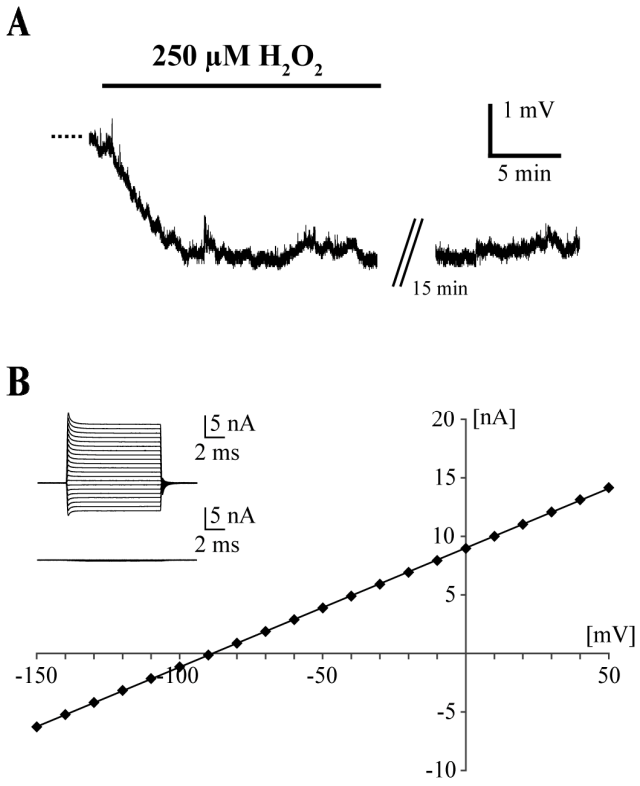

Figure 29: Membrane potential recording of an astrocyte during perfusion with H_2O_2.

A: Recording of E_m in an exemplary astrocyte was started after detection of a stable baseline (indicated by dashed line). It showed a hyperpolarization of about 2 mV during 20 min perfusion with ACSF containing 250 µM H_2O_2. After wash-out, E_m remained hyperpolarized for several minutes and showed an incomplete repolarization afterwards (not indicated).
B: Electrophysiological characterization of the astrocyte recorded in A, using a protocol from -150 to 50 mV. Insets on the left side show membrane currents before (top) and after (bottom) leak substraction. The resulting I/V-curve shows a linear current-voltage relationship typical for astrocytes at P15.
(P15; astrocyte in acute tissue slice)

Taken together, in mGluR activation experiments $[Ca^{2+}]_i$ of astrocytes was found to be drastically elevated by about 6,4% (increase in calculated ratio) after 45 minutes of prior treatment with 200 µM H_2O_2. Ca^{2+} response after activation of mGluR was significantly decreased with all three responses in one recording being affected in the same manner. To exclude that reduced Ca^{2+} responses originated from decreased filling levels of intracellular Ca^{2+} stores, experiments with CPA were performed. The results showed no significant decrease in filling levels, suggesting that Ca^{2+} uptake into the ER was not altered. Additionally, the membrane potential of astrocytes was measured during acute oxidative stress, to test for hints on ATP shortage. Decreased availability of ATP might have resulted in disturbed function of the Na^+/K^+-ATPases that would have led to a depolarization of the membrane. Because no depolarization was detected, shortage of ATP is rather unlikely to have occurred under acute oxidative stress, as it was induced in these experiments. This is also strengthened by the finding that ER filling levels were not altered significantly, because ATP would have been necessary for Ca^{2+} uptake into the ER by the SERCAs.

3.5 Medium-term effects of acute oxidative stress in organotypic slice cultures

Experiments with acute oxidative stress resulted in drastic changes of metabotropic Ca^{2+} signaling. But they did not answer the question, if cells will undergo other, non-acute changes, such as altered gene expression resulting in astrogliosis. For investigation of this issue, organotypic slices of 4 animals were treated with concentrations of 10, 100 and 200 µM H_2O_2 for 45 minutes, followed by 3 days of postincubation to allow for development of astrogliosis. All concentrations, as well as ACSF for controls, were applied in each culture batch to avoid misinterpretation of received data. For analysis an overall number of 23 slices with 304 astrocytes were evaluated. In detail, 7 slices with 10 µM (n = 98), 5 slices with 100 µM (n = 64) and 6 slices with 200 µM H_2O_2 (n = 90) treatment, as well as 5 slices for controls (n = 52) were analyzed. After fixation and immunohistochemical staining, astrocytes were identified by GFAP-labeled processes and their soma was localized by S100β (see figure 30).

Analysis was performed in maximum projection images of confocal 7-8 layer stacks with 0.5 µm thickness, at which interest was focused on staining against GFAP. Based on this staining, diameters of the 4 thickest primary processes of each astrocyte were measured in close proximity to the soma (see figure 31) and the total number of processes was counted. Diameters were averaged afterwards with those of astrocytes in slices that had been treated the same way and statistically validated (see figure 32 A). Comparison showed no significant difference between control, treatment with 10 µM and treatment with 100 µM H_2O_2. Only 45 minute treatment with 200 µM H_2O_2 exhibited a significant increase in diameter of about 0.07 µm (*p*-value = 0,06-0,28) on average to each other concentration. The number of processes was determined by counting those processes that were stained against GFAP and could be definitely assigned to the previously identified soma. Analysis showed no significant difference between any group (see figure 32 B).

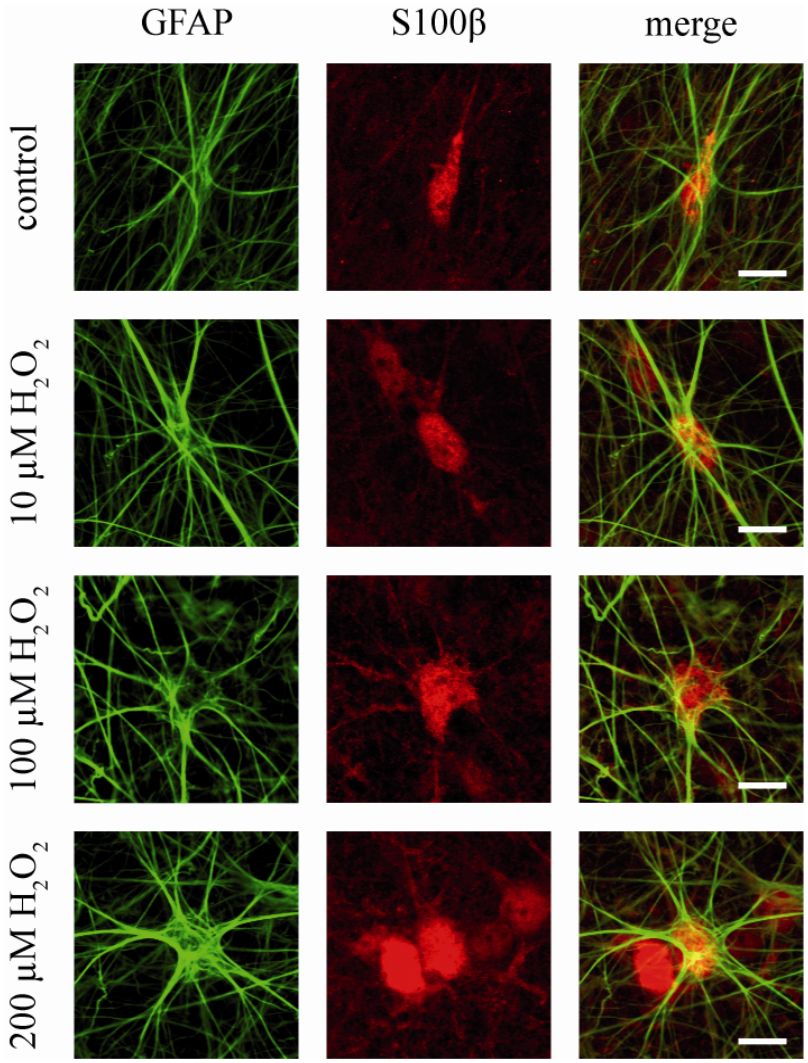

Figure 30: Imunhistochemical staining of organotypic slices after H_2O_2 treatment.

Organotypic slice cultures of mice were stained against GFAP, which labels intermediate filaments in astrocytes, and against S100β, which primary labels the soma. Treatment with 10 and 100 µM H_2O_2 for 45 minutes caused no increase in diameter of processes. Increase of diameter after treatment with 200 µM was still rather low.
All slices were kept 10 DIV before treatment and postincubated 3 more days afterwards. Scalebar: 10 µm

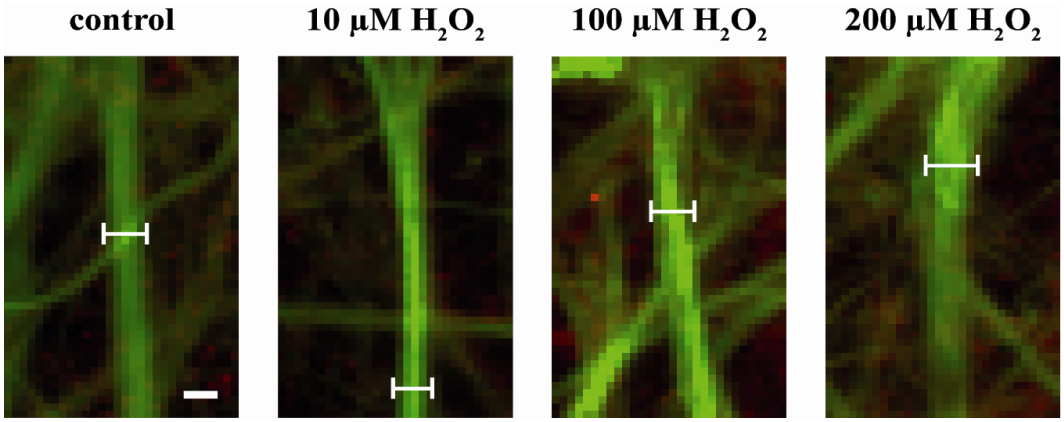

Figure 31: Analysis of process diameter.

Diameters of astrocytes' processes were analyzed in close proximity to the soma, where diameters did not change for several micrometers, as shown above. Treatment with 10 and 100 µM H_2O_2 showed no visible differences in diameter, whereas 200 µM resulted in a significant increase of diameter (see figure 32).
(merged image; green: GFAP, red: S100β; Scalebar: 1 µm)

In summary, oxidative stress was shown not only to induce acute effects, but medium-term effects as well when applied to astrocytes in the same manner, in which analysis of metabotropic receptor activation was performed. GFAP expression was altered, as measured by increase in astrocyte processes' diameter after immunohistochemical staining. This gives a hint towards an astrogliosis, caused by H_2O_2 treatment, although the number of processes was unaltered.

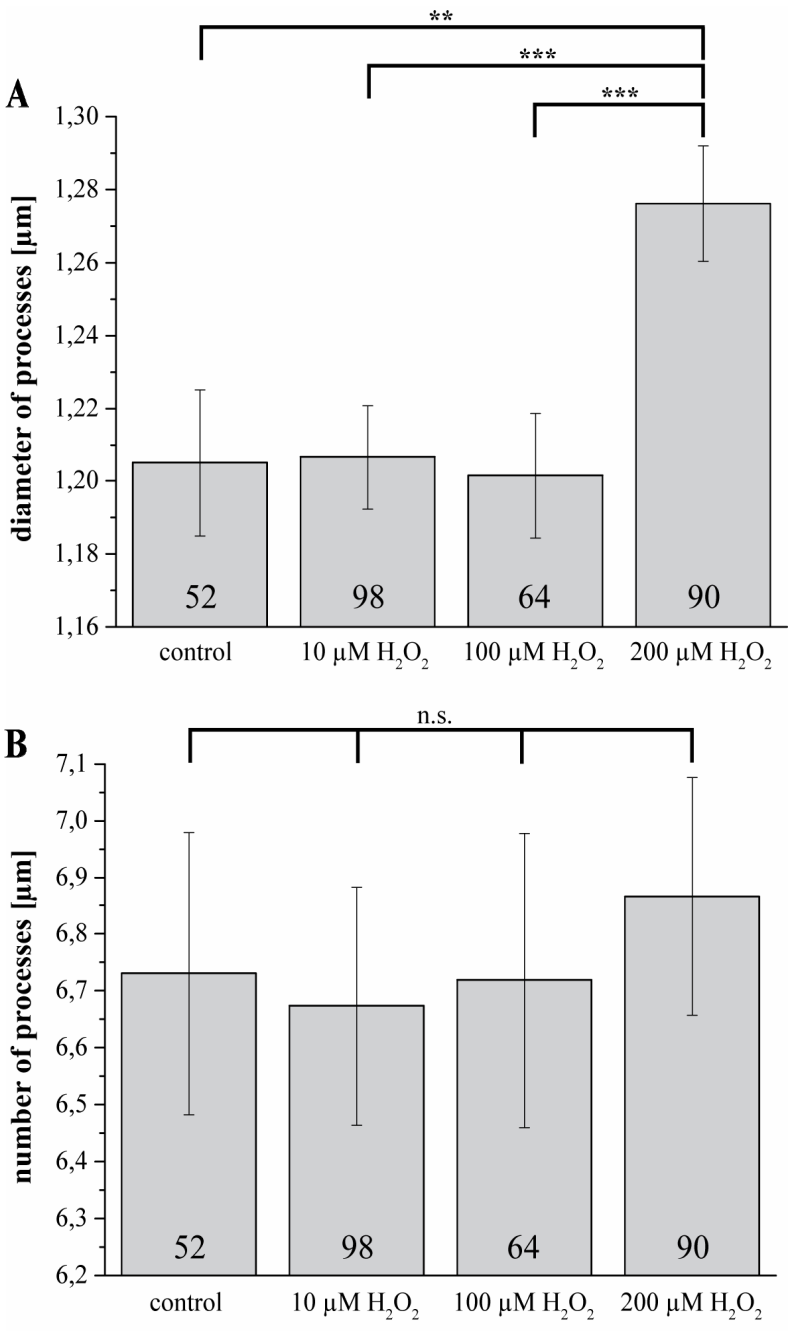

Figure 32: Morphological changes in astrocyte processes after H_2O_2 treatment.

Analysis of the 4 thickest processes of astrocytes (**A**) showed no changes in diameter after treatment with 10 or 100 µM H_2O_2, compared with controls. After treatment with 200 µM H_2O_2 a significant increase was found. In contrast, the number of astrocyte processes was not significantly altered (**B**). All slices were kept 10 DIV before treatment and postincubated 3 more days afterwards. All values are given as means ± S.E.M.
(each group consisted of 5-7 slice from 3-4 animals; number of analyzed cells are named in the bars; significance: n.s. = not significant ($p > 0,05$); * = $p < 0,05$; ** = $p < 0,01$; *** = $p < 0,001$)

4 Discussion

4.1 Analysis of USSCs

The potential of USSCs from human cord blood to replace cells which had underwent apoptosis, was investigated in the DFG research project FOR717 ("Unrestricted Somatic Stem Cells from Human Umbilical Cord Blood"). As a part of this, the subproject A2 concentrated on the differentiation of USSCs into cells of the CNS and their integration into the tissue. USSCs were prepared and treated with differentiation medium to induce development into neurons in the laboratory of Prof. Dr. H.W. Müller (department of neurology). About 2.5 weeks later, I tested those differentiated USSCs for neuronal functionality. Analysis focused on induction of Ca^{2+} response by application of receptor stimulating substances, because intracellular Ca^{2+} signaling is a reliable hint on signal processing activity of neurons. Using fluorescence widefield imaging, response behavior to application of K^{+}_{high} ACSF, glutamate, ATP and GABA was analyzed. Cells were found to show a variety of different morphologies and lacked response to most substances. Only one morphological group (T4), in which cells showed 3-4 processes with minor branching, contained cells that exhibited a repeatable rise in $[Ca^{2+}]_i$ after exposure to ATP.

Response to ATP has also been shown in other cell types of the CNS than neurons, e.g. astrocytes and microglia (Verderio and Matteoli, 2001; Wang et al., 2005; Light et al., 2006; North and Verkhratsky, 2006). ATP functions as neurotransmitter as well as signaling molecule for cellular damage to the surrounding tissue (Wang et al., 2005; North and Verkhratsky, 2006) and gives no distinct hint on the cell type. Although responses proved that some of the tested cells were capable of signal processing, lack of response to K^{+}_{high} ACSF indicated missing or at least non-functional voltage-dependant channels, which are crucial in neurons for signal conduction. However, this is in accordance with earlier findings of Greschat et al., which were also unable to detect functional voltage-gated Na^{+} channels although channel proteins were found (Greschat et al., 2008). Nonetheless, lack of response to glutamate or GABA further left open the question, if these differentiated USSCs would have excitatory or inhibitory function.

Additionally, integration of USSCs into CNS tissue of mice was tested by transplantation of these cells into the lesion of organotypic (tissue) slices cultures of mice, which were injured with a cut before. In 6 of 44 slices USSCs were detected after 7 days of postincubation but not after 10 or 14 days. On the one hand, these findings differ from earlier experiments (Schira et al., 2012), in which USSCs were detected even after 3 weeks. Axonal regrowth was also found in those experiments, whereas in my studies cells did not even show hints on accumulation near the borders of the lesion. On the other hand, experiments of Schira et al. were performed in the spinal cord of living rats and not in a hippocampal model system of mice. This gives two possible explanations for the small number of hippocampal tissue slices with USSCs after 7 days. In addition, Schira et al. did not find USSCs to develop into neurons; they were found to support axonal regrowth instead. With USSCs, which were transplanted into hippocampal slice cultures of mice, vanishing after one week, it was not possible to detect similar effects.

In summary, analysis of differentiated USSCs gave more hints on non-neural identity of the analyzed cells than on neurons, although earlier studies reported the ability of USSCs to develop into dopaminergic neurons (Greschat et al., 2008). The ability of USSCs to integrate into tissue cultures was found to be low and to last only for a short period of time. Nonetheless, USSCs survive in living animals and decrease the consequences of spinal cord injury (Schira et al., 2012). It is therefore obvious that the different results originate from the different model systems and possibly also from the related treatment parameters, i.e. cerebrospinal fluid of the rat in contrast to culture medium.

4.2 Identification of astrocytes in tissue slices

Analysis of astrocyte response to a given stimulus required a reliable identification of these cells in tissue slices first. Although performance of identification experiments would have been easier in primary cultures, astrocytes and neurons are known to influence each other during development (Bordey and Sontheimer, 1997), which made this work in the model systems of later experiments necessary. For primary cultures, mostly animals of early postnatal age (P0-2) are used, in which astrocytes and neurons

have not yet developed into fully functional cells. Reliability of data received from these cultures might therefore be not usable for experiments in tissue slices of P18+ animals. For identification experiments in tissue slices, labeling with SR101 and testing for Ca^{2+} signals, which are induced by an astrocyte specific Kir channel, were compared in accordance with earlier work (Dallwig et al., 2000; Dallwig and Deitmer, 2002; Nimmerjahn et al., 2004; Kafitz et al., 2008). During perfusion with K^+_{low} ACSF, influx of Ca^{2+} was found in astrocytes of acute tissue slices with variable amplitudes, whereas presumed neurons showed no alterations of $[Ca^{2+}]_i$. Signaling was also found in astrocytes that were not supposed to possess functional Kir channels respective to the animal's age, but a clear differentiation between astrocytes and neurons was possible though. Use of $BaCl_2$ for blocking the rise in $[Ca^{2+}]_i$ during K^+_{low} ACSF perfusion turned out to be only partially removable in slices of older animals.

In 2000, Dallwig et al. detected an increase of $[Ca^{2+}]_i$ in cerebellar astrocytes of rats, when extracellular concentration of potassium was reduced from 5 to less than 1 mM. Additionally they found that this effect was based on barium-sensitive Kir channels (Dallwig et al., 2000). Subsequent experiments revealed that astrocytes and neurons in acute tissue slices could be distinguished by this effect, because it was restricted to astrocytes only (Dallwig and Deitmer, 2002). These findings could be confirmed in my studies as well as the described heterogeneity in signal amplitudes. Although alterations in $[Ca^{2+}]_i$ during perfusion with K^+_{low} ACSF that were detected in P5 animals, have not been described earlier, functionality of ion channels in astrocytes of immature rodents was reported (Bordey and Sontheimer, 1997, , 2000; Li et al., 2001). Potassium currents through Kir channels have been shown to be present in 40-50 % of hippocampal astrocytes (Bordey and Sontheimer, 2000). Therefore it appears coherent that Kir channels in slices of P5 animals also allowed Ca^{2+} currents in K^+_{low} ACSF. However, in the older animals removal of the channel-blocking effect of Ba^{2+} was rather unreliable and potential stress by alternating potassium concentrations, to test for astrocytes identity, cannot be totally ruled out. Therefore this technique for cell identification was not applied in experiments, which dealt with oxidative stress and was not further validated statistically.

Use of SR101 was introduced as an astrocyte-specific and robust labeling method by Nimmerjahn et al. in 2004. Cells that had taken up this dye also expressed EGFP under the GFAP promoter, which is typical for astrocytes and therefore verified these cells as astrocytes. Additionally, these cells showed Ca^{2+} signals with a slow

elevation, in contrast to neurons that show fast transients (Nimmerjahn et al., 2004). In 2008, Kafitz et al. adapted this technique and analyzed it in detail in acute hippocampal slices. SR101 was found, independent of the developmental stage, to label almost all classical astrocytes in acute hippocampal tissue slices of rodents, which was confirmed by analyzing electrophysiological properties (Kafitz et al., 2008). Neither in that study nor in the work to this one was SR101 found to affect performed experiments, e.g. Ca^{2+} imaging. Staining quality was also comparable with earlier studies. Additional labeling with SR101 during experiments with Ca^{2+} influx through Kir channels was in consistence with cells that showed the described rise in $[Ca^{2+}]_I$ (Dallwig et al., 2000). The only work that assessed use of SR101 critically was published by Kang et al. in 2010. They described SR101 to lower the necessary threshold of membrane depolarization for the induction of an action potential in neurons. Some results of the performed experiments in that study remain questionable though. Analysis of NMDA receptor currents, for example, was performed with decreased Mg^{2+} concentrations (0 mM) and bicuculline, a blocker for (inhibitory) GABA-mediated signaling, in the used ACSF. Under these conditions, one does not have to be surprised, that recorded currents were found to be increased because all inhibitory mechanisms were removed. Additionally, findings of increased spontaneous neuronal signaling activity in the study of Kang et al., which result from SR101 application, could not be confirmed during my experiments. Hence, SR101 was used for astrocyte identification during all following live cell imaging experiments.

4.3 Acute oxidative stress

One major topic of this study was the analysis of effects on metabotropic Ca^{2+} signaling of astrocytes, resulting from oxidative stress. Metabotropic Ca^{2+} signaling in astrocytes has been found to arise after stimulation with several neurotransmitters (Kim et al., 1994; Chen et al., 1995; Zhu and Kimelberg, 2001) and to be important for a variety of functions (for review see Verkhratsky et al., 2011). Ca^{2+} release from the ER in astrocytes is involved in gliotransmission (release of glutamate and ATP), which modulates the activity of synaptic transmission, i.e. presynaptic release of neurotransmitters and postsynaptic efficacy in neurons (Volterra and Meldolesi, 2005;

Pirttimaki et al., 2011). It also regulates the local blood flow by inducing the release of vasoactive substances and it can control apoptosis of astrocytes (Verkhratsky et al., 2011). Aside from Ca^{2+} signaling, the ER has various other functions as well, such as intracellular transport of molecules and involvement in protein synthesis. Because these functions are affected by Ca^{2+} release from the ER itself, Ca^{2+} signaling links cell activity to specific biochemical processes (Verkhratsky et al., 2011).

Oxidative stress is capable of disturbing cellular Ca^{2+} homeostasis in the CNS by oxidizing regulatory proteins, e.g. CaM (see also chapter 1.3.2; Squier and Bigelow, 2000; Bond and Greenfield, 2007; Nedergaard and Verkhratsky, 2010) and might thus impair metabotropic Ca^{2+} signaling as well. Therefore I addressed the question, if each induced metabotropic Ca^{2+} signal is affected by acute oxidative stress and if those effects are similar or if signals are altered in an accumulative manner. The hypothesis was that a disturbance of Ca^{2+} homeostasis would affect Ca^{2+} release from the ER and that repeated stimulation would result in decreased signal amplitudes. In context with this, I also wanted to trace the origin for a potential alteration by analyzing Ca^{2+} filling levels of the ER and test for hints on energy shortage that might affect a decreased refill of intracellular Ca^{2+} stores. Additionally, experiments were attempted to be performed in acute and cultured tissue to find an adequate model system for these questions.

4.3.1 Astrocytes and neurons differ in dose-response behavior

As a prerequisite for oxidative stress analysis, a proper treatment for induction of oxidative stress had to be found first. In the past, H_2O_2 treatment had already been used for this purpose, either to simulate effects of aging (Gille and Joenje, 1992; Gottfried et al., 2002; Lu et al., 2004; Pertusa et al., 2007) or to analyze oxidation on cellular functions (Desagher et al., 1996; Gottfried et al., 2002; Souza dos Santos et al., 2007; Voss et al., 2008; Wilkinson et al., 2008; Gerich et al., 2009). To find a concentration that induces oxidative stress to astrocytes in tissue slices without irreversibly impairing neuronal cells, dose-response experiments were performed. Slices were perfused with H_2O_2 concentrations ranging from 0.1 to 2 mM for 10 minutes, and alterations in $[Ca^{2+}]_i$ were recorded by widefield imaging. Alterations in $[Ca^{2+}]_i$ and malfunction in Ca^{2+} homeostasis have been described before as a consequences of oxidative stress (Nicotera et al., 1992; Squier and Bigelow, 2000; Nedergaard and Verkhratsky, 2010) and were

therefore used to assess effects on measured cells. In my experiments, neurons were found to show a more intense increase in $[Ca^{2+}]_i$ than astrocytes. Results also suggested to apply a maximum of 200 µM H_2O_2 for 45 minutes to avoid overstressing of the vellular antioxidant mechanisms (see also chapter 3.4.2).

In literature, neurons in primary culture have been described as particularly vulnerable to oxidative stress (Thery et al., 1991; Desagher et al., 1996). This might be due to the fact that peroxide detoxification via the glutathione system is less efficient in neurons than in astrocytes (Dringen et al., 1999). Astrocytes also contain higher amounts of antioxidants and antioxidant enzymes, suggesting a neuroprotective role (Desagher et al., 1996; Dringen, 2000; Takuma et al., 2004). In contrast to that, astrocytes in organotypic slice cultures were found to be as vulnerable to hydrogen peroxide as neurons, and perhaps even more (Feeney et al., 2008). Data that was received in acute tissue slices during my work, is in line with those earlier results as neurons were found to respond with a stronger rise in $[Ca^{2+}]_i$ than astrocytes during perfusion with H_2O_2. Based on the calculated $\Delta F/F$ values, neurons began to approach maximum peak amplitude at 1 mM H_2O_2, whereas astrocytes showed a linear rise in $[Ca^{2+}]_i$ up to highest concentration used (2 mM). This indicates that astrocytes in acute tissue slices are capable of compensating higher amounts of oxidative stress than neurons because Ca^{2+} homeostasis in astrocytes becomes less affected. Additionally, these findings support the assumption of increased antioxidant substances in astrocytes not only to be true for primary cell cultures but for acute tissue slices as well.

Similar to findings of Gülden et al. in astroglioma cells (Gulden et al., 2010), a biphasic dose-response curve was expected for both cell types. Glutathione peroxidase activity would limit increase in $[Ca^{2+}]_i$ to a certain degree during the first phase. In the second phase, $[Ca^{2+}]_i$ would rapidly increased and finally end in maximum peak amplitude, marking the failure of all antioxidant processes. However, received data gave indications for a sigmoid curve progression only for neurons. Astrocytes showed a nearly linear dose-response behavior, at least for the tested concentrations. With further increase of H_2O_2 concentration, these cells would have also reached their maximum peak amplitude as soon as their antioxidant mechanisms had reached their limit. Hence, the chosen linear fitting curve can only be assessed in dependence to the range of tested concentrations. It is also noteworthy that the equation of the sigmoid fitting curve is based on 4 variables. With 5 concentrations tested, the reliability is low, although the value for R^2 is nearly 1.

As mentioned above, the increase of $[Ca^{2+}]_i$ in neurons was nearly linear up to a perfusion with 1 mM H_2O_2 for 10 minutes but reduced during use of higher concentrations. This treatment was therefore assessed as the limit of what should be done to the acute tissue slices, because the intention was to find a way to induce acute oxidative stress but not to overstress antioxidant mechanisms. Similar to the free "radical theory of aging" (Harman, 1956), which considers aging to be an accumulation of damage over time (see also chapter 1.3.2), a relation between concentration and time of treatment was assumed for perfusion with H_2O_2 as well. A correlation of both was also confirmed by Gülden et al. (2010), but in contrast to their work, H_2O_2 concentration was unable to decrease during my experiments because ACSF with H_2O_2 was constantly renewed. Therefore I assumed the effects of H_2O_2 perfusion, which was an increase of $[Ca^{2+}]_i$ in my work, to be based on a linear instead on an exponential relation between concentration and time. Dose-response experiments showed a nearly linear increase in $[Ca^{2+}]_i$ of astrocytes and neurons when the treatment time was kept constant, at least up to the treatment described above. In reverse I concluded that when the H_2O_2 concentration would be kept constant, adequate changes in the treatment time would induce a similar increase in $[Ca^{2+}]_i$. 45 minute treatment with 200 µM H_2O_2 was therefore expected to have the same results concerning increase in $[Ca^{2+}]_i$ as a 10 minute perfusion with 900 µM. This is shortly before neurons began to fade towards their maximum peak amplitude in dose-response experiments. 60 minute treatment with 200 µM would relate to more than 1 mM H_2O_2 in 10 minutes, where cells had already began to do so and which would expose them to a high risk of irreversible damage. This was strengthened by the initial mGluR activation experiments in which 2/3 of the cells did not respond to DHPG application after 60 minute of H_2O_2 treatment in contrast to ~20 % after 45 minutes (see also chapter 3.4.3). Consequently, treatment with 200 µM H_2O_2 for 45 minutes was used for further experiments. Minor rise in $[Ca^{2+}]_i$ that was found in astrocytes and neurons of controls was not taken into account further, because this alteration was presumably a slight stress response to prior handling, i.e. preparation, insertion into the experimental chamber and variations of temperature.

4.3.2 Organotypic slice culture vs. acute tissue

Cells of organotypic (tissue) slice cultures are structural closer to those of acute tissue than cells of primary cultures, while giving the opportunity to carry out pharmacological treatments for several days (Gahwiler, 1988; Stoppini et al., 1991; Gahwiler et al., 1997). In the past, they have been used for different studies, e.g. analysis of calcium waves (Harris-White et al., 1998) or analysis of regional vulnerability to endogenous and exogenous oxidative stress (Vornov et al., 1998), but the effects of oxidative stress on Ca^{2+} signaling were not further elucidated in this model system. Organotypic slice cultures were therefore intended to be used for analysis of mild oxidative stress via Ca^{2+} imaging in my work. Induction of oxidative stress would have been carried out by application of H_2O_2 for multiple days. In the end, imaging experiments had to be stopped after numeral difficulties in staining with Fura-2 arose (see chapter 3.3.1). Neither cellular loss in the *stratum pyramidale* nor rise of $[Ca^{2+}]_i$ without experimental interference was tolerable. A correction of collected data afterwards could also not have been performed, because this rise showed no linearity (see figure 28). Nonetheless, Ca^{2+} imaging in organotypic slices has been found realizable in experiments of Harris-White et al. (1999). This might be due to staining procedures at RT instead of staining in the incubator or because no detergent was used by this group to facilitate the staining process, although this method has proven well in experiments with acute tissue slices (see below). As a prerequisite for use of organotypic slices in future experiments, the Fura-2 staining protocol has to be revised first. Bolus staining was found to be feasible as a replacement in my studies, yet staining of neurons was poor (see figure 27) and dose-response experiments of astrocytes resulted in questionable data (see figure 29).

Over the years, use of acute tissue slices has become a common method to perform experiments very close to *in vivo* conditions (Carmignoto et al., 1998; Latour et al., 2001; Aguado et al., 2002; Dallwig and Deitmer, 2002; Zur Nieden and Deitmer, 2006; Stangl and Fromherz, 2008; Langer et al., 2012). Earlier ion imaging experiments in other institutes as well as in our institute showed that Bolus staining (pressure injection of a fluorescent dye) works well with this model system (Stosiek et al., 2003; Meier et al., 2006; Kafitz et al., 2008) and consequently it was used in this study as well. Minor increase in $[Ca^{2+}]_i$ (< 20 nM) without experimental interference during dose-response experiments (0 mM H_2O_2) were linked to potential stress before experiments, leading subsequently to Ca^{2+} signaling and an increase in the $[Ca^{2+}]_i$

baseline (see also chapter 4.3.1). Modification or degradation of Fura-2 molecules, due to the used light intensities, are improbable because this dye has been shown to be relatively photostable (Becker and Fay, 1987; Hayashi and Miyata, 1994; Paredes et al., 2008) and is widely used for Ca^{2+} imaging (Verkhratsky et al., 1998; Dallwig and Deitmer, 2002; Wilkinson et al., 2008; Stoppelkamp et al., 2010). To minimize implication on later analysis, recording times, and with this also exposure to light, were kept short, i.e. 3 x 5 minutes for DHPG application experiments and 20 minutes for CPA experiments. In short, for experiments dealing with oxidative stress, acute tissue slices were preferred, because of the established staining method. Analysis of effects resulting from mild oxidative stress for several days was postponed.

4.3.3 Effect of acute oxidative stress on metabotropic Ca^{2+} signals

Accumulation of intracellular Ca^{2+}, as it has been found in this study, is in line with earlier observations in primary cell cultures of neurons (Gerich et al., 2009) and astrocytes of the hippocampus (Robb et al., 1999; Gonzalez et al., 2006; Bond and Greenfield, 2007), where it was described as result of oxidative stress and failure of Ca^{2+} homeostasis (see also Squier and Bigelow, 2000; Nedergaard et al., 2010). These studies used peroxides, e.g. H_2O_2 to induce oxidative stress and found an increase in $[Ca^{2+}]_i$ of astrocytes as well as neurons based on depletion of the intracellular Ca^{2+} stores, i.e. the ER (Robb et al., 1999; Gonzalez et al., 2006; Gerich et al., 2009). They also detected an influx of Ca^{2+} from the extracellular space to occur via VGCCs in astrocytes after exposure to oxidative stress (Bond and Greenfield, 2007). In addition to both, disturbances of Ca^{2+} regulatory mechanisms have been described to result in persisting alterations of $[Ca^{2+}]_I$ as well. Reduced function of antioxidant enzymes which leads to an excess of ROS, causes oxidation of redox-sensitive proteins such as the intracellular Ca^{2+}-sensor protein CaM and the plasma membrane Ca^{2+}-ATPase (Squier and Bigelow, 2000; Souza dos Santos et al., 2007). CaM coordinates the regulation of a huge number of enzymes, channels and receptors, such as the plasma membrane Ca^{2+}-ATPase, which itself has been found to be highly sensitive to oxidation and to be impaired in aged animals where reduced function is linked with accumulation of ROS during aging (Michaelis et al., 1996; Zaidi et al., 1998; Squier and Bigelow, 2000). As a consequence, Ca^{2+}-removal from the cytosol becomes impaired and $[Ca^{2+}]_i$ increases.

Similar to findings of Desagher et al. (1996), who described neurons to be less resistant to oxidative stress than astrocytes based on analysis of cell survival, my work showed a higher increase in $[Ca^{2+}]_i$ of neurons than in astrocytes after H_2O_2 treatment. This supports the previous findings because increase in $[Ca^{2+}]_i$ has been shown in several studies to be a preceding step of cell death (Barnham et al., 2004; Berliocchi et al., 2005; Zundorf and Reiser, 2011). When activation of mGluR takes place under these conditions, temporal and spatial coding of intracellular Ca^{2+} signals is expected to be affected as well. Proper function of processes that are regulated by metabotropic Ca^{2+} signaling, e.g. release of neurotransmitters and K^+ buffering of astrocytes, would be at risk (see chapter 1.3.2).

Application of the mGluR agonist DHPG resulted in different amplitudes of Ca^{2+} signals in astrocytes between control recordings and recordings after H_2O_2 perfusion. Yet, the course of the signals allowed no conclusion on an altered Ca^{2+} removal from the intracellular space after depletion (see figure 20). Instead, a slight decrease in amplitudes between the first and the second Ca^{2+} signal of each experiment was found, whereas the second and third were nearly identical. This indicated desensitization within the mGluR-coupled Ca^{2+} signaling cascade, which can take place on different levels within the cell (for review see Dhami and Ferguson, 2006). The fact that the second and third signals were similar even strengthens this assumption, for similar results can also be found in the excitability of neurons within the refractory period, where only a decreased amount of channels are able to open, resulting in lower membrane potential changes. Interestingly, reduction of all averaged Ca^{2+} signal's amplitudes (TTX control compared with H_2O_2 treatment) was about 36,5 %, which indicated an effect on the amplitude that is independent of the intracellular Ca^{2+} store filling level and ATP availability. This is because otherwise at least the third signal would have been expected to exhibit a stronger decrease. Consequently, the results rather gave a hint towards an equally altered receptor (-protein) function. In parallel the question arose, if Ca^{2+} uptake into intracellular stores, namely the ER, was altered by oxidative stress although this would be in contradiction with earlier observations. SERCA of rat brain has been found to be relatively resistant against oxidation by H_2O_2, even when this process is amplified by adding Fe^{2+} to induce a Fenton reaction (Souza dos Santos et al., 2007). Therefore, further analysis of ER filling levels and availability of ATP was necessary to search for more hints on or against the involvement of both on reduced DHPG-response amplitudes.

4.3.4 Decrease in metabotropic Ca^{2+} signal amplitude after oxidative stress is independent of ER filling levels and apparently also of ATP availability

Analysis of intracellular Ca^{2+} store filling levels was performed to receive an answer on the question, if acute oxidative stress, H_2O_2 respectively, reduced function of the SERCA in my model system and might therefore have led to a decreased Ca^{2+} response after mGluR activation. In consistence with results of mGluR activation experiments (see chapter 3.4.3 and 4.3.3), intracellular Ca^{2+} baseline levels were also increased after 45 minutes of H_2O_2 treatment in these experiments. Use of CPA for ER depletion (see also Kahlert and Reiser, 2000) resulted in ratio values, by which $[Ca^{2+}]_i$ was detected being higher after H_2O_2 treatment than in controls. This is not surprising, as $[Ca^{2+}]_i$ is not only increased by intracellular Ca^{2+} store depletion, but by effects of previous H_2O_2 perfusion as well. Yet, mGluR activation experiments already indicated that the ER filling levels might not have been affected by H_2O_2 treatment because the second and third Ca^{2+} signal were nearly identical after treatment. A further decrease would have been expected instead (see also chapter 4.3.3). The data recorded in CPA experiments confirmed this assumption as they showed no significant difference in $\Delta F/F$ based intracellular Ca^{2+} increase of astrocytes between controls and H_2O_2 treated tissue (see figure 22). This supports the hypothesis that decreased amplitudes of Ca^{2+} signals after mGluR activation were independent from ER filling levels in astrocytes. In 2007, Souza dos Santos and coworkers analyzed Ca^{2+}-ATPases in isolated membrane vesicles from plasma membrane and endoplasmic reticulum of rat brain on their susceptibility for oxidative stress. Additionally, activity of SERCAs from rabbit skeletal muscle cells was analyzed in this study and found to be reduced by oxidative stress, similar to plasma membrane Ca^{2+}-ATPases. SERCAs of the brain tissue in contrast appeared to be resistant against oxidative stress. Souza dos Santos et al. proposed that this might result from the SERCA isoform SERCA2b, which is predominantly expressed in the CNS (Souza dos Santos et al., 2007). Consequently, it is unlikely that SERCAs in my work were affected by H_2O_2 induced oxidative stress, although a different model system was used.

Another aspect that may have led to increase of $[Ca^{2+}]_i$ and decrease of SERCA activity, would have been shortage of ATP availability. Under conditions of long-term oxidative stress, which has been proposed to occur during aging for example (von Zglinicki et al., 2001; Lin et al., 2007; Pertusa et al., 2007), ATP levels were found to

be reduced because of deficits in ATP synthesis (Joo et al., 1999; Lu et al., 2004; Boveris and Navarro, 2008). Considering this, ATPases like the plasma membrane Ca^{2+}-ATPase and the SERCA might also function less efficiently under conditions of acute oxidative stress. By recording E_m during perfusion with H_2O_2, we therefore tested for hints on decreased availability of ATP in astrocytes. The homeostasis of Na^+ and K^+, and therefore of E_m as well, is highly dependant on proper function of the Na^+/K^+-pump, which is also an ATPase. Dysfunction of this protein results in a breakdown of the K^+ gradient as well as in an imbalance of the ionic distribution. Consequently, the cellular membrane becomes depolarized (Kimelberg et al., 1979; Hertz, 1986; Lees, 1991; Sontheimer et al., 1994). We used patch-clamp recordings to monitor potential alterations in E_m, which could be interpreted as a hint on ATP shortage. If acute oxidative stress would lead to reduced ATP levels, Na^+/K^+-pumps might also be affected and measurements of the E_m of astrocytes would show a depolarization. However, a depolarization was not detected. Although treatment time during patch-clamp recordings was reduced to 20 minutes and only 5 cells were analyzed, astrocytes reacted nearly instantly. But instead of a depolarization, a hyperpolarisation of about 2 mV occurred (see figure 23) that persisted until the end of recording. As a result, no hint on ATP shortage during acute oxidative stress was found in this study. This further supports the assumption that the SERCAs in astrocytes were not affected by acute oxidative stress, which might have led to the observed decrease in metabotropic Ca^{2+} signaling.

Mechanisms leading to a decrease in metabotropic $[Ca^{2+}]_i$ signal amplitude under conditions of acute oxidative stress, could not finally be revealed in this study. Yet, a decrease in filling levels of intracellular Ca^{2+} stores was excluded and hints on reduced ATP availability were not found. That leaves basically two more possible causes. The metabotropic glutamate receptor itself becomes either oxidized, resulting in decreased PLC mediated signaling, or one element of the metabotropic signaling cascade, e.g. the IP_3 receptor becomes impaired, inducing a decreased Ca^{2+} release from the ER after stimulation of metabotropic glutamate receptors (see figure 33).

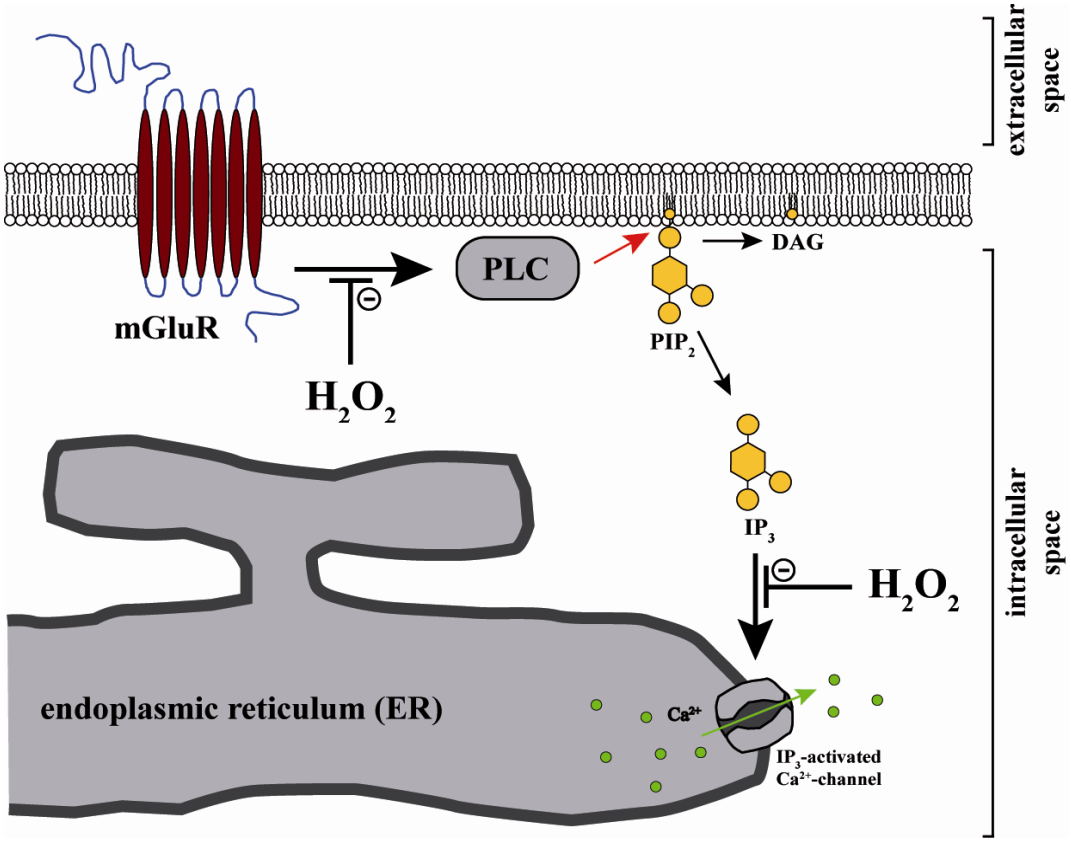

Figure 33: Increase of $[Ca^{2+}]_i$ after mGluR activation.

Stimulation of mGluRs 1+5 by DHPG leads to activation of phopholipase C (PLC). PLC then cleaves (red arrow) the membrane-bound phophatidylinositol 4,5-biphosphate (PIP_2) into inositol 1,4,5-triphosphate (IP_3) and diacylglycerol (DAG). DAG remains in the cell membrane, whereas IP_3 activates Ca^{2+} channels of the ER. Ca^{2+} is released into the cytosol and increases $[Ca^{2+}]_i$.
The two probable points of intervention by acute oxidative stress, H_2O_2 respectively, are indicated. Either the signaling between the mGluR and the PLC is impaired or the IP_3 is unable to activate the receptors in the ER membrane.

4.4 Medium-term effects of acute oxidative stress

Aside from the acute effects of oxidative stress on metabotropic signaling, I addressed the question, if other, non-acute changes, will arise, such as altered gene expression and astrogliosis. In CNS tissue, harmful incidents normally result in astrogliosis, which is hallmarked by hypertrophy, increased number of processes (Yong et al., 1991; Ridet et al., 1997; Tamagno and Schiffer, 2006; Wilhelmsson et al., 2006) and increased expression of the intermediate filament GFAP in astrocytes (Bignami et al., 1972; Ridet

et al., 1997; Eng et al., 2000; Sofroniew, 2005). Astrogliosis originates from microglial cells, which detect the occurrence of damage and secrete signaling molecules, i.e. cytokines, to induce protective processes (Ridet et al., 1997; Faulkner et al., 2004; Hauwel et al., 2005; Buffo et al., 2010). Consequently, H_2O_2 treatment used for analysis of metabotropic signaling was tested for indications of astrogliosis in an immunohistochemical approach. After three days of postincubation, prior treatment for 45 minutes with 200 µM H_2O_2 was found to result in a slight but significant increase in processes' diameter of astrocytes, visualized by staining against GFAP (see figure 32 A). The number of processes was not altered significantly (see figure 32 B). Staining of S100β was performed for proper cell soma identification, but not analyzed further. Although increased expression has been described during aging and subsequent to oxidative stress (Sheng et al., 1996; Pertusa et al., 2007; Modi and Kanungo, 2010), this would have only been realizable with a molecular approach, not by visual quantification.

Earlier studies showed that oxidative stress is a major factor in cell death cascades (Barnham et al., 2004; Valko et al., 2007; Bai and Lipski, 2010) and that several proteins, responsible for regulation of $[Ca^{2+}]_i$, e.g. the Ca^{2+}-ATPases, become impaired (Squier and Bigelow, 2000; Cotrina and Nedergaard, 2002; Souza dos Santos et al., 2007). Failure of Ca^{2+} homeostasis with subsequent rise in $[Ca^{2+}]_i$ triggers cell death (Schanne et al., 1979; Nicotera et al., 1992; Nedergaard et al., 2010; Nedergaard and Verkhratsky, 2010), which means a harmful incident to the tissue. Considering that reactive astrocytes, which are the prominent indicators for astrogliosis (Eddleston and Mucke, 1993; Ridet et al., 1997; Faulkner et al., 2004; Liberto et al., 2004), were described to protect against oxidative stress amongst other functions (Sofroniew, 2009), it seemed obvious that expression of GFAP had to be increased after H_2O_2 treatment, indicating astrogliosis. Additionally, astrogliosis and increased expression of GFAP have been found in aged individuals (Nichols, 1999; Cotrina and Nedergaard, 2002; Pertusa et al., 2007) and described as a consequence of accumulated oxidative stress (Harman, 1981; Gille and Joenje, 1992; Cotrina and Nedergaard, 2002).

Analysis of astrocytes' number of processes did not result in significant evidence for astrogliosis in treated slices. Compared to earlier findings, which dealt with induction of astrogliosis (Kehl, 2007) and findings of Wilhelmsson et al. in 2006 who described the increase in astrocytic primary processes as one hallmark of reactive astrocytes, not even a tendency towards astrogliosis was found in the current study.

Using the number of astrocytes' processes should therefore be considered a rather vague hint on astrogliosis. In contrast to that, analysis of averaged processes' diameter in this study showed a slight but significant increase after treatment with 200 µM H_2O_2 (see figure 32 A), indicating astrogliosis. This is also in consistence with earlier work performed in this lab, in which increase in process' diameter was verified to indicate astrogliosis (Kehl, 2007; Lepka, 2010) and with work of other groups who described increase in diameter of astrocytic processes as hallmark of astrogliosis before (for review see Ridet et al., 1997; Liberto et al., 2004; Sofroniew, 2009). The rather slight increase in processes' diameter of astrocytes in the current work was presumably the direct effect of ROS, which are one group of trigger molecules for the induction of astrogliosis. Release of other modulating molecules such as ATP, interleukine-6 and TNF-α (for review see Sofroniew, 2009) by dead cells and microglia might have occurred as well, finally leading to further activation of astrocytes and altered GFAP expression (Ridet et al., 1997; Liberto et al., 2004; Wilhelmsson et al., 2004; Sofroniew, 2005). However, this remains speculative because the current work did not test for the eventually involved molecules. The detection of astrogliosis confirms in parallel the former decision to decrease treatment time to 45 minutes as 2/3 of cells did not respond to DHPG application after 60 minute treatment (see also chapter 4.3.1). Although testing for cell death was not performed explicitly, it cannot be excluded that these cells had begun with apoptosis as a consequence of Ca^{2+} homeostasis failure or other oxidative damage.

Taken together, use of 200 µM H_2O_2 for 45 minutes induces a mild, yet statistically provable form of astrogliosis in organotypic culture slices. It is therefore plausible that at least a beginning astrogliosis is induced in acute tissue slices, which are able to detoxify higher amounts of ROS due to their higher number of cells, by this treatment. Consequently, and in parallel to alteration of metabotropic Ca^{2+} signaling, acute oxidative stress leads to non-acute changes in form of alteration in gene expression and subsequent astrogliosis.

4.5 Conclusions and perspectives

In conclusion, differentiated USSCs were not found to show response behavior typical for neurons and the amount of cells integrating into hippocampal tissue cultures from mice was rather low. Because earlier experiments have detected positive effects of USSCs on functional recovery after spinal cord injury in rats (Schira et al., 2012) though, general functionality of USSCs is assured. Reasons for the aberrant results remain therefore speculative. The most likely one is that differences result from the different model systems, i.e. rat and mouse. It might have also been that USSCs vanished and lacked neuronal response abilities because they support recovery but do not replace neurons and their functions. This was also suggested before by Schira et al. in 2012.

The earlier described method to differentiate between astrocytes and neurons by Dallwig & Deitmer (Dallwig and Deitmer, 2002) proved usable in acute tissue but not in slice cultures. Labeling with SR101 (Kafitz et al., 2008) instead was useful in both, acute and organotypic culture slices, and was consequently preferred. Hence, I used SR101 labeling in acute tissue slices to identify astrocytes for subsequent analysis of metabotropic signaling in astrocytes under conditions of acute oxidative stress.

Acute oxidative stress was found to drastically impair metabotropic Ca^{2+} signaling of astrocytes in my studies. This was not caused by decreased filling levels of intracellular Ca^{2+} stores and hints on ATP shortage, causing a slow refill, were also not found. Further research is necessary to elucidate, if oxidation of membrane proteins or impairment of the intracellular signaling cascade is responsible. Besides that, results underline that for acute H_2O_2 treatment, consideration of concentration- and time-dependency is crucial to avoid unintended apoptosis.

In context with aging, it is difficult to transfer the obtained results from experiments with acute oxidative stress. The simulated aspects of oxidative stress in this study cover only a few aspects of oxidative stress as it comes with aging. This is mainly because a short treatment with high concentrations of H_2O_2 induces acute effects such as cell death resulting from oxidative damage. Whereas chronic effects, e.g. alteration in gene expression (see also chapter 4.4), develop over time, i.e. with age, and can only be analyzed after several days (see immunohistochemical analysis in chapter 3.5). For this long-term analysis, acute tissue slices are an improper model system as they cannot be

used for more than 8 hours and should therefore be replaced. Pertusa et al. (2007) for example performed analysis on astrocytes and neurons in primary cell cultures which were aged for up to 90 days *in vitro*. Nonetheless the results obtained in the current study provide insight into potential effects of ROS during aging, when function of antioxidant enzymes becomes impaired. Future experiments dealing with long-term effects of oxidative stress will have to be carried out in organotypic tissue cultures to overcome the difficulties mentioned before. Yet, this requires improvement of staining procedures first. Additional consideration concerning use of other substances e.g. BSO, to induce oxidative stress, might be necessary. This is especially important after H_2O_2 has been found to be degraded after contact with cellulose-mixed ester membranes, as they were used in tissue culture (Lepka, 2010), and concentrations diminish fast in presence of great cell numbers (Gille and Joenje, 1992).

5 References

Abbott NJ, Ronnback L, Hansson E (2006) Astrocyte-endothelial interactions at the blood-brain barrier. Nat Rev Neurosci 7:41-53.

Aguado F, Espinosa-Parrilla JF, Carmona MA, Soriano E (2002) Neuronal activity regulates correlated network properties of spontaneous calcium transients in astrocytes in situ. J Neurosci 22:9430-9444.

Akopian G, Kressin K, Derouiche A, Steinhauser C (1996) Identified glial cells in the early postnatal mouse hippocampus display different types of Ca2+ currents. Glia 17:181-194.

Andersen JK, Mo JQ, Hom DG, Lee FY, Harnish P, Hamill RW, McNeill TH (1996) Effect of buthionine sulfoximine, a synthesis inhibitor of the antioxidant glutathione, on the murine nigrostriatal neurons. J Neurochem 67:2164-2171.

Araque A, Parpura V, Sanzgiri RP, Haydon PG (1998) Glutamate-dependent astrocyte modulation of synaptic transmission between cultured hippocampal neurons. Eur J Neurosci 10:2129-2142.

Arcuino G, Lin JH, Takano T, Liu C, Jiang L, Gao Q, Kang J, Nedergaard M (2002) Intercellular calcium signaling mediated by point-source burst release of ATP. Proc Natl Acad Sci U S A 99:9840-9845.

Armstrong JS, Steinauer KK, Hornung B, Irish JM, Lecane P, Birrell GW, Peehl DM, Knox SJ (2002) Role of glutathione depletion and reactive oxygen species generation in apoptotic signaling in a human B lymphoma cell line. Cell Death Differ 9:252-263.

Bai JZ, Lipski J (2010) Differential expression of TRPM2 and TRPV4 channels and their potential role in oxidative stress-induced cell death in organotypic hippocampal culture. Neurotoxicology.

Balaban RS, Nemoto S, Finkel T (2005) Mitochondria, oxidants, and aging. Cell 120:483-495.

Barnham KJ, Masters CL, Bush AI (2004) Neurodegenerative diseases and oxidative stress. Nat Rev Drug Discov 3:205-214.

Becher B, Bechmann I, Greter M (2006) Antigen presentation in autoimmunity and CNS inflammation: how T lymphocytes recognize the brain. J Mol Med 84:532-543.

Bechmann I, Galea I, Perry VH (2007) What is the blood-brain barrier (not)? Trends Immunol 28:5-11.

Becker PL, Fay FS (1987) Photobleaching of fura-2 and its effect on determination of calcium concentrations. Am J Physiol 253:C613-618.

Berliocchi L, Bano D, Nicotera P (2005) Ca2+ signals and death programmes in neurons. Philos Trans R Soc Lond B Biol Sci 360:2255-2258.

Berridge MJ, Lipp P, Bootman MD (2000) The versatility and universality of calcium signalling. Nat Rev Mol Cell Biol 1:11-21.

Bezprozvanny I, Mattson MP (2008) Neuronal calcium mishandling and the pathogenesis of Alzheimer's disease. Trends Neurosci 31:454-463.

Bignami A, Eng LF, Dahl D, Uyeda CT (1972) Localization of the glial fibrillary acidic protein in astrocytes by immunofluorescence. Brain Res 43:429-435.

Bindokas VP, Jordan J, Lee CC, Miller RJ (1996) Superoxide production in rat hippocampal neurons: selective imaging with hydroethidine. J Neurosci 16:1324-1336.

Bolkent S, Zierold K (2002) Effects of the ionophores valinomycin, ionomycin and gramicidin A on the element compartmentation in cultured rat hepatocytes. Toxicol In Vitro 16:159-165.

Bond CE, Greenfield SA (2007) Multiple cascade effects of oxidative stress on astroglia. Glia 55:1348-1361.

Bonfanti L, Peretto P (2011) Adult neurogenesis in mammals--a theme with many variations. Eur J Neurosci 34:930-950.

Bordey A, Sontheimer H (1997) Postnatal development of ionic currents in rat hippocampal astrocytes in situ. J Neurophysiol 78:461-477.

Bordey A, Sontheimer H (2000) Ion channel expression by astrocytes in situ: comparison of different CNS regions. Glia 30:27-38.

Boveris A, Navarro A (2008) Brain mitochondrial dysfunction in aging. IUBMB Life 60:308-314.

Buffo A, Rolando C, Ceruti S (2010) Astrocytes in the damaged brain: molecular and cellular insights into their reactive response and healing potential. Biochem Pharmacol 79:77-89.

Burke SN, Barnes CA (2009) Senescent synapses and hippocampal circuit dynamics. Trends Neurosci 33:153-161.

Bushong EA, Martone ME, Jones YZ, Ellisman MH (2002) Protoplasmic astrocytes in CA1 stratum radiatum occupy separate anatomical domains. J Neurosci 22:183-192.

Cai Z, Zhao B, Ratka A (2011) Oxidative stress and beta-amyloid protein in Alzheimer's disease. Neuromolecular Med 13:223-250.

Camello-Almaraz C, Gomez-Pinilla PJ, Pozo MJ, Camello PJ (2006) Mitochondrial reactive oxygen species and Ca2+ signaling. Am J Physiol Cell Physiol 291:C1082-1088.

Carmignoto G, Pasti L, Pozzan T (1998) On the role of voltage-dependent calcium channels in calcium signaling of astrocytes in situ. J Neurosci 18:4637-4645.

Chen ZP, Levy A, Lightman SL (1995) Nucleotides as extracellular signalling molecules. J Neuroendocrinol 7:83-96.

Cotrina ML, Nedergaard M (2002) Astrocytes in the aging brain. J Neurosci Res 67:1-10.

Cotrina ML, Nedergaard M (2009) Physiological and pathological functions of P2X7 receptor in the spinal cord. Purinergic Signal 5:223-232.

Dallwig R, Deitmer JW (2002) Cell-type specific calcium responses in acute rat hippocampal slices. J Neurosci Methods 116:77-87.

Dallwig R, Vitten H, Deitmer JW (2000) A novel barium-sensitive calcium influx into rat astrocytes at low external potassium. Cell Calcium 28:247-259.

Deitmer JW, Schild D (2000) 2.2 Fura-2. In: Ca^{2+} und pH (Labor im Fokus), Spektrum Verlag 2000, pp22-pp33

Desagher S, Glowinski J, Premont J (1996) Astrocytes protect neurons from hydrogen peroxide toxicity. J Neurosci 16:2553-2562.

Dhami GK, Ferguson SS (2006) Regulation of metabotropic glutamate receptor signaling, desensitization and endocytosis. Pharmacol Ther 111:260-271.

Dringen R (2000) Metabolism and functions of glutathione in brain. Prog Neurobiol 62:649-671.

Dringen R, Kussmaul L, Gutterer JM, Hirrlinger J, Hamprecht B (1999) The glutathione system of peroxide detoxification is less efficient in neurons than in astroglial cells. J Neurochem 72:2523-2530.

Droge W, Schipper HM (2007) Oxidative stress and aberrant signaling in aging and cognitive decline. Aging Cell 6:361-370.

Eddleston M, Mucke L (1993) Molecular profile of reactive astrocytes--implications for their role in neurologic disease. Neuroscience 54:15-36.

Eng LF, Ghirnikar RS, Lee YL (2000) Glial fibrillary acidic protein: GFAP-thirty-one years (1969-2000). Neurochem Res 25:1439-1451.

Facecchia K, Fochesato LA, Ray SD, Stohs SJ, Pandey S (2011) Oxidative toxicity in neurodegenerative diseases: role of mitochondrial dysfunction and therapeutic strategies. J Toxicol 2011:683728.

Faulkner JR, Herrmann JE, Woo MJ, Tansey KE, Doan NB, Sofroniew MV (2004) Reactive astrocytes protect tissue and preserve function after spinal cord injury. J Neurosci 24:2143-2155.

Feeney CJ, Frantseva MV, Carlen PL, Pennefather PS, Shulyakova N, Shniffer C, Mills LR (2008) Vulnerability of glial cells to hydrogen peroxide in cultured hippocampal slices. Brain Res 1198:1-15.

Fellin T (2009) Communication between neurons and astrocytes: relevance to the modulation of synaptic and network activity. J Neurochem 108:533-544.

Finkel T, Holbrook NJ (2000) Oxidants, oxidative stress and the biology of ageing. Nature 408:239-247.

Foster TC (2007) Calcium homeostasis and modulation of synaptic plasticity in the aged brain. Aging Cell 6:319-325.

Gahwiler BH (1988) Organotypic cultures of neural tissue. Trends Neurosci 11:484-489.

Gahwiler BH, Capogna M, Debanne D, McKinney RA, Thompson SM (1997) Organotypic slice cultures: a technique has come of age. Trends Neurosci 20:471-477.

Garden GA, Moller T (2006) Microglia biology in health and disease. J Neuroimmune Pharmacol 1:127-137.

Gerich FJ, Funke F, Hildebrandt B, Fasshauer M, Muller M (2009) H(2)O(2)-mediated modulation of cytosolic signaling and organelle function in rat hippocampus. Pflugers Arch 458:937-952.

Ghosh R, Mitchell DL (1999) Effect of oxidative DNA damage in promoter elements on transcription factor binding. Nucleic Acids Res 27:3213-3218.

Giaume C, Venance L (1998) Intercellular calcium signaling and gap junctional communication in astrocytes. Glia 24:50-64.

Gille JJ, Joenje H (1992) Cell culture models for oxidative stress: superoxide and hydrogen peroxide versus normobaric hyperoxia. Mutat Res 275:405-414.

Glorioso C, Sibille E (2010) Between destiny and disease: Genetics and molecular pathways of human central nervous system aging. Prog Neurobiol.

Golovina VA, Blaustein MP (2000) Unloading and refilling of two classes of spatially resolved endoplasmic reticulum Ca(2+) stores in astrocytes. Glia 31:15-28.

Gomi H, Yokoyama T, Fujimoto K, Ikeda T, Katoh A, Itoh T, Itohara S (1995) Mice devoid of the glial fibrillary acidic protein develop normally and are susceptible to scrapie prions. Neuron 14:29-41.

Gonzalez A, Granados MP, Pariente JA, Salido GM (2006) H2O2 mobilizes Ca2+ from agonist- and thapsigargin-sensitive and insensitive intracellular stores and stimulates glutamate secretion in rat hippocampal astrocytes. Neurochem Res 31:741-750.

Gottfried C, Tramontina F, Goncalves D, Goncalves CA, Moriguchi E, Dias RD, Wofchuk ST, Souza DO (2002) Glutamate uptake in cultured astrocytes depends on age: a study about the effect of guanosine and the sensitivity to oxidative stress induced by H(2)O(2). Mech Ageing Dev 123:1333-1340.

Greschat S, Schira J, Kury P, Rosenbaum C, de Souza Silva MA, Kogler G, Wernet P, Muller HW (2008) Unrestricted somatic stem cells from human umbilical cord blood can be differentiated into neurons with a dopaminergic phenotype. Stem Cells Dev 17:221-232.

Griffith OW, Meister A (1979) Potent and specific inhibition of glutathione synthesis by buthionine sulfoximine (S-n-butyl homocysteine sulfoximine). J Biol Chem 254:7558-7560.

Grynkiewicz G, Poenie M, Tsien RY (1985) A new generation of Ca2+ indicators with greatly improved fluorescence properties. J Biol Chem 260:3440-3450.

Gulden M, Jess A, Kammann J, Maser E, Seibert H (2010) Cytotoxic potency of H2O2 in cell cultures: impact of cell concentration and exposure time. Free Radic Biol Med 49:1298-1305.

Harman D (1956) Aging: a theory based on free radical and radiation chemistry. J Gerontol 11:298-300.

Harman D (1981) The aging process. Proc Natl Acad Sci U S A 78:7124-7128.

Harman D (2003) The free radical theory of aging. Antioxid Redox Signal 5:557-561.

Harris-White ME, Zanotti SA, Frautschy SA, Charles AC (1998) Spiral intercellular calcium waves in hippocampal slice cultures. J Neurophysiol 79:1045-1052.

Hartel K, Singaravelu K, Kaiser M, Neusch C, Hulsmann S, Deitmer JW (2007) Calcium influx mediated by the inwardly rectifying K+ channel Kir4.1 (KCNJ10) at low external K+ concentration. Cell Calcium 42:271-280.

Hauwel M, Furon E, Canova C, Griffiths M, Neal J, Gasque P (2005) Innate (inherent) control of brain infection, brain inflammation and brain repair: the role of microglia, astrocytes, "protective" glial stem cells and stromal ependymal cells. Brain Res Brain Res Rev 48:220-233.

Hayashi H, Miyata H (1994) Fluorescence imaging of intracellular Ca2+. J Pharmacol Toxicol Methods 31:1-10.

Hertz L (1986) Potassium transport in astrocytes and neurons in primary cultures. Ann N Y Acad Sci 481:318-333.

Hibino H, Inanobe A, Furutani K, Murakami S, Findlay I, Kurachi Y (2010) Inwardly rectifying potassium channels: their structure, function, and physiological roles. Physiol Rev 90:291-366.

Holthoff K, Witte OW (2000) Directed spatial potassium redistribution in rat neocortex. Glia 29:288-292.

Hou JG, Cohen G, Mytilineou C (1997) Basic fibroblast growth factor stimulation of glial cells protects dopamine neurons from 6-hydroxydopamine toxicity: involvement of the glutathione system. J Neurochem 69:76-83.

Jacobson J, Duchen MR (2002) Mitochondrial oxidative stress and cell death in astrocytes--requirement for stored Ca2+ and sustained opening of the permeability transition pore. J Cell Sci 115:1175-1188.

Jendelova P, Sykova E (1991) Role of glia in K+ and pH homeostasis in the neonatal rat spinal cord. Glia 4:56-63.

Johnson CM, Hill CS, Chawla S, Treisman R, Bading H (1997) Calcium controls gene expression via three distinct pathways that can function independently of the Ras/mitogen-activated protein kinases (ERKs) signaling cascade. J Neurosci 17:6189-6202.

Joo HJ, Ma JY, Choo YG, Choi BK, Jung KY (1999) Age-related alteration of intracellular ATP maintenance in the cell suspensions of mice cerebral cortex. Mech Ageing Dev 110:1-12.

Kafitz KW, Meier SD, Stephan J, Rose CR (2008) Developmental profile and properties of sulforhodamine 101--Labeled glial cells in acute brain slices of rat hippocampus. J Neurosci Methods 169:84-92.

Kahlert S, Reiser G (2000) Requirement of glycolytic and mitochondrial energy supply for loading of Ca(2+) stores and InsP(3)-mediated Ca(2+) signaling in rat hippocampus astrocytes. J Neurosci Res 61:409-420.

Kehl C (2007) Immunhistochemische Charakterisierung von Gliazellen. Diploma thesis. Institute for Neurobiology, Heinrich-Heine-University Düsseldorf

Kelly T, Kafitz KW, Roderigo C, Rose CR (2009) Ammonium-evoked alterations in intracellular sodium and pH reduce glial glutamate transport activity. Glia 57:921-934.

Kim JV, Dustin ML (2006) Innate response to focal necrotic injury inside the blood-brain barrier. J Immunol 177:5269-5277.

Kim WT, Rioult MG, Cornell-Bell AH (1994) Glutamate-induced calcium signaling in astrocytes. Glia 11:173-184.

Kimelberg HK (2004) The problem of astrocyte identity. Neurochem Int 45:191-202.

Kimelberg HK, Anderson E, Kettenmann H (1990) Swelling-induced changes in electrophysiological properties of cultured astrocytes and oligodendrocytes. II. Whole-cell currents. Brain Res 529:262-268.

Kimelberg HK, Bowman C, Biddlecome S, Bourke RS (1979) Cation transport and membrane potential properties of primary astroglial cultures from neonatal rat brains. Brain Res 177:533-550.

Kofuji P, Newman EA (2004) Potassium buffering in the central nervous system. Neuroscience 129:1045-1056.

Kuchibhotla KV, Lattarulo CR, Hyman BT, Bacskai BJ (2009) Synchronous hyperactivity and intercellular calcium waves in astrocytes in Alzheimer mice. Science 323:1211-1215.

Kuchibhotla KV, Goldman ST, Lattarulo CR, Wu HY, Hyman BT, Bacskai BJ (2008) Abeta plaques lead to aberrant regulation of calcium homeostasis in vivo resulting in structural and functional disruption of neuronal networks. Neuron 59:214-225.

Langer J, Stephan J, Theis M, Rose CR (2012) Gap junctions mediate intercellular spread of sodium between hippocampal astrocytes in situ. Glia 60:239-252.

Latour I, Gee CE, Robitaille R, Lacaille JC (2001) Differential mechanisms of Ca2+ responses in glial cells evoked by exogenous and endogenous glutamate in rat hippocampus. Hippocampus 11:132-145.

Lavenex P, Banta Lavenex P, Amaral DG (2007) Postnatal development of the primate hippocampal formation. Dev Neurosci 29:179-192.

Lees GJ (1991) Inhibition of sodium-potassium-ATPase: a potentially ubiquitous mechanism contributing to central nervous system neuropathology. Brain Res Brain Res Rev 16:283-300.

Lehnardt S, Wennekamp J, Freyer D, Liedtke C, Krueger C, Nitsch R, Bechmann I, Weber JR, Henneke P (2007) TLR2 and caspase-8 are essential for group B Streptococcus-induced apoptosis in microglia. J Immunol 179:6134-6143.

Lepka KM (2010) Influence of oxidative stress on glial GFAP-expression. Bachelor thesis. Institute for Neurobiology, Heinrich-Heine-University Düsseldorf

Li L, Head V, Timpe LC (2001) Identification of an inward rectifier potassium channel gene expressed in mouse cortical astrocytes. Glia 33:57-71.

Liberto CM, Albrecht PJ, Herx LM, Yong VW, Levison SW (2004) Pro-regenerative properties of cytokine-activated astrocytes. J Neurochem 89:1092-1100.

Light AR, Wu Y, Hughen RW, Guthrie PB (2006) Purinergic receptors activating rapid intracellular Ca increases in microglia. Neuron Glia Biol 2:125-138.

Lin DT, Wu J, Holstein D, Upadhyay G, Rourk W, Muller E, Lechleiter JD (2007) Ca2+ signaling, mitochondria and sensitivity to oxidative stress in aging astrocytes. Neurobiol Aging 28:99-111.

Liu X, Li C, Gebremedhin D, Hwang SH, Hammock BD, Falck JR, Roman RJ, Harder DR, Koehler RC (2011) Epoxyeicosatrienoic acid-dependent cerebral vasodilation evoked by metabotropic glutamate receptor activation in vivo. Am J Physiol Heart Circ Physiol 301:H373-381.

Lledo PM, Alonso M, Grubb MS (2006) Adult neurogenesis and functional plasticity in neuronal circuits. Nat Rev Neurosci 7:179-193.

Lu T, Pan Y, Kao SY, Li C, Kohane I, Chan J, Yankner BA (2004) Gene regulation and DNA damage in the ageing human brain. Nature 429:883-891.

Martensson J, Jain A, Stole E, Frayer W, Auld PA, Meister A (1991) Inhibition of glutathione synthesis in the newborn rat: a model for endogenously produced oxidative stress. Proc Natl Acad Sci U S A 88:9360-9364.

Meier SD, Kovalchuk Y, Rose CR (2006) Properties of the new fluorescent Na+ indicator CoroNa Green: comparison with SBFI and confocal Na+ imaging. J Neurosci Methods 155:251-259.

Meier SD (2007) GABA-Induced Ca^{2+} Signaling in Rat Hippocampal Astrocytes. Doctoral thesis. Institute for Neurobiology, Heinrich-Heine-University Düsseldorf

Metea MR, Newman EA (2006) Glial cells dilate and constrict blood vessels: a mechanism of neurovascular coupling. J Neurosci 26:2862-2870.

Michaelis ML, Bigelow DJ, Schoneich C, Williams TD, Ramonda L, Yin D, Huhmer AF, Yao Y, Gao J, Squier TC (1996) Decreased plasma membrane calcium transport activity in aging brain. Life Sci 59:405-412.

Modi PK, Kanungo MS (2010) Age-dependent expression of S100beta in the brain of mice. Cell Mol Neurobiol 30:709-716.

Morgan TE, Rozovsky I, Goldsmith SK, Stone DJ, Yoshida T, Finch CE (1997) Increased transcription of the astrocyte gene GFAP during middle-age is attenuated by food restriction: implications for the role of oxidative stress. Free Radic Biol Med 23:524-528.

Moser KV, Humpel C (2007) Primary rat monocytes migrate through a BCEC-monolayer and express microglia-markers at the basolateral side. Brain Res Bull 74:336-343.

Nagler K, Mauch DH, Pfrieger FW (2001) Glia-derived signals induce synapse formation in neurones of the rat central nervous system. J Physiol 533:665-679.

Navarro A, Boveris A (2004) Rat brain and liver mitochondria develop oxidative stress and lose enzymatic activities on aging. Am J Physiol Regul Integr Comp Physiol 287:R1244-1249.

Nedergaard M, Verkhratsky A (2010) Calcium dyshomeostasis and pathological calcium signalling in neurological diseases. Cell Calcium 47:101-102.

Nedergaard M, Takano T, Hansen AJ (2002) Beyond the role of glutamate as a neurotransmitter. Nat Rev Neurosci 3:748-755.

Nedergaard M, Ransom B, Goldman SA (2003) New roles for astrocytes: redefining the functional architecture of the brain. Trends Neurosci 26:523-530.

Nedergaard M, Rodriguez JJ, Verkhratsky A (2010) Glial calcium and diseases of the nervous system. Cell Calcium 47:140-149.

Nichols NR (1999) Glial responses to steroids as markers of brain aging. J Neurobiol 40:585-601.

Nicotera P, Bellomo G, Orrenius S (1992) Calcium-mediated mechanisms in chemically induced cell death. Annu Rev Pharmacol Toxicol 32:449-470.

Nimmerjahn A, Kirchhoff F, Kerr JN, Helmchen F (2004) Sulforhodamine 101 as a specific marker of astroglia in the neocortex in vivo. Nat Methods 1:31-37.

Nolte C, Matyash M, Pivneva T, Schipke CG, Ohlemeyer C, Hanisch UK, Kirchhoff F, Kettenmann H (2001) GFAP promoter-controlled EGFP-expressing transgenic mice: a tool to visualize astrocytes and astrogliosis in living brain tissue. Glia 33:72-86.

North RA, Verkhratsky A (2006) Purinergic transmission in the central nervous system. Pflugers Arch 452:479-485.

Obara M, Szeliga M, Albrecht J (2008) Regulation of pH in the mammalian central nervous system under normal and pathological conditions: facts and hypotheses. Neurochem Int 52:905-919.

Olanow CW (1993) A radical hypothesis for neurodegeneration. Trends Neurosci 16:439-444.

Paredes RM, Etzler JC, Watts LT, Zheng W, Lechleiter JD (2008) Chemical calcium indicators. Methods 46:143-151.

Parpura V, Grubisic V, Verkhratsky A (2011) Ca(2+) sources for the exocytotic release of glutamate from astrocytes. Biochim Biophys Acta 1813:984-991.

Parpura V, Basarsky TA, Liu F, Jeftinija K, Jeftinija S, Haydon PG (1994) Glutamate-mediated astrocyte-neuron signalling. Nature 369:744-747.

Pekny M, Nilsson M (2005) Astrocyte activation and reactive gliosis. Glia 50:427-434.

Perea G, Araque A (2005) Glial calcium signaling and neuron-glia communication. Cell Calcium 38:375-382.

Pertusa M, Garcia-Matas S, Rodriguez-Farre E, Sanfeliu C, Cristofol R (2007) Astrocytes aged in vitro show a decreased neuroprotective capacity. J Neurochem 101:794-805.

Peters A, Schweiger U, Pellerin L, Hubold C, Oltmanns KM, Conrad M, Schultes B, Born J, Fehm HL (2004) The selfish brain: competition for energy resources. Neurosci Biobehav Rev 28:143-180.

Pirttimaki TM, Hall SD, Parri HR (2011) Sustained neuronal activity generated by glial plasticity. J Neurosci 31:7637-7647.

Plenge-Tellechea F, Soler F, Fernandez-Belda F (1997) On the inhibition mechanism of sarcoplasmic or endoplasmic reticulum Ca2+-ATPases by cyclopiazonic acid. J Biol Chem 272:2794-2800.

Poopalasundaram S, Knott C, Shamotienko OG, Foran PG, Dolly JO, Ghiani CA, Gallo V, Wilkin GP (2000) Glial heterogeneity in expression of the inwardly rectifying K(+) channel, Kir4.1, in adult rat CNS. Glia 30:362-372.

Puro DG (1991) A calcium-activated, calcium-permeable ion channel in human retinal glial cells: modulation by basic fibroblast growth factor. Brain Res 548:329-333.

Raponi E, Agenes F, Delphin C, Assard N, Baudier J, Legraverend C, Deloulme JC (2007) S100B expression defines a state in which GFAP-expressing cells lose their neural stem cell potential and acquire a more mature developmental stage. Glia 55:165-177.

Reimann F, Ashcroft FM (1999) Inwardly rectifying potassium channels. Curr Opin Cell Biol 11:503-508.

Richter C, Park JW, Ames BN (1988) Normal oxidative damage to mitochondrial and nuclear DNA is extensive. Proc Natl Acad Sci U S A 85:6465-6467.

Ridet JL, Malhotra SK, Privat A, Gage FH (1997) Reactive astrocytes: cellular and molecular cues to biological function. Trends Neurosci 20:570-577.

Robb SJ, Robb-Gaspers LD, Scaduto RC, Jr., Thomas AP, Connor JR (1999) Influence of calcium and iron on cell death and mitochondrial function in oxidatively stressed astrocytes. J Neurosci Res 55:674-686.

Rolls A, Shechter R, Schwartz M (2009) The bright side of the glial scar in CNS repair. Nat Rev Neurosci 10:235-241.

Rose CR, Ransom BR (1997) Gap junctions equalize intracellular Na+ concentration in astrocytes. Glia 20:299-307.

Sarvazyan N, Swift L, Martinez-Zaguilan R (1998) Effects of oxidants on properties of fluorescent calcium indicators. Arch Biochem Biophys 350:132-136.

Schanne FA, Kane AB, Young EE, Farber JL (1979) Calcium dependence of toxic cell death: a final common pathway. Science 206:700-702.

Schira J, Gasis M, Estrada V, Hendricks M, Schmitz C, Trapp T, Kruse F, Kogler G, Wernet P, Hartung HP, Muller HW (2012) Significant clinical, neuropathological and behavioural recovery from acute spinal cord trauma by transplantation of a well-defined somatic stem cell from human umbilical cord blood. Brain 135:431-446.

Schoepp DD, Goldsworthy J, Johnson BG, Salhoff CR, Baker SR (1994) 3,5-dihydroxyphenylglycine is a highly selective agonist for phosphoinositide-linked metabotropic glutamate receptors in the rat hippocampus. J Neurochem 63:769-772.

Scoville WB, Milner B (1957) Loss of recent memory after bilateral hippocampal lesions. J Neurol Neurosurg Psychiatry 20:11-21.

Seifert G, Huttmann K, Binder DK, Hartmann C, Wyczynski A, Neusch C, Steinhauser C (2009) Analysis of astroglial K+ channel expression in the developing hippocampus reveals a predominant role of the Kir4.1 subunit. J Neurosci 29:7474-7488.

Sheng JG, Mrak RE, Rovnaghi CR, Kozlowska E, Van Eldik LJ, Griffin WS (1996) Human brain S100 beta and S100 beta mRNA expression increases with age: pathogenic implications for Alzheimer's disease. Neurobiol Aging 17:359-363.

Sofroniew MV (2005) Reactive astrocytes in neural repair and protection. Neuroscientist 11:400-407.

Sofroniew MV (2009) Molecular dissection of reactive astrogliosis and glial scar formation. Trends Neurosci 32:638-647.

Solovyova N, Verkhratsky A (2002) Monitoring of free calcium in the neuronal endoplasmic reticulum: an overview of modern approaches. J Neurosci Methods 122:1-12.

Somjen GG (1988) Nervenkitt: notes on the history of the concept of neuroglia. Glia 1:2-9.

Somjen GG (2002) Ion regulation in the brain: implications for pathophysiology. Neuroscientist 8:254-267.

Sontheimer H, Fernandez-Marques E, Ullrich N, Pappas CA, Waxman SG (1994) Astrocyte Na+ channels are required for maintenance of Na+/K(+)-ATPase activity. J Neurosci 14:2464-2475.

Souza dos Santos P, Saraiva DF, Ferraz da Costa DC, Scofano HM, de Carvalho-Alves PC (2007) Trifluoperazine protects brain plasma membrane Ca(2+)-ATPase from oxidative damaging. Exp Brain Res 177:347-357.

Squier TC, Bigelow DJ (2000) Protein oxidation and age-dependent alterations in calcium homeostasis. Front Biosci 5:D504-526.

Stangl C, Fromherz P (2008) Neuronal field potential in acute hippocampus slice recorded with transistor and micropipette electrode. Eur J Neurosci 27:958-964.

Steinhauser C, Gallo V (1996) News on glutamate receptors in glial cells. Trends Neurosci 19:339-345.

Stella F, Cerasti E, Si B, Jezek K, Treves A (2011) Self-organization of multiple spatial and context memories in the hippocampus. Neurosci Biobehav Rev.

Stoppelkamp S, Riedel G, Platt B (2010) Culturing conditions determine neuronal and glial excitability. J Neurosci Methods 194:132-138.

Stoppini L, Buchs PA, Muller D (1991) A simple method for organotypic cultures of nervous tissue. J Neurosci Methods 37:173-182.

Stosiek C, Garaschuk O, Holthoff K, Konnerth A (2003) In vivo two-photon calcium imaging of neuronal networks. Proc Natl Acad Sci U S A 100:7319-7324.

Szydlowska K, Tymianski M (2010) Calcium, ischemia and excitotoxicity. Cell Calcium 47:122-129.

Takano T, Tian GF, Peng W, Lou N, Libionka W, Han X, Nedergaard M (2006) Astrocyte-mediated control of cerebral blood flow. Nat Neurosci 9:260-267.

Takuma K, Baba A, Matsuda T (2004) Astrocyte apoptosis: implications for neuroprotection. Prog Neurobiol 72:111-127.

Tamagno I, Schiffer D (2006) Nestin expression in reactive astrocytes of human pathology. J Neurooncol 80:227-233.

Thery C, Chamak B, Mallat M (1991) Cytotoxic Effect of Brain Macrophages on Developing. Eur J Neurosci 3:1155-1164.

Toescu EC, Verkhratsky A (2003) Neuronal ageing from an intraneuronal perspective: roles of endoplasmic reticulum and mitochondria. Cell Calcium 34:311-323.

Ullian EM, Christopherson KS, Barres BA (2004) Role for glia in synaptogenesis. Glia 47:209-216.

Valko M, Leibfritz D, Moncol J, Cronin MT, Mazur M, Telser J (2007) Free radicals and antioxidants in normal physiological functions and human disease. Int J Biochem Cell Biol 39:44-84.

van de Water B, Zoeteweij JP, de Bont HJ, Mulder GJ, Nagelkerke JF (1994) Role of mitochondrial Ca2+ in the oxidative stress-induced dissipation of the mitochondrial membrane potential. Studies in isolated proximal tubular cells using the nephrotoxin 1,2-dichlorovinyl-L-cysteine. J Biol Chem 269:14546-14552.

Verderio C, Matteoli M (2001) ATP mediates calcium signaling between astrocytes and microglial cells: modulation by IFN-gamma. J Immunol 166:6383-6391.

Verkhratsky A (2006) Calcium ions and integration in neural circuits. Acta Physiol (Oxf) 187:357-369.

Verkhratsky A, Orkand RK, Kettenmann H (1998) Glial calcium: homeostasis and signaling function. Physiol Rev 78:99-141.

Verkhratsky A, Krishtal OA, Burnstock G (2009) Purinoceptors on neuroglia. Mol Neurobiol 39:190-208.

Verkhratsky A, Rodriguez JJ, Parpura V (2011) Calcium signalling in astroglia. Mol Cell Endocrinol 353:45-56.

Volterra A, Steinhauser C (2004) Glial modulation of synaptic transmission in the hippocampus. Glia 47:249-257.

Volterra A, Meldolesi J (2005) Astrocytes, from brain glue to communication elements: the revolution continues. Nat Rev Neurosci 6:626-640.

von Zglinicki T, Burkle A, Kirkwood TB (2001) Stress, DNA damage and ageing -- an integrative approach. Exp Gerontol 36:1049-1062.

Vornov JJ, Park J, Thomas AG (1998) Regional vulnerability to endogenous and exogenous oxidative stress in organotypic hippocampal culture. Exp Neurol 149:109-122.

Voss P, Engels M, Strosova M, Grune T, Horakova L (2008) Protective effect of antioxidants against sarcoplasmic reticulum (SR) oxidation by Fenton reaction, however without prevention of Ca-pump activity. Toxicol In Vitro 22:1726-1733.

Wang M, Kong Q, Gonzalez FA, Sun G, Erb L, Seye C, Weisman GA (2005) P2Y nucleotide receptor interaction with alpha integrin mediates astrocyte migration. J Neurochem 95:630-640.

Wilhelmsson U, Bushong EA, Price DL, Smarr BL, Phung V, Terada M, Ellisman MH, Pekny M (2006) Redefining the concept of reactive astrocytes as cells that remain within their unique domains upon reaction to injury. Proc Natl Acad Sci U S A 103:17513-17518.

Wilhelmsson U, Li L, Pekna M, Berthold CH, Blom S, Eliasson C, Renner O, Bushong E, Ellisman M, Morgan TE, Pekny M (2004) Absence of glial fibrillary acidic protein and vimentin prevents hypertrophy of astrocytic processes and improves post-traumatic regeneration. J Neurosci 24:5016-5021.

Wilkinson JA, Scragg JL, Boyle JP, Nilius B, Peers C (2008) H2O 2-stimulated Ca2+ influx via TRPM2 is not the sole determinant of subsequent cell death. Pflugers Arch 455:1141-1151.

Wojtowicz JM (2012) Adult neurogenesis. From circuits to models. Behav Brain Res 227:490-496.

Yodozawa S, Tsunoda Y, Funai T, Tashiro Y (1991) Dynamics of Ca2+ transients in norepinephrine-stimulated individual H-35 hepatoma cells: fura-2 digital imaging microscopy and high time-resolution microspectrofluorometry. J Histochem Cytochem 39:1311-1319.

Yong VW, Moumdjian R, Yong FP, Ruijs TC, Freedman MS, Cashman N, Antel JP (1991) Gamma-interferon promotes proliferation of adult human astrocytes in vitro and reactive gliosis in the adult mouse brain in vivo. Proc Natl Acad Sci U S A 88:7016-7020.

Zaidi A, Gao J, Squier TC, Michaelis ML (1998) Age-related decrease in brain synaptic membrane Ca2+-ATPase in F344/BNF1 rats. Neurobiol Aging 19:487-495.

Zhang Y, Rong Qi X, Gao Y, Wei L, Maitani Y, Nagai T (2007) Mechanisms of co-modified liver-targeting liposomes as gene delivery carriers based on cellular uptake and antigens inhibition effect. J Control Release 117:281-290.

Zhu Y, Kimelberg HK (2001) Developmental expression of metabotropic P2Y(1) and P2Y(2) receptors in freshly isolated astrocytes from rat hippocampus. J Neurochem 77:530-541.

Zhuo L, Sun B, Zhang CL, Fine A, Chiu SY, Messing A (1997) Live astrocytes visualized by green fluorescent protein in transgenic mice. Dev Biol 187:36-42.

Zundorf G, Reiser G (2011) Calcium dysregulation and homeostasis of neural calcium in the molecular mechanisms of neurodegenerative diseases provide multiple targets for neuroprotection. Antioxid Redox Signal 14:1275-1288.

Zur Nieden R, Deitmer JW (2006) The role of metabotropic glutamate receptors for the generation of calcium oscillations in rat hippocampal astrocytes in situ. Cereb Cortex 16:676-687.

Appendix

A Supplementary tables

amount for 500 ml	amount in %	substance	manufacturer
200 ml	40	Hank's Buffered Salt Solution (HBSS)	Gibco, Invitrogen, Paisley, U.K.
150 ml	30	Dulbecco's Modified Eagle Medium (DMEM)	Gibco, Invitrogen, Paisley, U.K.
150 ml	30	filtered horse serum	Gibco, Invitrogen, Paisley, U.K.

Table 2: Stock medium composition for cell culture medium.

amount for 500 ml	substance	manufacturer
6.25 ml	glucose (248 g/l)	Caelo, Ceasar & Lorenz GmbH, Hilden, Germany
250 ml	stock medium	---
1.5 ml	HCl (1N)	Merck KGaA, Darmstadt, Germany

Table 3: Culture medium composition.

amount	substance	manufacturer
6 g	Glycerol, 99 % GC	Sigma-Aldrich, Steinheim, Germany
2.4 g	Mowiol 4-88	Calbiochem (Merck, Darmstadt, Germany)
6 ml	aqua dest.	---
12 ml	0.2 M Tris-buffer, pH 8.0	Merck, Darmstadt, Germany
0.1 % (0..264 g)	DABCO	Fluka, Steinheim, Germany

Table 4: Composition of Mowiol solution.

	epitope	host	ex [nm]	manufacturer	dilution
primary antibodies	GFAP (monoclonal)	mouse	---	Sigma-Aldrich (Steinheim, Germany)	1:1000
	S100β (polyclonal)	rabbit	---	AbCam (Cambridge, U.K.)	1:200
secondary antibodies	Alexa Fluor anti-mouse	goat	488	molecular probes (Invitrogen, Karlsruhe, Germany	1:100
	Alexa Fluor anti-rabbit	goat	594	molecular probes (Invitrogen, Karlsruhe, Germany	1:100

Table 5: Antibodies used for immunohistochmical staining.

	procedure	time
	fixation in 4 % PFA at 4°C	overnight
	2x washing with PBS (on ice)	2x 10 min
	permeabilization and blocking in PBS with 0.25 % Triton-X and 2 % NGS at 4°C	1.5 h
	staining with primary antibodies (anti-GFAP and anti-S100) in PBS with 0.25 % Triton-X and 2 % NGS at 4°C	overnight
	3x washing with PBS (+ 0.25 % Triton-X and 2 % NGS) at RT	3x 15 min
work in the dark	staining with secondary antibodies (anti-mouse 488 and anti-rabbit 594) in PBS with 2 % NGS at RT	2 h
	6x washing with PBS	6x 10 min
	incubation with DAPI	15 min
	3x washing with PBS	3x 10 min

Table 6: Procedure for immunohistochemical staining.

B List of figures and tables

List of figures

List of tables

C Acknowledgement

I would like to thank a lot more people for their support in form of inspiration, motivation and criticism, than I can probably name here. At this place, I just want to give special mention to those, who were really close to me and my work in the past years, and I feel deeply indebted to.

First of all, I want to express my gratefulness to Prof. Dr. Christine R. Rose for the opportunity to write my doctoral thesis in her institute directly after finishing my diploma thesis. Her endurance during all the time, especially with all the difficulties that arose, is what I am deeply grateful for. I also want to thank Prof. Dr. Dieter Willbold for examination of this work, as well as the DFG for financial support of my work.

I am also thankful to current and former members of the institute for creating such a kind atmosphere and their support in different ways. In particular, I want to thank Karl for repeated proof-reading and comments on prior version of this work, and Klaudia Lepka for the helpful groundwork, which she performed with her bachelor thesis. I am also grateful to Claudia and Simone for their daily organization of the lab work and help whenever it was necessary, especially Simone's practical support by doing the immunohistochemistry.

To Jonathan, I want to address a big thank you for performing the patch-clamp experiments, additional proof-reading and for this unique working atmosphere in our room each single day.

Last but not least, I want to thank my family for their support, each one in their own way. I am in particular grateful to Jessie for enduring my fluctuating mood and numerous nights of working, where I went to sleep only 1-2 hours before she had to get up. For me, sleep is a precious thing and I really don't know how much sleep all of this has cost her.

D Declaration

Die hier vorgelegte Dissertation habe ich eigenständig und ohne unerlaubte Hilfe angefertigt. Die Dissertation wurde in der vorgelegten der in ähnlicher Form noch bei keiner anderen Institution eingereicht. Ich habe bisher keine erfolglosen Promotionsversuche unternommen.

Düsseldorf, den 27.07.2012

(Christian Kehl)